mgr farm. Paweł Kręcisz

# Opracowanie metod chromatograficznych w optymalizacji projektowania oraz otrzymywania nowych radiofarmaceutyków

# Development of chromatographic methods in optimization of design and synthesis of new radiopharmaceuticals

Promotor:

prof. dr hab. n. farm. Paweł Szymański

Promotor pomocniczy:

dr n. farm. Kamila Czarnecka

Uniwersytet Medyczny w Łodzi

Wydział Farmaceutyczny

Zakład Chemii Farmaceutycznej, Analizy Leków i Radiofarmacji

Łódź, 2021

## Spis treści

# Wykaz skrótów

| | | |
|---|---|---|
| ADME | - | Wchłanianie, Dystrybucja, Biotransformacja, Wydalanie (ang. Absorption, Distribution, Metabolism, Excretion) |
| CXCR4 | - | Receptor chemokiny C-X-C typu 4 |
| DOTA | - | Kwas 1,4,7,10-tetraazacylododekan-1,4,7,10-tetraoctowy |
| GC | - | Chromatografia gazowa (ang. Gas Chromatography) |
| HPLC | - | Wysokosprawna chromatografia cieczowa (ang. High Performance Liquid Chromatography) |
| HYNIC | - | Kwas 6-hydrazynonikotynowy |
| ICH | - | Międzynarodowa Rada do spraw Harmonizacji (ang. International Council for Harmonisation) |
| logP | - | Współczynnik podziału oktanol/woda |
| PET | - | Pozytonowa Tomografia Emisyjna (ang. Positron Emission Tomography) |
| PDA | - | Detektor UV wyposażony w układ fotodiod |
| pKa | - | Ujemny logarytm dziesiętny ze stałej dysocjacji kwasu |
| SFC | - | Chromatografia w stanie nadkrytycznym $CO_2$ (ang. Supercritical Fluid Chromatography) |
| SPECT | - | Tomografia Emisyjna Pojedynczego Fotonu (ang. Single Photon Emission Computed Tomography) |
| TLC | - | Chromatografia cienkowarstwowa (ang. Thin Layer Chromatography) |

# Wstęp

Zespół pod kierownictwem Pana prof. dr hab. n. farm. Pawła Szymańskiego z Zakładu Chemii Farmaceutycznej, Analizy Leków i Radiofarmacji Uniwersytetu Medycznego w Łodzi od lat pracuje nad pochodnymi takryny o wielkokierunkowym działaniu. Badania te pozwalają na opracowanie substancji o potencjalnym znaczeniu w leczeniu objawów choroby Alzheimera jak również dają nadzieję na opracowanie potencjalnego radiofarmaceutyku do wczesnej diagnostyki tego schorzenia. Modyfikacje struktury takryny dotyczyły połączenia układu 1,2,3,4-tetrahydroakrydyny za pomocą łańcucha węglowego o różnej długości z podstawnikami takimi jak kwas jodobenzoesowy [1], fluorobenzoesowy jako „zimne" analogi potencjalnych radiofarmaceutyków [2], dichloronikotynowy [3], a także kwas hydrazynonikotynowy, który był kompleksowany z promieniotwórczym technetem [4, 5] oraz dwufunkcyjny chelator DOTA (kwas 1,4,7,10-tetraazacylododekan-1,4,7,10-tetraoctowy) [6] (rycina 1, str. 6). Dla otrzymanych substancji badana była między innymi aktywność inhibicyjna oraz selektywność w stosunku do acetylocholinoesterazy oraz butyrylocholinoesterazy, ale także badane były właściwości neuroprotekcyjne pod kątem stresu oksydacyjnego czy zdolności hamowania agregacji płytek β amyloidu. Wykonywano badania toksyczności ostrej z wykorzystaniem kultur komórkowych oraz zwierząt. Prowadzone były również badania w kierunku wykazania działania przeciwdrobnoustrojowego [7], ponieważ pochodne akrydyny dzięki swojej strukturze są wykorzystywane w innych dziedzinach medycyny niż terapia choroby Alzheimera. Przykładem jest znany od wielu lat mleczan etakrydyny, będący substancją przeciwbakteryjną, przeciwgrzybiczą oraz wykorzystywaną jako środek antyseptyczny. Mechanizm działania przeciwdrobnoustrojowego mleczanu etakrydyny oraz innych barwników akrydynynowych związany jest z hamowaniem topoizomeraz bakteryjnych powodujących niewłaściwe skręcenie podwójnej helisy DNA podczas procesu replikacji. [8] Inną strukturą podobną do takryny jest chlorochina, która znalazła zastosowanie w terapii chorób pierwotniakowych takich jak malaria, będąca chorobą wywoływaną przez *Plasmodium falciparum.* Mechanizm działania przeciwpierwotniakowego chlorochiny polega na akumulacji substancji w wodniczkach trawiennych zarodźca malarii zmieniając w ich wnętrzu pH co prowadzi do zahamowania rozwoju komórki pierwotniaka. Chlorochina znalazła także zastosowanie jako środek przeciwzapalny w terapii reumatoidalnego zapalenia stawów oraz tocznia rumieniowatego. [9] Ponadto interesujące są badania będące efektem obecnej pandemii wirusa SARS-CoV-2 dotyczące efektywnego wykorzystania chlorochiny w terapii choroby COVID-19. [10] Mechanizm działania chlorochiny w terapii COVID-19 jest mocno złożony i nie został w pełni poznany, lecz istnieją dotyczące go hipotezy. Uważa się, że chlorochina wpływa na zależną od pH fuzję i replikację wirusa, zatrzymuje powstawanie glikoproteinowej otoczki wirusowej, a także glikozylację receptora gospodarza. Istnieje również hipoteza o osłabieniu ekspresji czynników prozapalnych i białek receptorowych odpowiedzialnych za wywoływanie zespołu ostrej niewydolności oddechowej. [11] Najnowsze badania dostarczają jednak informacji o niekorzystnych efektach zastosowania chlorochiny w terapii COVID-19. [12]

Wykorzystanie pochodnych 1,2,3,4-tetrahydroakrydyny jako nośników pierwiastków promieniotwórczych jest rozwinięciem prac zapoczątkowanych pod koniec

dwudziestego wieku, gdzie znakowano cząsteczkę 9-amino-1,2,3,4-tetrahydroakrydyny węglem $^{11}C$ poprzez metylację grupy aminowej. [13] Celem było opracowanie cząsteczek mogących znaleźć zastosowanie we wczesnej diagnozie choroby Alzheimera poprzez wykrywanie obszarów mózgu, w których występuje duże stężenie acetylocholinoesterazy. Pod kierownictwem profesora Pawła Szymańskiego opracowane zostały pochodne będące tzw. „zimnymi radiofarmaceutykami", czyli struktury w których znajdują się niepromieniotwórcze izotopy pierwiastków takich jak jod lub fluor. Zastosowanie do badań „zimnych radiofarmaceutyków" bardzo ułatwia uzyskiwanie informacji o właściwościach substancji bez ryzyka ekspozycji na promieniowanie. Taką strategię zastosowałem podczas opracowywania badań fizykochemicznych pochodnych takryny sprzężonych z kwasem jodobenzoesowym co zostało opisane w **publikacji 1**. Docelowo cząsteczki te będą zawierały w swojej strukturze izotop jodu $^{123}I$ będący emiterem promieniowania gamma z zastosowaniem w obrazowaniu metodami scyntylacyjnymi. Realizacja znakowania przewidziana jest poprzez wykorzystanie znakowanego promieniotwórczym jodem $^{123}I$ kwasu jodobenzoesowego w charakterze grupy prostetycznej. Schemat syntezy przewiduje reakcję tworzenia amidu indukowanego przez chlorek 4-(4,6-dimetoksy-1,3,5-triazyno-2-yl)-4-metylomofoliny w połączeniu z wolną grupą aminową łańcucha węglowego połączonego z cząsteczką 1,2,3,4-tetrahydroakrydyny. Mechanizm ten został dobrany na podstawie wysokiej wydajności uzyskiwania produktu reakcji, łagodnych warunków chemicznych i fizycznych oraz krótkiego czasu niezbędnego do przeprowadzania reakcji. Opracowane zostały również substancje, które mogłyby z powodzeniem zostać wykorzystane podczas obrazowania technikami tomografii emisyjnej pojedynczego fotonu (ang. Single Photon Emission Computed Tomography, SPECT) oraz pozytonowej tomografii emisyjnej (ang. Positron Emission Tomography, PET), znakowane technetem $^{99m}Tc$ [14], a także galem $^{68}Ga$ [6] z wykorzystaniem technik kompleksowania jonów metali za pomocą chelatorów dwufunkcyjnych takich jak kwas 1,4,7,10-tetraazacylododekan-1,4,7,10-tetraoctowy (DOTA) lub kwas 6-hydrazynonikotynowy (HYNIC). Technika ta jest obecnie szeroko stosowana w projektowaniu nowoczesnych nośników pierwiastków promieniotwórczych, co zostało opisane w formie przeglądu literatury w **publikacji 3**. W tej pracy zebrałem najnowsze dane na temat nowoczesnych radioznakowanych ligandów białkowych stosowanych w diagnostyce i terapii. Praca zawiera dane na temat nowo wprowadzonych małych białek, jak i dużych struktur takich jak przeciwciała monoklonalne. Została ona podzielona na sekcje dotyczące strategii receptorowej, radioimmunoterapii wraz z radioimmunodiagnostyką przy użyciu radioznakowanych przeciwciał oraz analizę badań klinicznych radioznakowanych pochodnych białkowych w latach 2008-2018. [15]

W swojej pracy przeglądowej zwróciłem uwagę na coraz bardziej intensywne badania nad metodą chelatowania jonów pierwiastków promieniotwórczych z zastosowaniem chelatorów dwufunkcyjnych. Zdolność tworzenia kompleksów przez ligandy jest możliwością wykorzystania danej substancji w szerszym spektrum zastosowań. Możliwość wyznakowania ligandu innym pierwiastkiem za pomocą szybkiej metody kompleksowania może pozwolić na zastosowanie innej techniki obrazowania zależnej od możliwości jednostki diagnostycznej lub wymaganej do określonych potrzeb jakości obrazowania, a nawet wykorzystania substancji pierwotnie stosowaną tylko do diagnostyki jako nośnik pierwiastków terapeutycznych, bez zaawansowanej ingerencji chemicznej w strukturę. [15]

Chelatowanie jonów metali jest także jednym z celów terapeutycznych substancji o wielokierunkowym działaniu, projektowanych w celu przeciwdziałania rozwojowi choroby Alzheimera. Związki te powinny wykazywać zdolność kompleksowania jonów miedzi $Cu^{2+}$, cynku $Zn^{2+}$ i żelaza $Fe^{3+}$ z powodu ich wpływu na mechanizm agregacji blaszki amyloidowej i jej działania neurotoksycznego. Jony miedzi są odpowiedzialne za usprawnienie procesu formowania się blaszki amyloidowej oraz biorą czynny udział w tworzeniu się reaktywnych form tlenu będących czynnikiem mechanizmu neurotoksycznego. Jony żelaza są odpowiedzialne w największym stopniu za powstawanie reaktywnych form tlenu poprzez łączenie się z blaszką amyloidową, a następnie reakcję redukcji $Fe^{3+}$ do $Fe^{2+}$. Jony cynku wpływają na stabilność powstałych agregatów β amyloidu co utrudnia usuwanie powstałych złogów, lecz jednocześnie ograniczaja wytwarzanie reaktywnych form tlenu, ponieważ cynk jest pierwiastkiem nie wykazującym właściwości redox. [16]

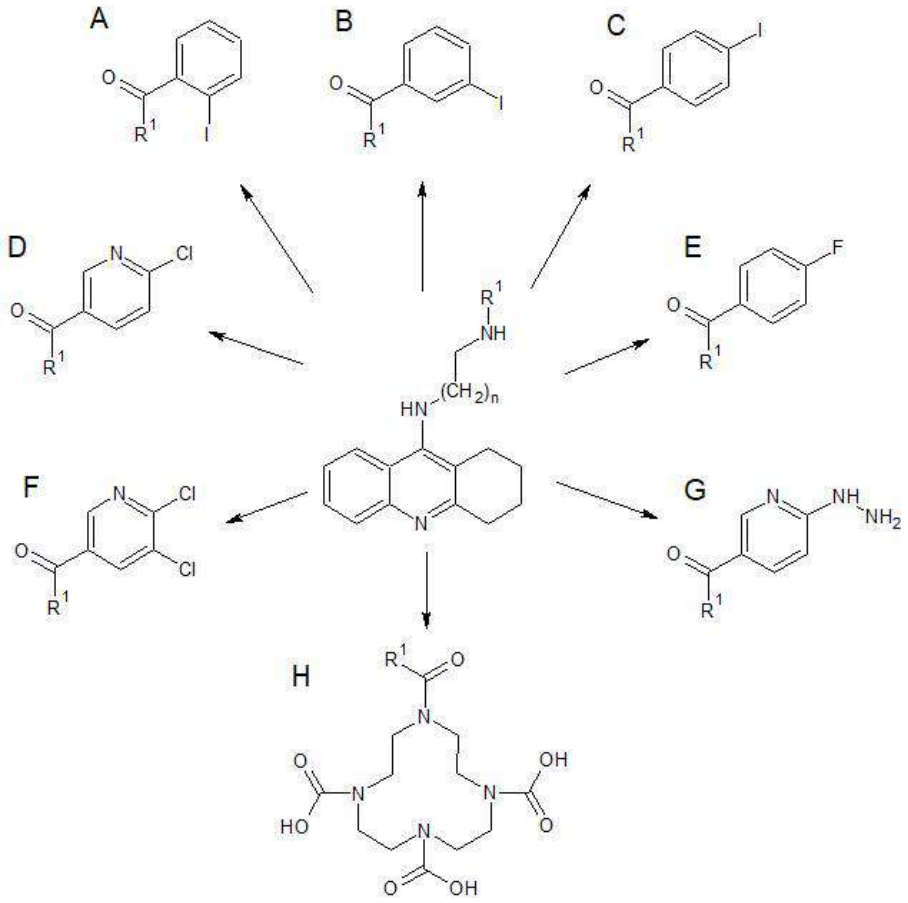


**Rycina 1.** Schemat poglądowy części struktur pochodnych tetrahydroakrydyny będących obiektem badań zespołu profesora Pawła Szymańskiego. A- kwas 2-jodobenzoesowy, B – kwas 3-jodobenzoesowy, C – kwas 4-jodobenzoesowy, D – kwas 6-chloronikotynowy, E – kwas 4-fluorobenzoesowy, F- kwas 5,6-dichloronikotynowy, G – kwas 6-hydrazynonikotynowy (HYNIC), H – kwas 1,4,7,10-tetraazacylododekan-1,4,7,10-tetraoctowy (DOTA)

W swojej pracy naukowej wykonywałem badanie zdolności kompleksowania metali pochodnych 1,3,4-tiazolorezorcynolu. Metoda oparta była o technikę analizy widm UV pod wpływem zachodzącej reakcji kompleksowania jonów $Cu^{2+}$, $Zn^{2+}$ oraz $Fe^{3+}$. [17]

Poza stwierdzeniem zdolności kompleksowania jonów metali przez badane związki wykonywałem badanie mające na celu określenie stosunku molowego kompleksu chelator : jon metodą Job'a. [18] Badania wykazały zdolność wszystkich badanych związków do chelatowania jonów miedzi oraz żelaza oraz połowy z nich do kompleksowania jonów cynku. Badanie stosunku molowego wykazało zmienność w budowie powstałych kompleksów zależnie od jonu oraz związku chelatującego. [17] Metoda ta znajdzie również zastosowanie w badaniu zdolności chelatujących dla innych substancji czynnych z różnymi jonami np. w badaniu zdolności chelatowania potencjalnych nośników jonów metali, których promieniotwórcze izotopy wykorzystywane są w diagnostyce i terapii.

# Cel pracy

Myślą przewodnią pracy było przygotowanie, opracowanie i optymalizacja procedur projektowania nowych cząsteczek mogących znaleźć zastosowanie w medycynie nuklearnej. Radiofarmacja jest obecnie jedną z najprężniej rozwijających się dziedzin z zakresu nauk farmaceutycznych, a jej rozwój przynosi coraz to nowe możliwości diagnostyczne oraz terapeutyczne chorób, które do niedawna wydawały się być wyrokiem dla pacjenta lub w ogóle były słabo poznane. [19]

Celem niniejszej pracy doktorskiej było zebranie informacji na temat obecnego stanu wiedzy o najnowszych radiofarmaceutykach, opracowanie metod pozwalających na uzyskanie danych o parametrach fizykochemicznych i stabilności biologicznie czynnych pochodnych 1,2,3,4-tetrahydroakrydyny będących nośnikami niepromieniotwórczych izotopów pierwiastków wykorzystywanych w diagnostyce obrazowej z dziedziny medycyny nuklearnej, a także usprawnienie procesu projektowania oraz otrzymywania nowych substancji leczniczych wykorzystujących techniki chromatograficzne, które w przyszłości z powodzeniem można będzie zastosować w badaniach nad nowymi radiofarmaceutykami.

Opracowanie metod pozwalających na uzyskanie danych dotyczących parametrów fizykochemicznych pochodnych 1,2,3,4-tetrahydroakrydyny takich jak logarytm P, $pK_a$ oraz opracowanie i zwalidowanie metody wysokosprawnej chromatografii cieczowej (ang. High Performance Liquid Chromatgraphy, HPLC) pozwalającej na zbadanie stabilności wyżej wymienionych pochodnych było niezbędnym elementem opracowania procedur mogących znaleźć zastosowanie w badaniach związków leczniczych o różnej budowie chemicznej. Optymalizacja procesu oczyszczania substancji z mieszanin poreakcyjnych lub ekstraktów naturalnych techniką chromatografii adsorpcyjnej typu flash pozwoli na usprawnienie procesu otrzymywania czystych chemicznie substancji biologicznie czynnych niezależnie od przyjętej skali projektu, aby usprawnić proces badawczy nad nowymi strukturami, zwłaszcza radiofarmaceutyków. Metody te mogą znaleźć zastosowanie w rutynowych procedurach projektowania i otrzymywania nowych substancji leczniczych w tym substancji stosowanych w medycynie nuklearnej. Badania wykonywane byłyby na strukturach zawierających atom izotopu niepromieniotwórczego pierwiastka, który docelowo zostałby zamieniony na izotop promieniotwórczy, co nie wpływałoby na parametry fizykochemiczne cząsteczki, a pozwoliłoby w sposób bezpieczny uzyskać dane o nowych radiofarmaceutykach. Taka strategia została wykorzystana w trakcie badań będących podstawą przedstawionej pracy doktorskiej.

# Parametry fizykochemiczne w naukach farmaceutycznych

Badania fizykochemiczne nowych substancji o potencjalnym działaniu biologicznym jest jednym z najbardziej kluczowych badań. Wiedza o podstawowych właściwościach fizykochemicznych takich jak pKa, logP, stabilności substancji chemicznych pozwala nie tylko przewidzieć właściwości substancji *in vivo*, ale także pozwala na odpowiednie postępowanie podczas przeprowadzania innych procedur prowadzących do lepszego poznania badanej substancji. [20]

Z punktu widzenia projektowania związków będących nośnikami pierwiastków promieniotwórczych prawidłowe oznaczenie parametrów fizykochemicznych takich substancji odgrywa jeszcze większą rolę niż w przypadku projektowania tradycyjnych ksenobiotyków. Substancja taka nie tylko powinna dotrzeć do celu terapeutycznego, ale także posiadać odpowiedni czas dystrybucji do określonego miejsca w organizmie. Czas ten jest w takim przypadku kluczowy, ponieważ jest on ograniczony okresem połowicznego rozpadu radionuklidu wbudowanego w strukturę radiofarmaceutyku. Co więcej, nośnik powinien precyzyjnie kumulować się tylko w miejscu, które jest istotne z punktu widzenia terapii lub diagnostyki, natomiast z innych rejonów organizmu powinien być szybko wydalany. Jest to ważne ze względu na jakość uzyskanego obrazowania, ograniczenia dawek promieniowania oraz bezpieczeństwa terapii. [21] Stabilność chemiczna nośników pierwiastków promieniotwórczych również jest istotna z punktu widzenia produkcji aktywnego radiofarmaceutyku oraz jego zastosowania, ponieważ nośnik musi wykazywać odpowiednią trwałość podczas reakcji znakowania oraz transportu z pracowni radiofarmaceutycznej do pracowni obrazowania lub odpowiedniego oddziału, w którym pacjenci poddawani są terapii. [22]

## Parametr $pK_a$

Wspólna zależność pH i $pK_a$ została opracowana na początku XX wieku przez Hendersona i Hasselbacha. Praca obu naukowców zaowocowała powstaniem równania Hendersona-Hasselbacha:

$$pH = pK_a + \log\left(\frac{[A^-]}{[HA]}\right)$$

*pH* – ujemny logarytm dziesiętny ze stężenia jonów wodorowych
*$pK_a$* – ujemny logarytm dziesiętny ze stałej dysocjacji kwasu
*$[A^-]$* – stężenie anionów zdysocjowanego kwasu
*[HA]* – stężenie cząsteczek niezdysocjowanego kwasu

Równanie to wskazuje, że pH i $pK_a$ jest powiązane równowagowymi stężeniami odpowiednio zdysocjowanego kwasu $[A^-]$ oraz niezdysocjowanego kwasu [HA]. Niezbędnymi danymi do obliczenia wartości $pK_a$ jest oznaczenie ilościowe odpowiednich form cząsteczki przy określonej wartości pH. Równanie to znajduje zastosowanie zarówno w przypadku cząsteczek substancji nieorganicznych, jak i organicznych. Istotnym faktem jest, że pomimo zależności opisanych przez równanie Hendersona-Hasselbacha na wartość $pK_a$ wpływają takie parametry jak temperatura oraz siła jonowa rozpuszczalnika. Równanie Hendersona-Hasselbacha wskazuje, że obliczeniom podlegają tylko cząsteczki kwasów zdolnych do dysocjacji. Należy wówczas pamiętać o ogólnych zasadach teorii kwasowo-zasadowych, które mówią o występowaniu sprzężonych

kwasów i zasad w równowadze kwasowo-zasadowej. W przypadku związków zasadowych należy rozważać formy uprotonowane jako formy niezdysocjowanego kwasu, natomiast struktury wolnej zasady jako formy zdysocjowanego kwasu. W literaturze można w takich przypadkach spotkać się z określeniem $pK_{BH+}$ będącym $pK_a$ sprzężonego kwasu związku zasadowego, który badamy. Cząsteczki organiczne substancji biologicznie czynnych często zawierają w swojej strukturze atomy azotu zdolne do przyjęcia dodatkowego protonu dzięki posiadaniu wolnej pary elektronowej. Tak uprotonowane cząsteczki tworzą kolejne formy protonowe, których oznaczenie jest kluczowe w przypadku wyznaczenia eksperymentalnych wartości $pK_a$ cząsteczki. Oznaczenia ilościowe kolejnych form protonowych było celem wielu naukowców od samego początku badań nad pKa. Dlatego opracowano metody potencjometryczne, konduktometryczne, spektrofotometryczne, chromatograficzne, fluorymetryczne, a nawet oparte na magnetycznym rezonansie jądrowym. [23]

W swojej pracy naukowej wykorzystywałem technikę spektrofotometrii UV w celu określenia wartości $pK_a$ pochodnych takryny w tym pochodnych będących „zimnymi" radiofarmaceutykami. Uzyskane w ten sposób parametry fizykochemiczne pozwoliły na obliczeniowe przewidywanie farmakokinetyki badanych substancji w oparciu o eksperymentalne dane co podnosi rzetelność uzyskanych predykcji. Analiza oparta na przesunięciu maksimów absorbcji pod wpływem zmiany pH pozwoliła na precyzyjne określenie wartości pKa pochodnych tetrahydroakrydyny sprzężonej z kwasem 3,5-dichlorobenzoesowym [24], kwasem 2-jodobenzoesowym, kwasem 3-jodobenzoesowym, kwasem 4-jodobenzoesowym [25], indometacyną [26] oraz pochodnych cyklopentachinoliny sprzężonej z kwasem 6-chloronikotynowym [27]. Metodologia przytoczona przez Musila i współpracowników [28] pozwoliła na opracowanie szybkiej metody z wykorzystaniem czytnika płytek UV-VIS polegającej na wykorzystaniu stosunku wartości absorbancji odczytywanej z dwóch długości fal co zapewniło wysoką powtarzalność i elastyczność metody przy jednoczesnym wykorzystaniu niewielkich próbek substancji badanej oraz małych ilości niezbędnych odczynników. Przykład wykresów regresji uzyskanej z wyników obliczeniowych znajduje się na rycinie 2, str. 11. Uzyskane wyniki zostały porównane z estymowanymi wartościami co potwierdziło przydatność wykonywania eksperymentalnych oznaczeń parametrów fizykochemicznych nowych substancji biologicznie czynnych i zostało opisane w **publikacji 1** dla pochodnych takryny sprzężonych z kwasem jodobenzoesowym.

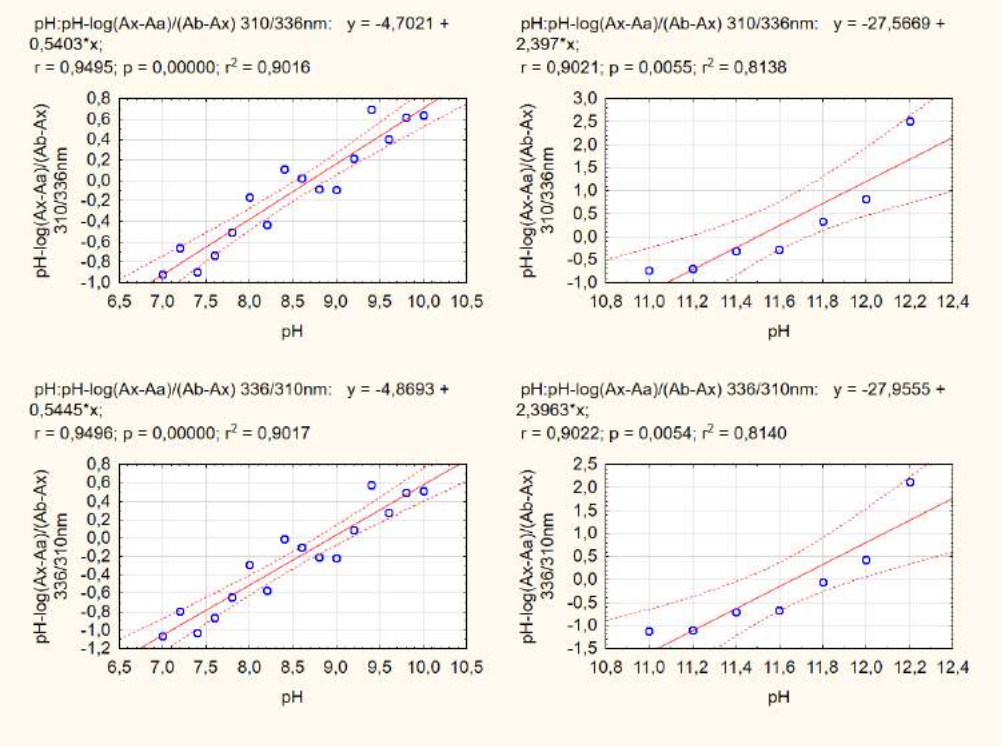


**Rycina 2.** Wykresy regresji liniowej wykreślone za pomocą oprogramowania STATISTICA 12 i uzyskane z obliczeń przewidzianych przez metodę badania wartości $pK_a$ pochodnych tetrahydroakrydyny sprzężonej z indometacyną. Punkt przecięcia linii regresji z punktem 0.0 na osi y wskazuje wartość $pK_a$ odczytywaną z osi x. [25]

## Logarytm P

Lipofilowość jest właściwością opisującą stopień powinowactwa cząsteczki do środowiska lipofilowego. [29] Parametrem wykorzystywanym do jej ilościowego wyrażenia jest zlogarytmowana wartość współczynnika podziału substancji w układzie dwufazowym złożonym z n-oktanolu i wody - logP. Parametr ten jest definiowany wzorem:

$$logP = logc_o - logc_w$$

Gdzie $c_o$ jest stężeniem badanej substancji w fazie organicznej, a $c_w$ jest stężeniem badanej substancji w fazie wodnej. [30] Pierwotnym sposobem wyznaczania parametru logP była metoda ekstrakcyjna. Metoda ta była jednak wyjątkowo czasochłonna oraz obarczona wieloma ograniczeniami. Pierwszym z nich był ograniczony zakres wartości logarytmu P jaki można było wyznaczyć tą metodą – od -3 do 3. Kolejnym ograniczeniem był fakt, że współczynnik podziału pomiędzy dwie fazy o różnej polarności musi być skorygowany pod kątem możliwości utworzenia się jonów substancji badanej w trakcie oznaczenia, co jest trudne w kontroli przy zastosowaniu metody ekstrakcyjnej szczególnie, gdy badana jest substancja posiadająca w swojej strukturze ugrupowania kwasowe i zasadowe jednocześnie. Problem dotyczył również substancji o właściwościach silnie hydrofilowych lub silnie hydrofobowych, które często wykazują słabą rozpuszczalność co może skutkować osadzaniem się na ściankach rozdzielacza lub generować wytwarzanie się emulsji podczas badania. Ostatnim ograniczeniem jest niezbędna, dość duża ilość oraz bardzo wysoka czystość substancji badanej, co

w przypadkach niektórych substancji jest trudne do osiągnięcia lub niezwykle kosztowne. [31, 32] Współcześnie stosowana jest metoda ekstrakcyjna w zmodyfikowanej formie wykorzystująca płytki 96 dołkowe, metody oparte na mikroekstrakcji z fazy stałej oraz techniki chromatograficzne. [33]

W swojej pracy naukowej wykorzystywałem technikę HPLC w celu wyznaczenia logarytmu P pochodnych tetrahydroakrydyny sprzężonej z kwasem 3,5-dichlorobenzoesowym [24], kwasem 2-jodobenzoesowym, kwasem 3-jodobenzoesowym, kwasem 4-jodobenzoesowym [25] oraz pochodnych cyklopentachinoliny sprzężonej z kwasem 6-chloronikotynowym [27]. Metoda wykorzystywana do tego celu została opracowana na podstawie metodologii przytoczonej przez Lianga i współpracowników. [34] Metodologia ta została wybrana z powodu możliwości zaprojektowania oznaczeń w sposób zautomatyzowany oraz szybkości uzyskiwania wyników dzięki opracowaniu krzywej wzorcowej stosowanej do uzyskania wyników wszystkich substancji badanych. [34] Metoda wymagała przygotowania serii oznaczeń substancji wzorcowych zbliżonych strukturalnie do substancji badanych z udokumentowaną eksperymentalną wartością logarytmu P oraz próbek badanych substancji. Oznaczenia wykonane były w odwróconym układzie faz wykorzystując elucję izokratyczną w pH zapewniającym neutralne formy protonowe cząsteczek z wykorzystaniem systemu HPLC wyposażonego w kolumnę C18 (4.6x50mm, 5µm) co pozwoliło na krótkie czasy rozdziałów. Uzyskane czasy retencji wzorców posłużyły najpierw do uzyskania ekstrapolowanej wartości $\log_{kw}$, a następnie stworzenia krzywej wzorcowej pozwalającej na odczyt wartości logarytmu P na podstawie ekstrapolowanej wartości $\log_{kw}$ co zostało wykonane dla próbek badanych. Uzyskane wyniki logP substancji badanych zostały również porównane z wartościami obliczonymi komputerowo. Znaczące różnice pomiędzy wartościami obliczonymi a eksperymentalnymi jeszcze silniej wskazało na konieczność eksperymentalnego uzyskiwania wartości fizykochemicznych nowych substancji biologicznie czynnych i zostało opisane w **publikacji 1** dla pochodnych takryny sprzężonej z kwasem jodobenzoesowym.

## Zależności $pK_a$ i logP w chemii obliczeniowej i projektowaniu związków

Logarytm P i $pK_a$ są jednymi z najważniejszych parametrów fizykochemicznych substancji leczniczych z punktu widzenia farmakokinetyki. Już na przełomie XIX i XX wieku Meyer i Overton, dwóch niezależnych badaczy, zwróciło uwagę na fakt, że siła działania anestetycznego różnych pod względem struktury związków organicznych rośnie wraz ze współczynnikiem ich podziału pomiędzy oliwą i wodą. [35, 36] Obecnie wiemy, że oba parametry odgrywają znaczącą rolę w każdym elemencie systemu ADME (ang. Absorption, Distribution, Metabolism, Excretion) - akronim od Wchłanianie, Dystrybucja, Biotransformacja, Wydalanie, a nawet biorą udział w mechanizmach toksyczności. Omawiane parametry fizykochemiczne mają znaczący wpływ na stopnień wchłaniania substancji leczniczej po podaniu *per os*, który jest jednym z najczęściej rekomendowanych sposobów podawania leku. Wchłanianie w jelitach wymaga od cząsteczki odpowiedniej lipofilowości w relatywnie wysokim pH panującym wewnątrz jelita. Nieodpowiednie parametry fizykochemiczne substancji mogą spowodować ograniczenie wchłaniania co prowadzi do spadku biodostępności i ostatecznie do słabego efektu farmakoterapii. Odpowiednia lipofilowość pozwala również na łatwiejszą penetrację cząsteczek poprzez błonę fosfolipidową komórek oraz transport

transkomórkowy, aby finalnie dotrzeć do światła naczyń krwionośnych i dalej zostać rozdysponowaną do poszczególnych rejonów organizmu. [33] Substancja lecznicza po przeniknięciu do krwioobiegu łączy się odwracalnie z białkami krwi w stopniu charakterystycznym dla niej samej. Stopień ten jest uwarunkowany między innymi lipofilowością i wartością $pK_a$. Kompleksy białko-lek pozwalają na swobodny transport cząsteczek substancji czynnej przez układ krwionośny, a pozostała wolna frakcja jest dostępna do przenikania w głąb tkanek i wywierania efektu terapeutycznego. Stopień wiązania z białkami nie może być zbyt niski, co prowadziłoby do szybkiego usunięcia ksenobiotyku z organizmu, ale także nie może być zbyt wysoki, ponieważ spowodowałoby to słaby efekt terapeutyczny przy jednoczesnej kumulacji substancji w organizmie oraz możliwość wystąpienia działań niepożądanych w przypadku zastosowania substancji potrafiących wyprzeć substancje czynne z kompleksu z białkiem takich jak np. kwas acetylosalicylowy. [37, 38] Nie można również pominąć wpływu parametrów fizykochemicznych na zdolność cząsteczek ksenobiotyków do pokonywania barier biologicznych takich jak np. bariera krew-mózg. [39] Ta właściwość jest jedną z najistotniejszych z punktu widzenia substancji mających zastosowanie w terapii chorób, których cele terapeutyczne znajdują się w obszarze ośrodkowego układu nerwowego – w tym chorób neurodegeneracyjnych. Zdolność ta jest również istotna z punktu widzenia toksyczności substancji czynnych, ponieważ wzmożona dystrybucja substancji do nieodpowiednich obszarów organizmu może nieść ze sobą poważne zagrożenia. Etapy biotransformacji i wydalania ksenobiotyków również nie pozostają bez wpływu parametrów fizykochemicznych. Najbardziej podstawowy model zakłada, że biotransformacja substancji leczniczej jest procesem złożonym z dwóch faz. Pierwsza faza biotransformacji polega na przeprowadzeniu szeregu procesów enzymatycznych, których efektem są przemiany cząsteczki leku takie jak utlenianie, redukcja czy hydroliza. Procesy te mają na celu wprowadzenie w strukturę związku wolnych grup funkcyjnych o charakterze polarnym takich jak np. grupa hydroksylowa, co skutkuje często zmniejszeniem lipofilowości cząsteczki i zwiększeniem jego rozpuszczalności w wodzie. Druga faza biotransformacji polega na sprzęganiu produktów pierwszej fazy np. z kwasem glukuronowym, octowym, jonami siarczanowymi lub aminokwasami, co w jeszcze silniejszym stopniu ułatwia ich wydalanie i zwykle dezaktywuje substancje czynne. Procesy te zachodzą w różnych obszarach organizmu, lecz najczęściej jest to wątroba, dlatego też parametry fizykochemiczne, które wpływają na dystrybucję cząsteczek substancji czynnych do tego narządu mogą wpływać na ich szybkość biotransformacji, ale także pośrednio na ich potencjalną toksyczność wywoływaną przez wciąż czynne produkty pierwszej fazy procesu biotransformacji. Co więcej, istnieją dowody, że substancje o wysokiej lipofilowości są wrażliwsze na działanie cytochromu P450, który bierze czynny udział w pierwszej fazie. Proces biotransformacji leku jest ściśle powiązany z procesem wydalania, ponieważ im sprawniej zachodzi proces biotransformacji cząsteczek ksenobiotyków tym szybciej zostaną one usunięte z organizmu. [40, 41]

Obecnie dostępne jest oprogramowanie komputerowe pozwalające na wyznaczanie właściwości fizykochemicznych. Obliczenia oparte są na algorytmach, a ich wyniki są mocno zbliżone do wyznaczanych eksperymentalnie wartości. Niestety, w przypadku prac badawczych nad związkami o działaniu biologicznym nawet niewielkie różnice pomiędzy estymowanymi a eksperymentalnymi wartościami potrafią wpłynąć np.

na wyniki przewidywania farmakokinetyki substancji aktywnej lub modelowania cząsteczkowego w tym analizy dokowania ligandu do miejsca aktywnego enzymu lub receptora, co może zaważyć na dalszych losach badanej struktury. [42]

W swojej pracy naukowej wykonywałem komputerowe analizy ADME wraz z symulacją wybranych działań toksycznych z wykorzystaniem oprogramowania ACDlabs Percepta (ver. 14.0.0, Advanced Chemistry Development, Inc. Metropolitan Toronto, Canada). Analizie zostały poddane pochodne tetrahydroakrydyny sprzężone z kwasem 3,5-dichlorobenzoesowym [24], cyklopentachinoliny sprzężone z kwasem 6-chloronikotynowym [27] oraz pochodne 1,3,4-tiazolorezorcynolu [17] i pochodne pirazolu [43]. W przypadku pochodnych tetrahydroakrydyny oraz cyklopentachinoliny do analizy ADME wraz z symulacją wybranych działań toksycznych zostały wykorzystane eksperymentalne wartości fizykochemiczne związków uzyskane metodami opisanymi wcześniej.

## Stabilność substancji czynnej w projektowaniu leków

Badanie stabilności chemicznej substancji leczniczych leży u podstaw procesu projektowania leków. Znajomość trwałości substancji wystawionych na warunki stresowe pozwala na odpowiednie przygotowanie oraz przechowywanie próbek, a w późniejszym okresie na odpowiedni sposób formulacji postaci leku, a także jego opakowanie i sposób oraz czas przechowywania. [44] Ponadto pozwala na zaprojektowanie odpowiednich procedur transportu tych substancji, co przekłada się w dalszej kolejności na rzetelność wyników badań, a finalnie na bezpieczeństwo terapii co jest szczególnie istotne w przypadku radiofarmaceutyków. [45] Rekomendowane metody badania stabilności chemicznej nowych substancji leczniczych są opisane w raporcie Q1A(R2) wydanego przez Międzynarodową Radę do spraw Harmonizacji (ang. International Council for Harmonisation, ICH). Raport ten jest podstawą do opracowywania raportów rejestracyjnych leków oraz zastosowań w przemyśle farmaceutycznym. Metody w nim przedstawione dotyczą badań stabilności chemicznej substancji czynnej lub produktu leczniczego w różnym pH, w wysokich oraz niskich temperaturach, w różnych wartościach wilgotności powietrza oraz w warunkach oksydacyjnych, a także sprawdzenie wpływu działania promieniowania UV. Ponadto rekomendowane jest badanie wpływu ochronnego różnego rodzaju opakowań. [46]

Metody opisane w raporcie ICH niestety trudno jest wykorzystać bez modyfikacji w skali laboratoryjnej do celów badawczych z powodu długich okresów pomiarowych – 3, 6 lub 9 miesięcy, a część badań nie jest niezbędna na etapie projektowania i optymalizacji struktury cząsteczki. Z tego też powodu w swojej pracy badawczej raport Q1(R2) był podstawą do opracowania metod pozwalających na szybkie zbadanie stabilności pochodnych tetrahydroakrydyny sprzężonych z kwasem 3-jodobenzoesowym w roztworze będącym w temperaturze pokojowej bez dostępu światła, w niskim i wysokim pH, podwyższonej temperaturze, warunkach stresu oksydacyjnego oraz wystawionych na działanie promieniowania UV. Badane próbki po testach stresowych zostały przeanalizowane za pomocą opracowanej i zwalidowanej metody HPLC w celu ilościowego określenia stopnia rozkładu substancji. Badanie to dostarczyło cennych informacji o wysokiej stabilności chemicznej badanych substancji w roztworach niezależnie od pH, temperatury i warunków stresu oksydacyjnego, ale także o znacznej fotolabilności tych pochodnych takryny (rycina 3, str. 15). [25] Uzyskane dane dotyczące

stabilności chemicznej „zimnych” jodopochodnych takryny dostarczają cennych informacji o sposobie postępowania z gotowym produktem, aby zapewnić maksymalne bezpieczeństwo oraz skuteczność zastosowania substancji u pacjenta.

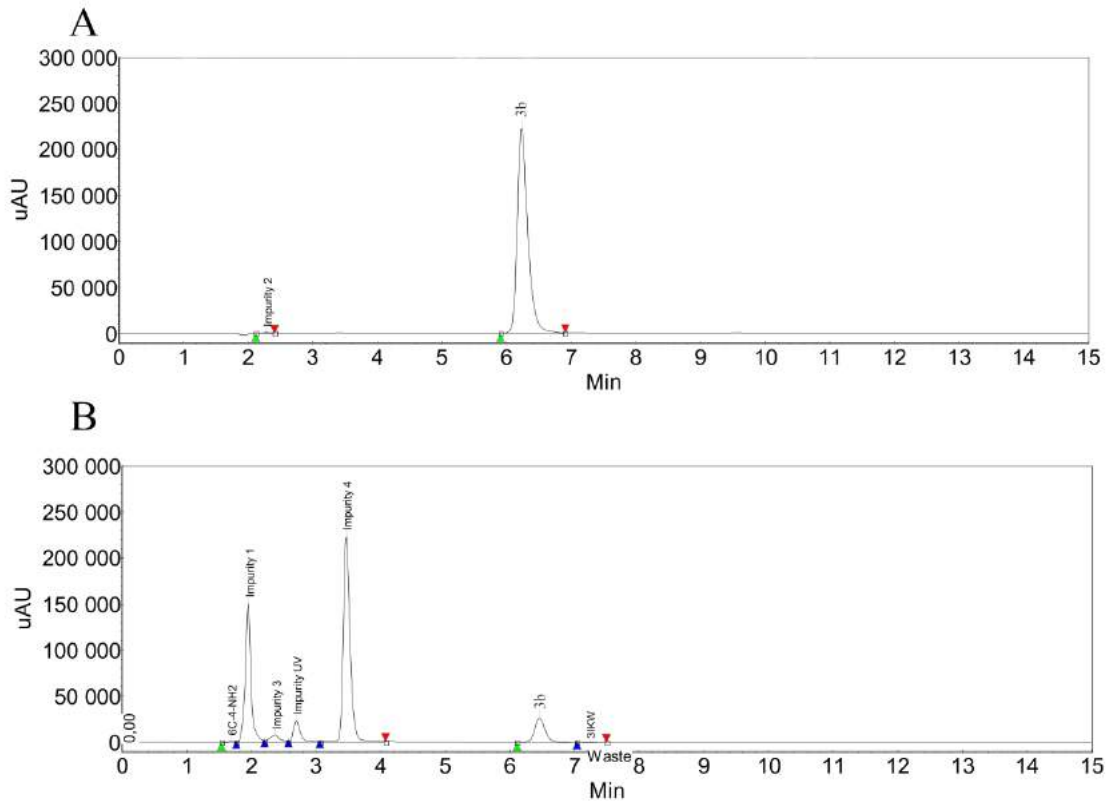


**Rycina 3.** Chromatogramy analizy próbek stabilności 3-jodo-N-[4-(1,2,3,4-tetrahydroakrydyno-9-ylamino)butyl]benzamidu (**3b**) wskazujące na znaczą fotolabilność związku. A – próbka przechowywana w temperaturze pokojowej w ciemności przez 48 godzin, B – próbka naświetlana promieniowaniem UV o długości fali 254nm przez 8 godzin w temperaturze pokojowej. [25]

## Chromatografia w analizie i preparatyce substancji leczniczych

Chromatografia jest techniką znaną od 1855 roku, kiedy Runge opublikował swoją pracę o separacji barwników na bibule, jednak za początki analizy chromatograficznej należy uznać prace Goppelsroedera i Schobeina z roku 1861, które również dotyczyły chromatografii bibułowej jednak już w aspekcie analitycznym. Początkiem chromatografii kolumnowej natomiast uważany jest 1893 rok kiedy Reed opublikował pierwsze eksperymenty z użyciem kolumn, by cztery lata później zademonstrować kolumnowy rozdział frakcji ropy naftowej. Chromatografia przechodziła ewolucje na przestrzeni dziesięcioleci dzięki czemu znamy teraz wiele technik chromatograficznych takich jak np. chromatografia bibułowa, kolumnowa (grawitacyjna oraz flash), planarna (ang. Thin Layer Chromatography, TLC), wysokosprawna chromatografia cieczowa (HPLC), gazowa (ang. Gas Chromatography, GC), chromatografia cieczowa w stanie nadkrytycznym $CO_2$ (ang. Supercritical Fluid Chromatography, SFC). Wraz z ewolucją technik zachodziła ewolucja metod i tak znamy dziś metody oparte na elucji izokratycznej oraz gradientowej (liniowej lub schodkowej). Należy również wspomnieć

o rozwoju metod chromatografii cieczowej opartych na układzie faz normalnych, gdzie faza ruchoma wykazuje się niższą polarnością od fazy stacjonarnej, lub kluczowych z punktu widzenia nauk farmaceutycznych metodach opartych na układzie faz odwróconych. [47]

## HPLC w analizie leku

Wybór pomiędzy zastosowanym rodzajem układu faz lub metody elucji to tylko podstawowe możliwości jakie dają współczesne systemy HPLC, bardzo precyzyjne i wielofunkcyjne urządzenia. Wielofunkcyjność tej techniki jest zapewniona przez modularną budowę systemów HPLC. Modyfikowalne metody podaży próbek pozwalają na dobranie odpowiedniej objętości nastrzyku do zakładanych celów. Różne średnice wewnętrzne oraz długości kolumn pozwalają uzyskać odpowiednią skalę do celów preparatywnych lub długość czasu rozdziałów do licznych oznaczeń analitycznych. Możliwość wyboru spośród bardzo dużej ilości kolumn charakteryzujących się różnym rodzajem wypełnienia pod kątem modyfikacji żelu krzemionkowego pozwala dopasować aparaturę do rodzaju substancji jaka będzie poddawana analizie. Ponadto dobór odpowiedniego wypełnienia może być oparty na doborze odpowiedniej wielkości cząstek żelu krzemionkowego, rodzaju tych cząstek (powierzchniowo-porowate lub objętościowo-porowate) oraz ich kształtu (sferyczne lub coraz rzadziej spotykane niejednorodne) co pozwala na uzyskanie lepszych wyników w procedurach analitycznych uzyskując większą rozdzielczość i mniejszą szerokość połówkową pików lub większą pojemność i niższe opory kolumny, co przełoży się na sprawniejsze rozdziały preparatywne. Zastosowanie odpowiedniego rodzaju detektora pozwala na odpowiednie użycie różnych procedur, a czasem umożliwia analizę specyficznych substancji jak jest w przypadku analizy radiofarmaceutyków i detektora radiometrycznego. Najczęściej stosowane detektory spektrofotometryczne w zakresie UV/VIS z możliwością regulacji długości fali odczytu lub fluorymetryczne nadają się do ilościowego oznaczania substancji oraz do oznaczeń ilościowo-jakościowych w metodach porównawczych z zastosowaniem odpowiednich wzorców, a także w detekcji pików podczas procedur preparatywnych. Detektory UV/VIS wyposażone w układ fotodiody (PDA) mogą posłużyć do oznaczeń ilościowo-jakościowych w metodach porównawczych dodatkowo opierając się o analizę widm UV. Detektor masowy sprzężony z systemem HPLC pozwala na uzyskanie wysokiej jakości widm masowych co znajduje zastosowanie w analizach jakościowych i potwierdzaniu tożsamości substancji. Zastosowanie dodatkowego modułu jakim jest automatyczny kolektor frakcji pozwala na wydajne i po odpowiedniej konfiguracji, praktycznie bezobsługowe zbieranie poszczególnych frakcji mieszanin w procedurach preparatywnych. [48]

Wszystkie te możliwości, które zapewnia system HPLC sprawiły, że technika ta jest obecnie złotym standardem w przemyśle farmaceutycznym, a także wiedzie prym jako jedna z najczęściej stosowanych technik w analizie leku. HPLC jest wykorzystywana na szeroką skalę w laboratoriach kontroli jakości i działach technologicznych koncernów farmaceutycznych. Międzynarodowa Rada do spraw Harmonizacji opublikowała swój raport dotyczący walidacji metody analitycznej Q2(R1) w oparciu głównie o technikę HPLC. [49]

W swojej pracy naukowej posłużyłem się raportem Q2(R1) do walidacji metody HPLC opracowanej na potrzeby oznaczeń ilościowo-jakościowych przy badaniu

stabilności chemicznej pochodnej tetrahydroakrydyny sprzężonej z kwasem 3-jodobenzoesowym. Metoda została opracowana i zwalidowana zgodnie z wymogami metody badawczej opisanymi w raporcie Q2(R1). Sprawdzeniu została poddana liniowość wraz z zakresem, precyzja, pośrednia precyzja, dokładność, specyficzność, czułość, elastyczność oraz zostały wprowadzone testy odpowiedniości systemu monitorujące każdy rozdział w czasie rzeczywistym. Limit detekcji oraz oznaczalności obliczono zgodnie ze wzorami rekomendowanymi przez ICH w oparciu o analizę szumu i nachylenia krzywej wzorcowej. Metoda przeszła z powodzeniem proces walidacyjny oraz pozwoliła na uzyskanie rzetelnych wyników oznaczeń próbek pochodzących z badania stabilności chemicznej. [25]

Technika HPLC znajduje zastosowanie nie tylko w analizie jakościowo-ilościowej. Zależności fizykochemiczne biorące udział w mechanizmie elucji są również przydatne w innych badaniach. Przykładem może być przytoczona już wcześniej metoda wyznaczenia parametru logarytmu P opracowana na potrzeby badań fizykochemicznych pochodnych tetrahydoakrydyny i cyklopentachinoliny. [24, 25, 27] Na szczególną uwagę zasługuje fakt, że dzięki zastosowaniu do badań pochodnych podstawionych izotopami stabilnymi radiacyjnie badanie to pozwoliło na uzyskanie wartości logarytmu P dla przyszłych radiofarmaceutyków.

## Zastosowanie technik chromatograficznych w preparatyce środków leczniczych na przykładzie radiofarmaceutyków

Techniki chromatograficzne znajdują obecnie zastosowanie w rutynowych procesach produkcji substancji leczniczych. Najbardziej zaawansowane zastosowanie tych technik można zaobserwować w dziedzinie syntezy przepływowej radiofarmaceutyków. Radiofarmaceutyki to grupa substancji o szerokim zastosowaniu w medycynie, która obecnie bardzo szybko się rozwija. [50] Obecnie wykorzystywanych jest wiele rodzajów pierwiastków emitujących cząstki α, strumień elektronów, pozytonów lub promieniowanie gamma. Ta różnorodność pozwala projektować substancje znajdujące zastosowanie w diagnostyce różnych chorób za pomocą techniki PET lub SPECT, ale także w terapii chorób onkologicznych, a nawet do zastosowań teranostycznych łączących obie te dziedziny. [51-54] Cechą charakterystyczną preparatów radiofarmaceutycznych jest określony i często krótki czas ich przydatności do użycia z powodu określonej trwałości izotopów promieniotwórczych dobranych do odpowiednich zastosowań. Z tego też powodu synteza preparatów radiofarmaceutycznych wymaga specyficznych warunków i bardzo często krótkiego okresu czasu pomiędzy rozpoczęciem syntezy a podaniem preparatu pacjentowi. Przykładowo substancje znakowane fluorem $^{18}F$ z powodu krótkiego czasu połowicznego rozpadu izotopu promieniotwórczego wynoszącego około 60 min muszą być produkowane w bardzo bliskim sąsiedztwie od miejsca podania pacjentowi. [55] Jednak, preparaty radiofarmaceutyczne bezwzględnie muszą spełniać wszelakie normy narzucane środkom leczniczym w tym odpowiednią czystość, dlatego też ich synteza wymaga specyficznych procedur. Bardzo często wykorzystuje się do tego celu technikę zautomatyzowanej syntezy przepływowej. System ten jest wyposażony w serię zaworów i pomp pozwalających na precyzyjne dostosowywanie odpowiedniej ilości substratów oraz czasu syntezy. Ponadto jest on wyposażony w zintegrowany system HPLC z różnymi rodzajami detektorów pozwalających na analizę jakościową oraz ilościową uzyskanego produktu.

W celu oczyszczenia produktu reakcji stosuje się tam kolumny chromatograficzne albo skomplikowany układ kolumn i rozpuszczalników do technik ekstrakcji z fazy stałej, które także są oparte o techniki chromatograficzne (rycina 4, str. 18). Przykładem zastosowania technik chromatograficznych w syntezie radiofarmaceutyków jest fluoryzacja izotopem $^{18}F$ grupy prostetycznej stosowanej do znakowania 6-[$^{18}F$]Py-CONH-T140 będącego inhibitorem receptora chemokinowego C-X-C typu 4 (CXCR4) na kolumnach jonowymiennych Sep-Pak PS-$HCO_3$ włączonych w system zautomatyzowanej syntezy przepływowej. [56]

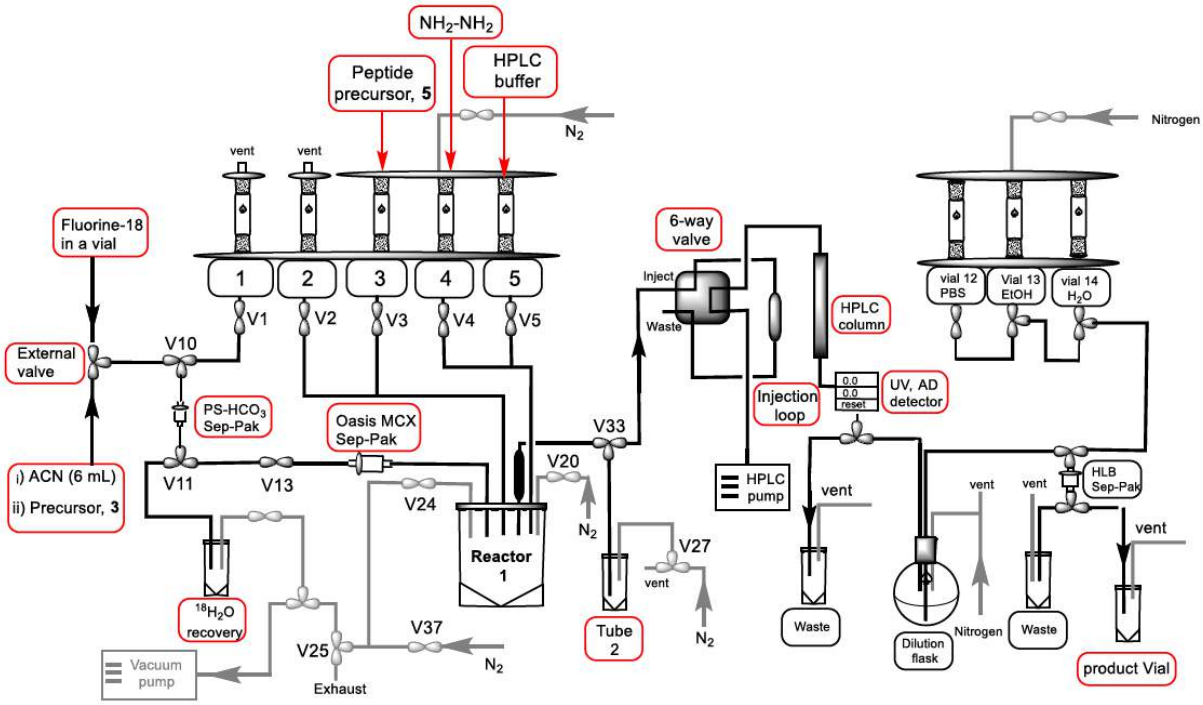


**Rycina 4.** Schemat systemu wykorzystywanego do automatycznej syntezy przepływowej 6-[$^{18}F$]Py-CONH-T140 metodą fluoryzacji na kartridżach Sep-Pak wraz ze zintegrowanym systemem HPLC służącym do analizy produktu. [56]

## Chromatografia typu flash w naukach farmaceutycznych

Radiofarmaceutyki, zwłaszcza te najnowsze, związane są z technikami oczyszczania i analizy wykorzystującymi metody chromatograficzne, co w połączeniu z intensywną pracą naukową nad kolejnymi pochodnymi takryny zainspirowało mnie do opracowania metody optymalizującej rozdziały chromatografii adsorpcyjnej typu flash wykorzystywanej w celu oczyszczania produktów reakcji i zostało opisane w **publikacji 2**.

Chromatografia typu flash jest rozwinięciem grawitacyjnej chromatografii kolumnowej, gdzie poza siłą grawitacji stosuje się dodatkowo ciśnienie, które przyspiesza przepływ fazy ruchomej. Pierwotnie ciśnienie nakładane było za pomocą kompresora na kolumnę już zalaną odpowiednią objętością fazy ruchomej. Współczesne aparaty flash swoją budową przypominają systemy HPLC, gdzie stosuje się pompy i mieszalniki dzięki czemu jest możliwość ustawienia składu fazy, korzystanie z elucji gradientowej i prowadzenie rozdziału przez dowolną ilość czasu, a także detektory i kolektory frakcji. Technika ta wykorzystuje różne rodzaje oraz wymiary jednorazowych kolumn

z wypełnieniem odpowiednim dla normalnego lub odwróconego układu faz. Ciśnienie odpowiednie dla tej techniki oscyluje między 1-6 bar, a maksymalne ciśnienie to zwykle do 22 bar. Chromatografia typu flash jest techniką preparatywną. Znajduje zastosowanie w metodach oczyszczania mieszanin poreakcyjnych, a także uzyskiwania czystych składników ekstraktów pozyskanych z surowców naturalnych przez co odgrywa znaczącą rolę w procesie poszukiwania nowych substancji leczniczych. Jej główne cechy przeważające nad systemami HPLC w kontekście rozdziałów preparatywnych to większa pojemność kolumn, szybsze procedury, łatwa możliwość przewidywania czasów retencji (za pomocą techniki TLC) oraz niższe koszty prowadzenia rozdziałów. [57] Zasada działania chromatografii typu flash i HPLC jest taka sama. Obie techniki opierają się na różnicach powinowactwa substancji badanych do fazy stacjonarnej i ruchomej. Z tego też powodu bardzo istotnym elementem opracowywania metody flash jest dobór odpowiedniego składu fazy ruchomej. Chromatografia typu flash bardzo często jest prowadzona w normalnym układzie faz w przeciwieństwie do metod HPLC stosowanych w analizie leku, dlatego też w tej technice kluczową rolę odgrywa „triada Snydera", będąca metodologią doboru rozpuszczalników do poprawnej elucji odpowiednich składników mieszanin. [58] Powiązanie czasu retencji wyrażonego w objętościach kolumny ze współczynnikiem retencji uzyskiwanym z rozdziałów TLC dodatkowo ułatwia dobór odpowiedniego składu fazy ruchomej. [59] Znaczącą różnicą pomiędzy współczesną techniką flash a HPLC jest metoda podaży próbek. HPLC wykorzystuje automatyczną lub coraz rzadziej, manualną podaż w formie roztworów. Chromatografia typu flash przewiduje tak zwane mokre lub suche podanie próbki. Mokre podanie próbki polega na naniesieniu roztworu próbki o odpowiednim stężeniu i objętości dopasowane do wymiarów i rodzaju kolumny na jej czoło. Suche podanie próbki wymaga zawieszenia cząsteczek próbki na cząstkach suchego żelu krzemionkowego, którego masa jest również dobrana do wymiarów oraz rodzaju kolumny, a następnie za pomocą odpowiedniego zestawu przygotowanie pre-kolumny wypełnionej właśnie tym żelem. Każda z tych technik ma swoje wady oraz zalety. Mokre podanie próbki jest techniką szybszą i prostszą, jednak mogącą wpływać na kształt pików poprzez wpływ rozpuszczalnika do przygotowania próbki. Suche podanie próbki jest techniką bardziej czasochłonną i trudniejszą pod względem wykonania. Wymaga zastosowania specjalnego zestawu do przygotowania pre-kolumny oraz w przypadku silnie higroskopijnych substancji wymaga doświadczenia operatora. Technika ta niweluje jednak całkowicie wpływ rozpuszczalnika próbki dając wyjątkowo symetryczne piki poszczególnych substancji co ma znaczenie w mieszaninach wieloskładnikowych i trudnych w rozdzieleniu. [57]

W swojej pracy naukowej opracowywałem metody rozdziałów mieszanin poreakcyjnych celem uzyskania czystych pochodnych tetrahydroakrydyny sprzężonych z kwasem 3,5-dichlorobenzoesowym [24], indometacyną [26], kwasem 2-jodobenzoesowym, 3-jodobenzoesowym i 4-jodobenzoesowym [25]. Doświadczenie zebrane podczas procedur mających na celu uzyskanie czystych związków biologicznie czynnych pozwoliło mi na opracowanie metody obliczania nachylenia gradientu w rozdziałach preparatywnych techniką chromatografii typu flash dopasowanej indywidualnie do mieszaniny poddawanej rozdziałowi w oparciu o dane pozyskane z chromatogramów TLC i sprecyzowanej na pojedynczy składnik tej mieszaniny (rycina 5, str. 20). Podstawa obliczeniowa metody silnie koresponduje z teorią elucji gradientowej przedstawionej przez Jandera i wsp. co jest dowodem rzetelności

uzyskanych danych obliczeniowych. [60, 61] Rozdziały w których zastosowano gradient opracowany tą metodą pozwalały na prawidłowe rozdzielenie składników mieszanin zachowując symetryczny kształt piku niezależnie od zastosowanej techniki podaży próbki. Ponadto metoda ta pozwala uzyskać zawsze ten sam czas rozdziału mierzony w objętościach kolumny, co nie ogranicza operatora pod względem skali procedury przy jednoczesnym ułatwieniu obliczeń niezbędnych objętości odczynników. Metoda ta zogniskowana jest na wykorzystaniu techniki mokrej podaży próbki i pozwala na zminimalizowanie nieoczekiwanego wpływu rozpuszczalnika próbki na kształt pików, co usprawnia i ułatwia proces oczyszczania substancji biologicznie czynnych. Cechy opracowanej metody optymalizacji gradientu pozwalają na szerokie zastosowanie jej w dziedzinie nauk farmaceutycznych. Może być ona stosowana w uzyskiwaniu czystych substancji pochodzenia naturalnego z ekstraktów roślinnych, a także oczyszczania substancji uzyskanych metodami syntetycznymi. [62] Szczególnym przykładem syntetycznych pochodnych, które wymagają szybkich oraz precyzyjnych procedur oczyszczania są radiofarmaceutyki. Wykorzystanie tej metody do opracowania metod oczyszczania gotowego produktu z zastosowaniem „zimnych" pochodnych w celu optymalizacji oraz odpowiedniego aparatu wyposażonego w detektor radiometryczny pozwoli na wydajny proces uzyskiwania produktów o czystości chromatograficznej.

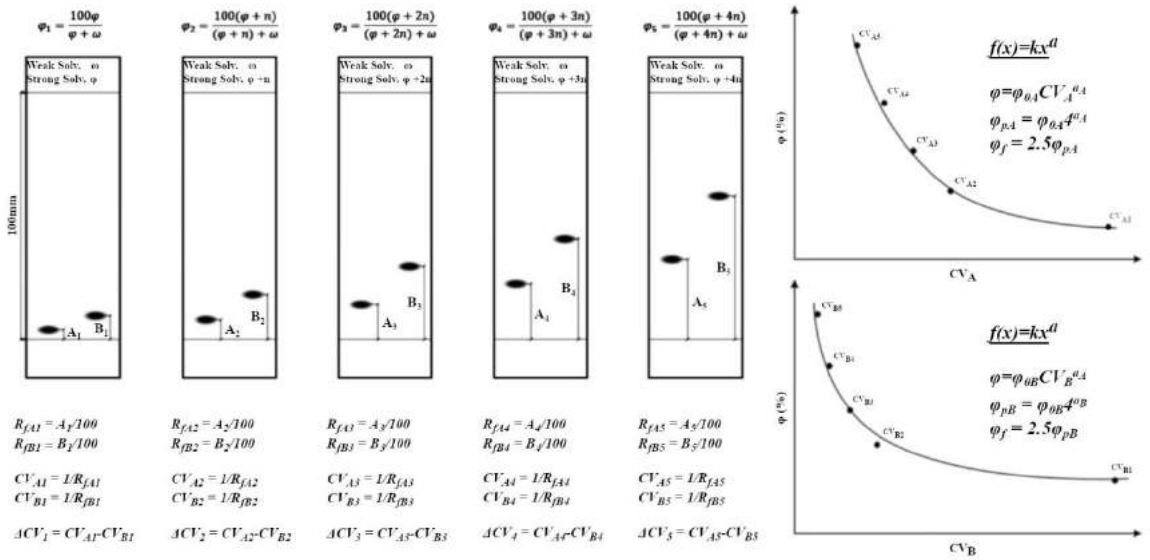


**Rycina 5.** Schemat naświetlający mechanizm metody optymalizacji nachylenia gradientu techniką TLC. [62]

## Podsumowanie i wnioski

Badania wchodzące w skład niniejszej pracy doktorskiej dostarczają narzędzi pozwalających na optymalizację projektowania i otrzymywania nowych struktur substancji biologicznie czynnych, w szczególności radiofarmaceutyków dzięki zastosowaniu strategii wykorzystania do badań „zimnych" analogów tych związków. Opracowane metody pozwalające na szybkie i rzetelne poznanie eksperymentalnych właściwości fizykochemicznych w połączeniu z technikami obliczeniowymi pozwala uzyskać dane wskazujące struktury o najlepszych parametrach, które w toku badań są syntetyzowane w większej ilości i oczyszczane. Etap oczyszczania, który jest również

kluczowym elementem badań nad nowymi strukturami, został poddany optymalizacji w celu dopełnienia myśli przewodniej niniejszej pracy doktorskiej, czyli opracowania procedur usprawniających proces otrzymywania nowych struktur radiofarmaceutyków.

Badania fizykochemiczne pochodnych 1,2,3,4-tetrahydroakrydyny sprzężonych z kwasem jodobenzoesowym posiadającym podstawnik halogenowy w położeniu *orto*, *meta* lub *para* wykazały średni wzrost wartości $pK_a$ 1 oraz spadek wartości $pK_a$ 2 wraz ze zwiększeniem długości łańcucha węglowego łączącego cząsteczkę 1,2,3,4-tetrahydroakrydyny z kwasem jodobenzoesowym. Miejsce podstawienia również nie pozostaje bez wpływu na wartości $pK_a$. Podstawienie atomu jodu w pozycji *orto* powodowało średnio najniższe wartości $pK_a$ 1 i najwyższe wartości $pK_a$ 2, natomiast podstawienie w ułożeniu *para* powodowało odwrotną tendencję. W przypadku wartości logarytmu P długość łańcucha węglowego wpływała znacząco na wzrost lipofilowości cząsteczki, ale wykazano, że ułożenie podstawnika również odgrywa istotną rolę w tym zakresie. Lipofilowość izomerów konstytucyjnych zawsze wzrastała w kolejności zgodnej z kolejnością podstawienia atomu jodu w pierścieniu aromatycznym kwasu benzoesowego, czyli najniższe wartości miały pochodne *orto*, a najwyższe pochodne *para*. Wyniki badań zostały porównane z obliczeniowymi wartościami parametrów $pK_a$ 1, $pK_a$ 2 oraz logarytmu P wygenerowanymi przez oprogramowanie ALOGPS 2.1 oraz Marvin (ChemAxon 2018). Wyniki porównania wskazują na znaczące różnice pomiędzy wartościami eksperymentalnymi a obliczeniowymi. Badania fizykochemiczne pozwalają na optymalizację struktury projektowanej cząsteczki pod kątem właściwości fizykochemicznych, które mają znaczący wpływ na farmakokinetykę ostatecznej struktury leku opierając się na eksperymentalnych wartościach parametrów fizykochemicznych cząsteczki. Dane uzyskane z tych badań mogą znacząco zoptymalizować proces projektowania radiofarmaceutyków, w szczególności diagnostycznych, których farmakokinetyka jest wyjątkowo istotna z punktu widzenia zastosowania tych substancji w medycynie.

Opracowana metoda HPLC pozwoliła na precyzyjne oznaczenie ilościowe próbek pochodzących z badania stabilności chemicznej 3-jodo-N-[4-(1,2,3,4-tetrahydroakrydyno-9-amino)butylo]benzamidu. Badania wykazały, że substancja jest trwała w roztworze metanolowo-wodnym przez 24 godziny w temperaturze pokojowej bez dostępu światła oraz jest odporna na czynniki utleniające. Wpływ środowiska silnie kwasowego lub silnie zasadowego jest niewielki na trwałość cząsteczki w roztworze. Badania wykazały natomiast, że cząsteczka 3-jodo-N-[4-(1,2,3,4-tetrahydroakrydyno-9-amino)butylo]benzamidu jest silnie wrażliwa na promieniowanie UV. Rzetelność oznaczeń została zapewniona poprzez pełną walidację metody HPLC zgodnie z protokołem Q2 opublikowanym przez Międzynarodową Radę ds. Harmonizacji. Badania stabilności chemicznej pozwalają na opracowanie procedur przechowywania oraz transportu substancji zarówno podstawionych stabilnym izotopem, jak i radiacyjnie promieniotwórczym izotopem już na etapie projektowania cząsteczki. Wykorzystanie „zimnych" radiofarmaceutyków do wyżej wymienionych badań jest dodatkowym atutem pozwalającym na bezpieczną pracę podczas procesu optymalizacji cząsteczki.

Opracowanie strategii optymalizacji gradientu dla chromatografii typu flash za pomocą analizy próbek techniką TLC pozwoliło na przyspieszenie i usprawnienie procesów oczyszczania pochodnych 1,2,3,4-tetrahydroakrydyny. Silnie korespondująca

z teorią elucji gradientowej opracowanej przez Jandera i wsp. podstawa obliczeniowa metody pozwala na precyzyjne zaprojektowanie rozdziału gradientowego, dzięki któremu można uzyskać produkt o czystości chromatograficznej przy jednoczesnym zminimalizowaniu ilości potrzebnego czasu oraz niezbędnych odczynników w dowolnej skali, dzięki zastosowaniu wartości objętości używanej kolumny do obliczeń. Ponadto metoda pozwala na wykorzystanie techniki mokrej podaży próbki na czoło kolumny, uzyskując rozdział o kształtach pików mocno zbliżonych do tych uzyskanych techniką suchej podaży próbki mimo wykorzystania rozpuszczalnika próbki zawierającym znaczną ilość silnego eluentu. Opracowana strategia optymalizacji gradientu dla chromatografii typu flash za pomocą analizy próbek techniką TLC pozwala na zminimalizowanie niekorzystnych cech techniki mokrej podaży próbki na czoło kolumny. Przyspiesza i upraszcza ona procedurę przygotowania próbki, pozwala na uzyskanie powtarzalnych i przewidywalnych czasów retencji substancji badanej, co ułatwia identyfikację odpowiednich pików na chromatogramie w przypadku złożonych mieszanin oraz nie jest ograniczona skalą projektu procesu oczyszczania dzięki wykorzystaniu wartości pojemności kolumny w obliczeniach. Strategia ta może znaleźć zastosowanie w wielu procedurach oczyszczania nowych substancji o potencjalnym działaniu biologicznym z naciskiem na opracowywanie nowych radiofarmaceutyków, które wymagają szybkich i wydajnych procedur z powodu ograniczeń narzuconych przez okres połowicznego rozpadu radionuklidów.

# Bibliografia


[1] Skibinski R, Czarnecka K, Girek M, Bilichowski I, Chufarova N, Mikiciuk-Olasik E and Szymanski P 2018 Novel tetrahydroacridine derivatives with iodobenzoic acid moiety as multifunctional acetylcholinesterase inhibitors *Chemical Biology & Drug Design* **91** 505-18

[2] Szymanski P, Karpinski A and Mikiciuk-Olasik E 2011 Synthesis, biological activity and HPLC validation of 1,2,3,4-tetrahydroacridine derivatives as acetylcholinesterase inhibitors *European Journal of Medicinal Chemistry* **46** 3250-7

[3] Czarnecka K, Chufarova N, Halczuk K, Maciejewska K, Girek M, Skibinski R, Jonczyk J, Bajda M, Kabzinski J, Majsterek I and Szymanski P 2018 Tetrahydroacridine derivatives with dichloronicotinic acid moiety as attractive, multipotent agents for Alzheimer's disease treatment *European Journal of Medicinal Chemistry* **145** 760-9

[4] Szymanski P, Markowicz M and Mikiciuk-Olasik E 2011 Synthesis and biological activity of derivatives of tetrahydroacridine as acetylcholinesterase inhibitors *Bioorganic Chemistry* **39** 138-42

[5] Szymanski P, Zurek E and Mikiciuk-Olasik E 2006 New tacrine-hydrazinonicotinamide hybrids as acetylcholinesterase inhibitors of potential interest for the early diagnostics of Alzheimer's disease *Pharmazie* **61** 269-73

[6] Gniazdowska E, Kozminski P, Halik P, Bajda M, Czarnecka K, Mikiciuk-Olasik E, Maslowska K, Rogulski Z, Cheda L, Kilian K and Szymanski P 2019 Synthesis, physicochemical and biological evaluation of tacrine derivative labeled with technetium-99m and gallium-68 as a prospective diagnostic tool for early diagnosis of Alzheimer's disease *Bioorganic Chemistry* **91** 12

[7] Czarnecka K, Lisiecki P, Szewczyk E, Chufarova N, Wojtowicz P, Krecisz P and Szymanski P 2020 New acridine derivatives as promising agents against methicillin-resistant staphylococci - From tests to in silico analysis *Computational Biology and Chemistry* **88** 6

[8] Wainwright M 2001 Acridine - a neglected antibacterial chromophore *Journal of Antimicrobial Chemotherapy* **47** 1-13

[9] Krogstad D J, Gluzman I Y, Kyle D E, Oduola A M J, Martin S K, Milhous W K and Schlesinger P H 1987 EFFLUX OF CHLOROQUINE FROM PLASMODIUM-FALCIPARUM - MECHANISM OF CHLOROQUINE RESISTANCE *Science* **238** 1283-5

[10] Gao J J, Tian Z X and Yang X 2020 Breakthrough: Chloroquine phosphate has shown apparent efficacy in treatment of COVID-19 associated pneumonia in clinical studies *Bioscience Trends* **14** 72-3

[11] Hu T Y, Frieman M and Wolfram J 2020 Insights from nanomedicine into chloroquine efficacy against COVID-19 *Nature Nanotechnology* **15** 247-9

[12] Kumar J, Jain S, Meena J and Yadav A 2021 Efficacy and safety of hydroxychloroquine/chloroquine against SARS- CoV-2 infection: A systematic review and meta-analysis *Journal of Infection and Chemotherapy* **27** 882-9

[13] Bonnot S, Prenant C and Crouzel C 1991 SYNTHESIS OF 9- C-11 METHYLAMINO-1,2,3,4-TETRAHYDROACRIDINE, A POTENT ACETYLCHOLINE ESTERASE INHIBITOR *Applied Radiation and Isotopes* **42** 690-1

[14] Gniazdowska E, Kozminski P, Wasek M, Bajda M, Sikora J, Mikiciuk-Olasik E and Szymanski P 2017 Synthesis, physicochemical and biological studies of

technetium-99m labeled tacrine derivative as a diagnostic tool for evaluation of cholinesterase level *Bioorganic & Medicinal Chemistry* **25** 912-20
[15] Kręcisz P, Czarnecka K, Królicki L, Mikiciuk-Olasik E and Szymański P 2021 Radiolabeled Peptides and Antibodies in Medicine *Bioconjugate Chemistry* **32** 25-42
[16] Finefrock A E, Bush A I and Doraiswamy P M 2003 Current status of metals as therapeutic targets in Alzheimer's disease *Journal of the American Geriatrics Society* **51** 1143-8
[17] Skrzypek A, Matysiak J, Karpińska M, Czarnecka K, Kręcisz P, Stary D, Kukułowicz J, Paw B, Bajda M, Szymański P and Niewiadomy A 2021 Biological evaluation and molecular docking of novel 1,3,4-thiadiazole-resorcinol conjugates as multifunctional cholinesterases inhibitors *Bioorganic Chemistry* **107** 104617
[18] Huang C Y 1982 DETERMINATION OF BINDING STOICHIOMETRY BY THE CONTINUOUS VARIATION METHOD - THE JOB PLOT *Methods in Enzymology* **87** 509-25
[19] Yordanova A, Eppard E, Krupig S, Bundschuh R A, Schonberger S, Gonzalez-Carmona M, Feldmann G, Ahmadzadehfar H and Essler M 2017 TheranosticsTheranostics in nuclear medicine practice *Oncotargets and Therapy* **10** 4821-8
[20] Martel S, Castella M E, Bajot F, Ottaviani G, Bard B, Henchoz Y, Valloton B G, Reist M and Carrupt P A 2005 Experimental and virtual physicochemical and pharmacokinetic profiling of new chemical entities *Chimia* **59** 308-14
[21] Mahajan S and Divgi C R 2016 The role of iodine-124 positron emission tomography in molecular imaging *Clinical and Translational Imaging* **4** 297-306
[22] Ramdhani D, Sriyani M E and Mustarichie R 2019 PHYSICOCHEMICAL CHARACTERIZATION OF (TECHNITIUM)-T-99m - LUTEOLIN AS RADIOPHARMACEUTICAL PREPARATION FOR ANTIOXIDANT COMPOUND *International Journal of Pharmaceutical Sciences and Research* **10** 3883-90
[23] Reijenga J, van Hoof A, van Loon A and Teunissen B 2013 Development of Methods for the Determination of pKa Values *Analytical Chemistry Insights* **8** ACI.S12304
[24] Czarnecka K, Girek M, Wójtowicz P, Kręcisz P, Skibiński R, Jończyk J, Łątka K, Bajda M, Walczak A, Galita G, Kabziński J, Majsterek I, Szymczyk P and Szymański P 2020 New Tetrahydroacridine Hybrids with Dichlorobenzoic Acid Moiety Demonstrating Multifunctional Potential for the Treatment of Alzheimer's Disease *International Journal of Molecular Sciences* **21**
[25] Krecisz P, Czarnecka K and Szymanski P 2020 Physicochemical evaluation of new tetrahydroacridine and iodobenzoic acid hybrids as the next step in the design of potential drugs for treating Alzheimer's disease *Biomedical Chromatography* 9
[26] Zawada K, Czarnecka K, Girek M, Kręcisz P, Trejtnar F, Mandíková J, Jończyk J, Bajda M, Staśkiewicz M, Wójtowicz P, Dziubek K, Skibiński R and Szymański P 2020 New hybrids of tacrine and indomethacin as multifunctional acetylcholinesterase inhibitors *Chemical Papers*
[27] Czarnecka K, Girek M, Krecisz P, Skibinski R, Latka K, Jonczyk J, Bajda M, Kabzinski J, Majsterek I, Szymczyk P and Szymanski P 2019 Discovery of New Cyclopentaquinoline Analogues as Multifunctional Agents for the Treatment of Alzheimer's Disease *International Journal of Molecular Sciences* **20** 22
[28] Musil K, Florianova V, Bucek P, Dohnal V, Kuca K and Musilek K 2016 Development and validation of a FIA/UV-vis method for pK(a) determination of

oxime based acetylcholinesterase reactivators *Journal of Pharmaceutical and Biomedical Analysis* **117** 240-6
[29] McNaught A D and Wilkinson A 1997 *Compendium of Chemical Terminology*: Blackwell Science)
[30] Dołowy M 2009 Determination of lipophilicity of dehydrocholic acid with use of different methods. *Farmacja Polska* **65** 689-93
[31] Danielsson L G and Zhang Y H 1996 Methods for determining n-octanol-water partition constants *Trac-Trends in Analytical Chemistry* **15** 188-96
[32] Sangster J 1997 *Octanol-water Partition Coefficients: Fundamentals and Physical Chemistry* (New York: Wiley)
[33] Rutkowska E, Pajak K and Jozwiak K 2013 LIPOPHILICITY - METHODS OF DETERMINATION AND ITS ROLE IN MEDICINAL CHEMISTRY *Acta Poloniae Pharmaceutica* **70** 3-18
[34] Liang C, Qiao J Q and Lian H Z 2017 Determination of reversed-phase high performance liquid chromatography based octanol-water partition coefficients for neutral and ionizable compounds: Methodology evaluation *Journal of Chromatography A* **1528** 25-34
[35] Meyer H 1899 Zur Theorie der Alkoholnarkose *Archiv für experimentelle Pathologie und Pharmakologie* **42** 109-18
[36] Overton C E 1901 *Studien über die Narkose: zugleich ein Beitrag zur allgemeinen Pharmakologie*: G. Fischer)
[37] Laznicek M and Laznickova A 1995 THE EFFECT OF LIPOPHILICITY ON THE PROTEIN-BINDING AND BLOOD-CELL UPTAKE OF SOME ACIDIC DRUGS *Journal of Pharmaceutical and Biomedical Analysis* **13** 823-8
[38] Soskic M and Magnus V 2007 Binding of ring-substituted indole-3-acetic acids to human serum albumin *Bioorganic & Medicinal Chemistry* **15** 4595-600
[39] Waterhouse R N 2003 Determination of lipophilicity and its use as a predictor of blood–brain barrier penetration of molecular imaging agents *Molecular Imaging & Biology* **5** 376-89
[40] Kansy M, Senner F and Gubernator K 1998 Physicochemical high throughput screening: Parallel artificial membrane permeation assay in the description of passive absorption processes *Journal of Medicinal Chemistry* **41** 1007-10
[41] van de Waterbeemd H, Smith D A and Jones B C 2001 Lipophilicity in PK design: methyl, ethyl, futile *Journal of Computer-Aided Molecular Design* **15** 273-86
[42] Mansouri K, Cariello N F, Korotcov A, Tkachenko V, Grulke C M, Sprankle C S, Allen D, Casey W M, Kleinstreuer N C and Williams A J 2019 Open-source QSAR models for pKa prediction using multiple machine learning approaches *Journal of Cheminformatics* **11** 20
[43] Czylkowska A, Szczesio M, Raducka A, Rogalewicz B, Kręcisz P, Czarnecka K, Szymański P, Pitucha M and Pawlak T 2021 Cytotoxic Activity against A549 Human Lung Cancer Cells and ADMET Analysis of New Pyrazole Derivatives *International Journal of Molecular Sciences* **22**
[44] Guo Y S 2010 An Overview of Physical Stability of Pharmaceuticals *Pharmaceutical Stability Testing to Support Global Markets* **12** 145-52
[45] Baertschi S W 2010 Forced Degradation and Its Relation to Real Time Drug Product Stability *Pharmaceutical Stability Testing to Support Global Markets* **12** 107-16
[46] ICH 2003 Stability Testing of New Drug Substances and Products Q1A(R2). (Geneve: International Conference on Harmonization) p 24

[47] Touchstone J C 1993 HISTORY OF CHROMATOGRAPHY *Journal of Liquid Chromatography* **16** 1647-65
[48] Witkiewicz Z and Kałużna-Czaplińska J 2017 *Podstawy Chromatografii i Technik Elektromigracyjnych* (Warszawa: Wydawnictwo Naukowe PWN)
[49] ICH 2005 Q2(R1) Validation of Analytical Procedures: Text and Methodology. In: *International Conference of Harmonization,* (Geneve
[50] Anderson C J, Ling X, Schlyer D J and Cutler C S 2019 *Radiopharmaceutical Chemistry,* (Cham: Springer International Publishing) pp 11-26
[51] Jackson I M, Scott P J H and Thompson S 2017 Clinical Applications of Radiolabeled Peptides for PET *Seminars in Nuclear Medicine* **47** 493-523
[52] Qaim S M 2019 Theranostic radionuclides: recent advances in production methodologies *Journal of Radioanalytical and Nuclear Chemistry* **322** 1257-66
[53] Berman D S, Kiat H, Van Train K, Friedman J D, Wang F P and Germano G 1994 Dual-Isotope Myocardial Perfusion Spect with Rest Thallium-201 and Stress Tc-99m Sestamibi *Cardiology Clinics* **12** 261
[54] Tolmachev V and Stone-Elander S 2010 Radiolabelled proteins for positron emission tomography: Pros and cons of labelling methods *Biochim. Biophys. Acta, Gen. Subj.* **1800** 487
[55] Charron C L, Hickey J L, Nsiama T K, Cruickshank D R, Turnbull W L and Luyt L G 2016 Molecular imaging probes derived from natural peptides *Natural Product Reports* **33** 761-800
[56] Basuli F, Zhang X, Phelps T E, Jagoda E M, Choyke P L and Swenson R E 2020 Automated Synthesis of Fluorine-18 Labeled CXCR4 Ligand via the Conjugation with Nicotinic AcidN-Hydroxysuccinimide Ester (6- F-18 SFPy) *Molecules* **25** 14
[57] Roge A B, Firke S N, Kawade R M, Sarje S K and Vadvalkar S M 2011 BRIEF REVIEW ON: FLASH CHROMATOGRAPHY *International Journal of Pharmaceutical Sciences and Research* **2** 1930-7
[58] Snyder L R 1978 CLASSIFICATION OF SOLVENT PROPERTIES OF COMMON LIQUIDS *Journal of Chromatographic Science* **16** 223-34
[59] Stevens W C and Hill D C 2009 General methods for flash chromatography using disposable columns *Molecular Diversity* **13** 247-52
[60] Jandera P and Churacek J 1974 GRADIENT ELUTION IN LIQUID-CHROMATOGRAPHY .1. INFLUENCE OF COMPOSITION OF MOBILE PHASE ON CAPACITY RATIO (RETENTION VOLUME, BAND WIDTH, AND RESOLUTION) IN ISOCRATIC ELUTION - THEORETICAL CONSIDERATIONS *Journal of Chromatography* **91** 207-21
[61] Jandera P and Churacek J 1974 GRADIENT ELUTION IN LIQUID-CHROMATOGRAPHY .2. RETENTION CHARACTERISTICS (RETENTION VOLUME, BAND WIDTH, RESOLUTION, PLATE NUMBER) IN SOLVENT-PROGRAMMED CHROMATOGRAPHY - THEORETICAL CONSIDERATIONS *Journal of Chromatography* **91** 223-35
[62] Kręcisz P, Czarnecka K and Szymański P 2021 Thin-Layer Chromatography Gradient Optimization Strategy for Wet Load Adsorption Flash Chromatography *Journal of Chromatographic Science*

# Publikacja 1

Received: 1 March 2020 | Revised: 14 May 2020 | Accepted: 19 May 2020
DOI: 10.1002/bmc.4906



RESEARCH ARTICLE

Biomedical Chromatography WILEY

# Physicochemical evaluation of new tetrahydroacridine and iodobenzoic acid hybrids as the next step in the design of potential drugs for treating Alzheimer's disease

Paweł Kręcisz | Kamila Czarnecka | Paweł Szymański

Department of Pharmaceutical Chemistry, Drug Analyses and Radiofarmacy, Medical University of Lodz, ul. Muszyńskiego 1, Łódź, 90-151, Poland

**Correspondence**
Paweł Szymański, Department of Pharmaceutical Chemistry, Drug Analyses and Radiofarmacy, Medical University of Lodz, ul. Muszyńskiego 1, 90-151 Lodz, Poland.
Email: pawel.szymanski@umed.lodz.pl

**Funding information**
National Science Centre, Grant/Award Number: 2015/19/B/NZ7/02847

## Abstract

Tacrine derivatives containing iodobenzoic acid were developed as a novel multitarget-directed ligand and find potential application in the treatment of Alzheimer's disease. The aim of this study is to perform a physicochemical profile of this series. Experimental log *P* and $pK_a$ values were determined and compared with those already calculated. The results indicated better values of the tested compounds than the values predicted using computer software. The stability report was obtained using the developed HPLC method. The stability assay in different environment conditions provided information about the photosensitivity of these compounds and a proper method for the storage of this series of compounds.

**KEYWORDS**
Alzheimer's disease, HPLC, log *P* determination, method validation, $pK_a$ determination, tacrine

## 1 | INTRODUCTION

The significance of physicochemical properties in drug discovery is incontestable. The preclinical profiling of new compounds reduces drug failures resulting from various problems in human pharmacokinetics during clinical trials. Defining physicochemical properties of new potent drugs helps develop more efficient drugs and safer clinical trials, and reduce expenditures (D. T. Manallack, Prankerd, Yuriev, Oprea, & Chalmers, 2013). One of the first attempts to studying the dependence of pharmacokinetic properties on physicochemical properties was made by Lipinski et al. who described the well-known "rule of five." Lipinski's rule of five implies good pharmacokinetics for a compound if it fulfills two or more of `the following criteria: molecular weight < 500, log *P* < 5, H-bond acceptors < 10, and H-bond donors < 5 (Lipinski, Lombardo, Dominy, & Feeney, 1997). Subsequently, other researchers improved the methods of evaluating the pharmacokinetic properties of novel potent medicines (Meanwell, 2011). Several studies have reported that acid/base properties and the octanol/water partition coefficient are the most important physicochemical properties for drug development. The $pK_a$ value is crucial in determining the absorption, permeability, and bioavailability of the drug because the varying ability to permeate through biological barriers depends on the charge (Gleeson, 2008). Acid/base characteristics are also important for the estimation of plasma protein binding and, indirectly, the volume of distribution (F. L. Zhang, Xue, Shao, & Jia, 2012). Log *P* value is one of the most important properties determining the distribution of drug and its brain permeation (Clark, 2003; Gleeson, 2008). Wager et al. combined both these properties to analyze $ClogD_{7.4}$ and proved that compounds with $ClogD_{7.4}$ values in the range of 2.0–4.0 can be considered central nervous system drugs because they can permeate the brain and bind to brain tissue (Wager, Hou, Verhoest, & Villalobos, 2010). Nowadays, in silico estimation of pharmacokinetic properties of a drug using computers is invaluable in drug development, especially if crucial input data such as $pK_a$ and log *P* are experimentally determined.

Alzheimer's disease (AD) is a progressive neurodegenerative disorder and is the most common neurodegenerative disease among the elderly. The most common symptoms of AD are memory loss, dysfunction of cognitive ability, and behavioral disorders, which lead to deterioration in the quality of life and ultimately death. The number of patients with AD is growing every year, and

  

it is estimated to reach 114 million by 2050 (Hamulakova et al., 2016; C. Zhang et al., 2016). Its diagnosis is very difficult. Nowadays, the disease is diagnosed based on biomarkers, psychological tests, and imaging. Its pathophysiology is also complex. Scheltens et al. published an excellent paper about AD in which they provided information about pathophysiology, diagnosis, and epidemiology (Scheltens et al., 2016).

Now, pharmacotherapy, which slows down the progress of AD, is being used. In an earlier study, Skibiński et al. (Skibiński et al., 2018) developed a new tetrahydroacridine derivative that exhibited an inhibitory activity against acetylcholinesterase and beta-amyloid aggregation. Such multitarget-directed ligands offer hope for AD therapy by decreasing the symptoms of the disease and making the therapy simpler.

In this study, we developed assays that evaluate basic physicochemical properties of a series of compounds developed by (Skibiński et al., 2018) (Figure 1). Moreover, we developed quantitative methods with validation and stability tests for determining the most biologically active compound in this series. UV spectrophotometric methods provided the $pK_a$ value, one of the most important properties of a drug. It impacts lipophilicity, solubility, protein binding, and permeability of a drug. (David T. Manallack, 2007). Log *P*, one of the most relevant lipophilicity descriptors, was studied next. It is also of paramount importance as a parameter in pharmacokinetic predictions and studies (Mazak & Noszal, 2014). Log *P* values of the compounds were obtained using HPLC, which was optimized using the results of the $pK_a$ tests. This was due to the presence of noncharged structures in the assay. These parameters affect the pharmacokinetic profile of a compound.

More advanced pharmacokinetic studies require advanced quantitative methods; therefore, we developed a simple isocratic HPLC method for the spectrophotometric quantification of the most biologically active compound in the series developed by Skibiński et al (Skibiński et al., 2018). Full validation was performed according to the ICH guidelines Q2(R1) (ICH, 2005). The method can also be used in quality assays for identification of specific compounds among a series of compunds or in impurities assays, and therefore it was used in stability tests. This method may also be used in future pharmacokinetic studies involving blood samples after an appropriate sample preparation. (Sulochana, Sharma, Mullangi, & Sukumaran, 2014)

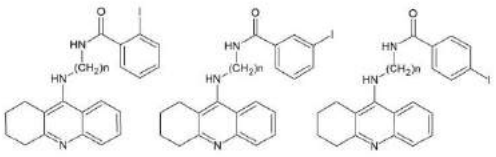


**FIGURE 1** Structures and names of tested compounds

## 2 | MATERIALS AND METHODS

### 2.1 | Reagents

Potassium dihydrogen phosphate, potassium hydroxide, methanol, potassium phosphate monobasic, and phosphoric acid were purchased from POCH (Gliwice, Poland). Triethylamine (TEA), 3-iodobenzoic acid (3IKW), and a 0.45 μm nylon filter membrane were purchased from Sigma-Aldrich (Steinheim, Germany). HPLC-grade methanol and acetonitrile were purchased from Baker (Deventer, The Netherlands). Milli-Q® Advantage AIO with qualification IQ/OQ was used as demineralized water source.

### 2.2 | $pK_a$ assay

Potassium dihydrogen phosphate, potassium hydroxide, and methanol were used to prepare a buffer solution. Methanol–water mixture (1:1) was used as a dissolvent due to the weak water solubility of the test compounds. Potassium dihydrogen phosphate (0.01 M) in methanol–water mixture (1:1) was used as a stock buffer solution. The test buffer solutions were prepared by titrating the stock buffer solution with 0.1 M potassium hydroxide in methanol–water mixture (1:1). The pH values of the test buffer solutions were set from 5.6 to 12.4 in steps of 0.2 pH. The pH range was limited by the $pK_a$ values of potassium dihydrogen phosphate and tripotassium phosphate. The pH-meter Mettler Toledo FiveEasy with Lab pH electrode LE438 (Mettler Toledo) was used for measurement at 23°C. Test compounds were 5 μM solutions in methanol–water (1:1) mixture.

Spectrophotometric measurement was performed in 96 well plates using Synergy H1 microplate reader (BioTek) coupled with Gen5 software (BioTek). The full assay of one test compound consisted of 35 UV spectra measurements, one for each test buffer solution. For the assay, in 35 wells, 180 μL of the sequent test buffer solution and 20 μL of the tested compound solution were added. For blanks, in 35 wells, 200 μL of the sequent test buffer was added. The measurement was performed at 23°C; the spectra range was 280–380 nm in steps of 1 nm. This spectra range was used because of the occurrence of the absorption spectra with a maximum at 336 nm with pH 5.6. The largest variability in the absorbance was observed at 310 and 336 nm, and therefore this wavelength range was used to perform the calculations. The method developed by Musil et al. (2016) was used for the calculations. To avoid the influence of detector noise, all calculations were performed using ratios of 310/336 and 336/310 nm. The absorbance values obtained from 310/336 and 336/310 nm ratios were analyzed to determine the range of pH values in which the absorbance was stable. Absorbance was considered stable when the difference between the values obtained at two subsequent measurements was at a minimum. Three points were determined for all test compounds. The average value of the absorbance ratio was calculated for all stable points, and these values were used in the following function (Equation 1):

**TABLE 1** Compounds used to perform calibration curve

| Compound name | Experimental properties | |
|---|---|---|
| | Log *P* (Hansch, Leo, & Hoekman, 1995) | $pK_a$ |
| Procainamide HCl | 0.88 | 9.32 (Sangster, 1997) |
| Tacrine | 2.71 | 9.95 (Perrin, 1972) |
| Thymol | 3.30 | – |
| Naphthalene | 3.60 | – |
| Promazine HCl | 4.55 | 9.36 (Sangster, 1997) |
| Promethazine HCl | 4.81 | 9.10 (Sangster, 1997) |
| Chlorpromazine HCl | 5.41 | 9.30 (Hansch et al., 1995) |
| Thioridazine HCl | 5.90 | 9.50 (*The Merck Index: An Encyclopedia of Chemicals, Drugs, and Biologicals*, 14th ed., 2006) |

$$f(pH) = pH - \log\frac{A_x - A_a}{A_b - A_x}, \quad (1)$$

where pH is the pH value of the analyzed sample, $A_x$ is the value of absorbance ratio of the analyzed sample, $A_a$ is the average value of the absorbance ratio at the stable point at a lower pH, $A_b$ is the average value of the absorbance ratio at the stable point at a higher pH. The zero point of this function was determined via the linear regression method. The pH value corresponding to the zero point of the function was the $pK_a$ value of the analyzed test compound. Because of the occurrence of three stable points for all compounds, this procedure was performed twice for both ratios to determine two $pK_a$ values. The final $pK_a$ value of each test compound was the average of the results of the two ratios. The obtained results were compared with the $pK_a$ value calculated using online software (ChemAxon 2018).

## 2.3 | Log *P* assay

Demineralized water, trimethylamine, and methanol were used to form the mobile phase. The neutral form of the basic substances was required to perform the assay. TEA was used to achieve pH 10 in mobile phases. The basic properties of the mobile phases did not affect retention times of neutral compounds. TEA was dissolved in methanol and water to obtain two solutions of 30 mM TEA. Ten varying binary mobile phases were required to assay. The first mobile phase contained 50% 30 mM TEA methanol solution and 50% 30 mM TEA aqueous solution. Each of the next mobile phases contained 5% more 30 mM TEA methanol solution and 5% less 30 mM TEA aqueous solution. A mixture of 95% 30 mM TEA methanol solution and 5% 30 mM TEA aqueous solution was used as the last mobile phase.

The compounds used for calibration are listed in Table 1. These substances were selected due to their similarity in structure with the test compounds. Stock solutions of calibration compounds and test compounds were 1 mg/mL. The injection concentration and the injection volume were 100 μg/mL and 7 μL, respectively. All injection samples were prepared in the mobile phase with the weakest eluting power.

The apparatus used was a Waters 600 HPLC system with a photodiode array detector. The detector was set at the optimum absorption wavelength for each compound. The chromatographic column used was Xbridge C18 50 × 4.6 mm i.d., 3.5 μm (Waters, Milford, MA, USA). Data acquisition and processing were performed using a Waters Millennium software.

The procedure used in this assay was developed by Liang et al. (2017). Dead time ($t_0$) was measured using sodium nitrate in methanol in a water 50:50 mixture (100 μg/mL) at a wavelength of 210 nm. The $t_0$ value was measured five times and averaged for each mobile phase. To prepare the calibration curve, each calibration substance was eluted by all mobile phases. All obtained retention times (tR) are shown in Equation 2:

$$\log k = \log\left(\frac{tR - t_0}{t_0}\right). \quad (2)$$

The results were used to calculate $\log k$ values for each sample and then $\log k_w$ values by linear regression and extrapolation for each of the calibration compounds. These results were used to generate a calibration curve.

The same procedure was used to obtain $\log k_w$ values of the test compounds. Log *P* values were read from the calibration curve. Experimental log *P* values were compared with the estimated values of log *P* using online software (ChemAxon 2018).

## 2.4 | Development of the validated analytical HPLC method

Samples of 3-iodo-*N*-[4-(1,2,3,4-tetrahydroacridin-9-ylamino)butyl] benzamide (**3b**), 9-chloro-1,2,3,4-tetrahydroacridin (9Cl-THA), and N1-(1,2,3,4-tetrahydroacridin-9-yl)butane-1,4-diamine (6C-4-NH) were synthesized in-house. HPLC-grade methanol, acetonitrile, and demineralized water were used. Potassium phosphate monobasic and phosphoric acid were used to prepare the buffer solution. Isocratic mobile phase was filtered under vacuum using a 0.45 μm nylon filter membrane.

### 2.4.1 | Determination of a suitable wavelength

A PerkinElmer Lambda 25 UV/VIS spectrophotometer and UV WINLAB version 2.85.04 software (PerkinElmer Inc., 2000) were used to obtain the UV spectra of 3IKW, 9Cl-THA, 6C-4-NH, and

**3b**. All sample solutions were prepared in methanol/aqueous 30 mM $KH_2PO_4$ solution (50:50) mixture with pH 3.03.

#### 2.4.2 | Chromatographic system

Analytical and validation procedures were performed using a Varian ProStar HPLC system with an isocratic pump PS210, UV/Vis detector PS325, manual injector, and Galaxie Chromatography Data System software version 1.9.302.530 (Varian Inc., Palo Alto, CA, USA). A mixture of methanol/acetonitrile/30 mM potassium dihydrogen phosphate buffer (25:35:40) was used as the mobile phase. The pH of the mobile phase was set at 3.03 by using 10% phosphoric acid. All experiments were performed at room temperature (RT). Chromatograms were recorded at 223 nm. Waters Atlantis T3 C18 (4.6 × 150 mm, particle size 5 μm) with a guard cartridge (Waters) was used as the analytical column. The flow rate was set at 1.00 mL/min.

#### 2.4.3 | Analytical HPLC procedure

All stock solutions (1 mg/mL) were prepared in methanol/water (50:50) mixture. Five dilution levels (70, 85, 100, 115, and 130%) of working solutions were prepared for **3b**. A 100% dilution level was about 0.1 mg/mL. The injection volume was 10 μL.

#### 2.4.4 | System suitability

Internal system suitability test in Galaxy Software was used. The acceptability criteria were ≤2 tailing factor (As USP) and ≥3000 theoretical plates (NTP USP).

#### 2.4.5 | Method validation

The analytical method validation was carried out according to the ICH Q2(R1) method validation guidelines. The following validation parameters were checked: accuracy, selectivity, linearity, limit of detection (LOD), limit of quantification (LOQ), robustness, and the stability of 6C-4-3IKW in the diluent. Two samples, **3a** and **2c**, at a concentration of 0.1 mg/mL were prepared for selectivity. Intermediate precision was performed 1 week after the precision evaluation. Additional stability tests were performed. The stability was checked for five kinds of stress conditions: acid hydrolysis (0.5 M HCl at RT, 48 h in the dark), base hydrolysis (0.5 M NaOH at RT, 48 h in the dark), oxidation (3% $H_2O_2$ at RT, 48 h in the dark), thermal stress (60°C, 8 h), and UV irradiation (254 nm, 8 h). A 254 nm UV lamp was used for UV irradiation. The sample was prepared in a quartz cuvette and was not exposed to daylight during UV irradiation.

## 3 | RESULTS AND DISCUSSION

### 3.1 | $pK_a$ assay

$pK_a$ assays were performed to evaluate basic physiochemical properties, which were necessary to determine the log *P* values of test compounds. The experimental $pK_a$ results were compared with those calculated using online software (ChemAxon 2018). The experimental and calculated $pK_a$ values are presented in Table 2. For strong bases, $pK_a$ values calculated by ChemAxon software were close to the experimental $pK_{a1}$ values. For strong acids, the experimental $pK_{a2}$ values were lower than those calculated using ChemAxon software. The differences between experimental and predicted results may be because of the characteristic of the obtained data. The predicted results were obtained via an algorithm using similar input data, and therefore all results for strong bases are the same. The results for strong acids are also similar. A few obtained results have a $pK_a$ value greater than 14. The experimental results indicated that the length of the carbon chain has an impact on the average value of $pK_{a1}$ and $pK_{a2}$ in groups of three derivatives with the same number of carbon atoms in their alkyl chain. In addition, the experimental results showed the significant role of the position of iodine in the aromatic ring on the $pK_a$ values, which was impossible to notice in computer-calculated results.

### 3.2 | Log *P* assay

Our procedure is a modified method developed by Chao Liang and allows for the fast, simple, and inexpensive determination of log *P*. The coefficient of determination was over 0.96 for the calibration curve. The log *P* values of all test compounds were lower than 5. The results are presented in Table 3.

The results obtained indicate a significant influence of the iodine position in the aromatic ring on the log *P* value. The log *P* value increases with the position number of iodine in the aromatic ring, and

**TABLE 2** Experimental and computer-calculated $pK_a$ values

| | Experimental | | Calculated (ChemAxon 2018) | |
|---|---|---|---|---|
| Compound | $pK_{a1}$ | $pK_{a2}$ | $pK_a$ (strong base) | $pK_a$ (strong acid) |
| **1a** | 8.09 | 11.82 | 8.89 | 13.53 |
| **2a** | 8.26 | 11.28 | 8.89 | 13.55 |
| **3a** | 8.19 | 11.64 | 8.89 | 13.55 |
| **1b** | 8.25 | 11.60 | 8.89 | 14.67 |
| **2b** | 8.10 | 11.44 | 8.89 | 14.68 |
| **3b** | 8.44 | 11.20 | 8.89 | 14.69 |
| **1c** | 8.36 | 11.47 | 8.89 | 14.79 |
| **2c** | 8.28 | 11.50 | 8.89 | 14.81 |
| **3c** | 8.59 | 11.37 | 8.89 | 14.81 |

**TABLE 3** Experimental and computer-calculated log *P* values of test compounds

| Compound | Experimental log *P* | Calculated log *P* (ChemAxon 2018) | Calculated log *P* (ALOGPS 2.1) |
|---|---|---|---|
| **1a** | 3.520 | 4.73 | 4.91 |
| **2a** | 3.771 | 4.79 | 5.24 |
| **3a** | 3.745 | 5.31 | 5.72 |
| **1b** | 4.143 | 4.73 | 4.94 |
| **2b** | 4.509 | 4.79 | 5.34 |
| **3b** | 4.530 | 5.31 | 5.73 |
| **1c** | 4.239 | 4.73 | 4.94 |
| **2c** | 4.529 | 4.79 | 5.35 |
| **3c** | 4.525 | 5.31 | 5.73 |

the largest increase is observed between position numbers 2 and 3. The most distinct differences between log *P* values are between compounds with two carbon atoms in alkyl chains and compounds with three and four carbon atoms in alkyl chains in a series of derivatives with the same iodobenzoic group. Log *P* values of compounds with three and four carbon atoms in alkyl chains and the same iodobenzoic group are very similar. All log *P* calculations obtained using ChemAxon or ALOGPS 2.1 were higher than the experimental values. Values predicted by ALOGPS (Tetko et al., 2005) were even higher than those by ChemAxon algorithm. Both predicted methods underestimated the role of the position number of iodine in the aromatic ring, and they are generally based on the length of the alkyl chain. The experimental log *P* values lower than 5 were optimal, as they potentially offered improved biodistribution for the tested series of compounds.

## 3.3 | HPLC quantification and method validation

### 3.3.1 | Determination of a suitable wavelength

The detection wavelength was determined by obtaining the UV spectra for 3IKW, 9Cl-THA, 6C-4-NH2, and **3b** before developing the chromatographic methodology applied. The samples were dissolved in methanol/aqueous 30 mM $KH_2PO_4$ solution (50:50) mixture (pH = 3.03) to observe the UV spectra at the appropriate pH value. UV scans were performed in the range of 200-400 nm. The UV spectra of four compounds are illustrated in Figure 2.

The maximum absorbance for **3b** appears at 223 nm. 6C-4-NH2, 9Cl-THA, and 3IKW exhibit maximum absorbance at 246, 238, and 218 nm, respectively. The response of 6C-4-NH2 and 3IKW was twice as high as that of **3b**. The response of 9Cl-THA was four times stronger than that of **3b**. We chose 223 nm as an analytical wavelength used in the HPLC quantification method and validation procedure.

### 3.3.2 | Method development and validation

The working pH of the mobile phase was determined using the experimental $pK_a$ values of **3b** and the estimated $pK_a$ values from online software (ChemAxon 2018) for 3IKW, 9Cl-THA, and 6C-4-NH2. The mobile phase was prepared at a pH in the range of 5–6 and adjusted to 3.03 with 10% phosphoric acid solution. The binary (methanol:buffer solution) isocratic mobile phase was investigated by various ratios, but acquisition length and peak shape were unsatisfactory. The addition of acetonitrile improved these parameters and led to an appropriate acquisition time, resolution, and peak shape. The developed method can separate impurities and

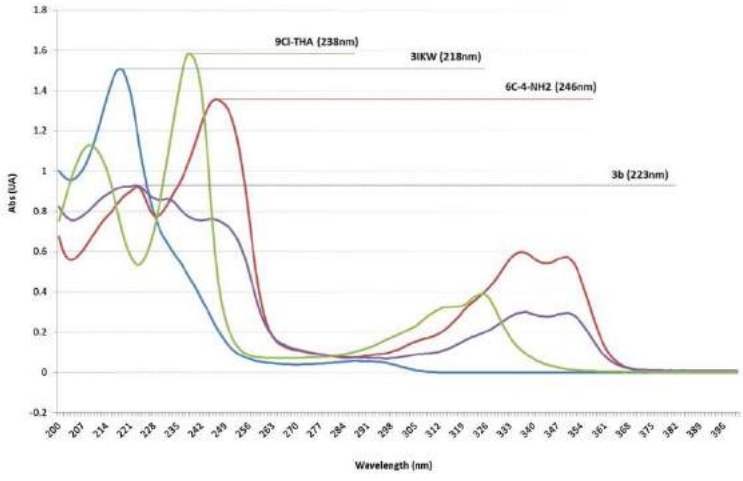


**FIGURE 2** UV absorption spectra of tested compounds from 200 to 400 nm. Concentration: 3IKW (0.015 mg/mL), 9Cl-THA (0.0075 mg/mL), 6C-4-NH2 (0.015 mg/mL), and **3b** (0.035 mg/mL)

quantify **3b** in samples. A concentration of 0.1 mg/mL was used as the main working solution. Five levels of dilution were performed over the range of 70–130% for the main concentration sample (about 0.1 mg/mL) according to the ICH guidelines Q2(R1). The resultant graph indicates that the method is linear over this range (Figure 3).

### 3.3.3 | Selectivity

HPLC chromatograms were recorded for **3b**, **2b**, and **3a** at a concentration of about 0.1 mg/mL, thrice for each compound. Retention times were obtained and used to calculate relative retention times with respect to the main compound **3b** and resolution USP factor according to the US Pharmacopeia 32 definition (Table 4). Compound **3a** had the smallest retention time, so its resolution USP factor was calculated for compound and impurities peak according to the US Pharmacopeia Resolution factor equation.

### 3.3.4 | Precision and repeatability

System precision was evaluated by calculating relative standard deviation (RSD%) based on three samples taken at five concentration

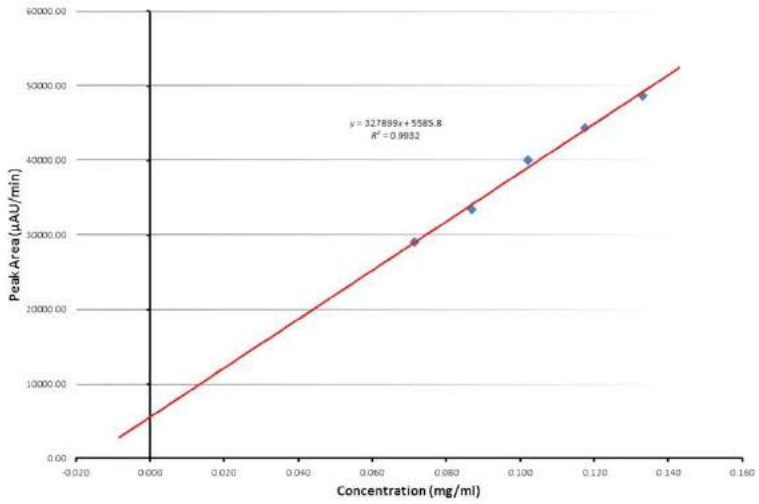


**FIGURE 3** Calibration curve of 3b. Regression line is marked by a red continuous line. The linear equation and the coefficient of determination are marked on plots area. The residual sum of squares is equal to 1,719,694.522

**TABLE 4** Selectivity results (acceptable criteria of resolution USP factor is greater than 1)

| | Retention times (min) | | | Relative retention times (%) | | | Resolution USP factor | | |
|---|---|---|---|---|---|---|---|---|---|
| | 3a | 3b | 2b | 3a | 3b | 2b | Impurities/3a | 3a/3b | 3b/2b |
| | 4.11 | 6.39 | 6.71 | 64 | 100 | 105 | 2.27 | 9.31 | 1.07 |
| | 4.10 | 6.38 | 6.71 | 64 | 100 | 105 | 2.25 | 9.12 | 1.10 |
| | 4.11 | 6.38 | 6.71 | 64 | 100 | 105 | 2.24 | 9.08 | 1.10 |
| Average | 4.11 | 6.38 | 6.71 | 64 | 100 | 105 | 2.25 | 9.17 | 1.09 |

**TABLE 5** Precision and intermediate precision results

| | Precision | | | Intermediate precision | | |
|---|---|---|---|---|---|---|
| Concentration level (%) | Average peak area (µAU/min) | SD | RSD% | Average peak area (µAU/min) | SD | RSD% |
| 70 | 29 024.67 | 132.91 | 0.46 | 29 784.77 | 459.31 | 1.54 |
| 85 | 33 385.27 | 281.19 | 0.84 | 34 215.57 | 106.99 | 0.31 |
| 100 | 40 050.23 | 505.81 | 1.26 | 40 895.47 | 174.58 | 0.43 |
| 115 | 44 417.97 | 230.89 | 0.52 | 44 225.13 | 186.00 | 0.42 |
| 130 | 48 646.77 | 201.84 | 0.41 | 50 444.47 | 382.03 | 0.76 |

levels. All RSD% values complied with the ICH proposed acceptance criteria (no more than 2%) for precision and intermediate precision (Table 5).

Abbreviations: RSD%, relative standard deviation; SD, standard deviation.

### 3.3.5 | Limit of detection and limit of quantification

LoD and LoQ were calculated using an equation based on the standard deviation of response and slope according to the ICH Q2(R1) guidelines. The standard deviation of noise was used as the standard deviation of response. Noise measurement was performed during all HPLC separations by an integration event using Compute noise in Galaxy software. The LoD and LoQ for our HPLC method was 1.364 and 4.133 μg/mL, respectively.

### 3.3.6 | Accuracy (recovery%)

The accuracy was determined by the recovery of **3b** at five levels of concentration (70–130%). The samples at each concentration were measured thrice. The results are presented in Table 6.

### 3.3.7 | Robustness

The method robustness was checked by performing HPLC separation at varying temperatures, mobile phase compositions, and flow rate. Asymmetry USP factor, resolution USP factor between peak **3b** and **3b**, and many theoretical plates' USP were checked for each measurement of the sample separation at a concentration of 0.1 mg/mL. The results are presented in Table 7.

Abbreviations: ACN, acetonitrile; MeOH, methanol.

**TABLE 6** Summary for recovery% of **3b**

| Concentration level (%) | Recovery% |
|---|---|
| 70 | 99.89 |
| 85 | 97.57 |
| 100 | 102.82 |
| 115 | 100.74 |
| 130 | 98.82 |

**TABLE 7** Results of robustness

| | Value of tested parameter | As USP 3b | NTP USP 3b | Resolution USP 3b/3a |
|---|---|---|---|---|
| Temperature (°C) | 25 | 1.37 | 7568.74 | 9.17 |
| | 35 | 1.40 | 7374.69 | 8.80 |
| Flow rate (mL/min) | 1.0 | 1.37 | 7568.74 | 9.17 |
| | 1.5 | 1.40 | 6036.26 | 7.88 |
| Organic modifier in mobile phase (%) | 60 (ACN, 35%; MeOH, 25%) | 1.37 | 7568.74 | 9.17 |
| | 70 (ACN, 40%; MeOH, 30%) | 1.31 | 5923.38 | 4.47 |

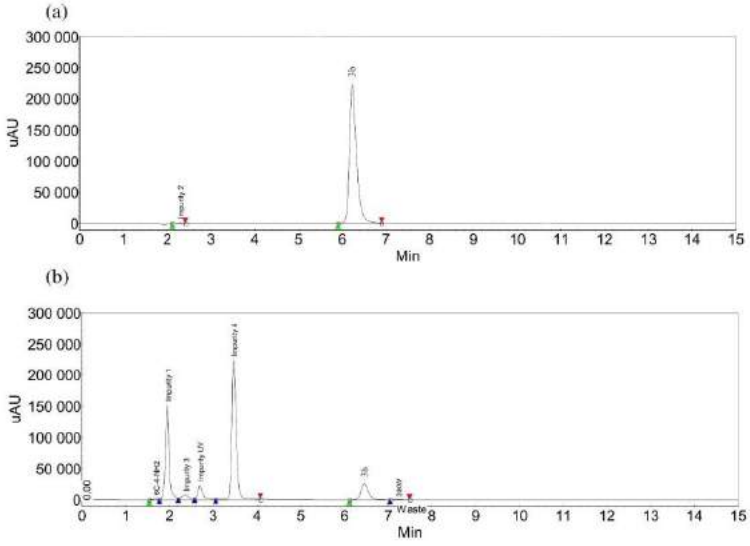


**FIGURE 4** Chromatograms obtained from stability tests of compound **3b**. (a) 48 h, room temperature, inthe dark; (b) 8 h, RT, UV (254 nm) irradiation. Impurities 1, 2, 3, and 4 are unknown peaks that occurred in a pure sample as traces. "Impurity UV" is a specific peak derived from compound degradation product created under a specific stress condition

**TABLE 8** Results of stability tests

| Stress condition | Time (h) | Recovery% 3b | % Peak area 3b | Remarks |
|---|---|---|---|---|
| Stability over time (in the dark at RT) | 48 | 100.38 | 99.33 | No degradation products formed (total unknown less than 1%) |
| Acid hydrolysis (0.5 M HCl at RT in the dark) | 48 | 95.25 | 97.29 | Some unknown degradation products formed (total unknown about 2.5%) |
| Base hydrolysis (0.5 M NaOH at RT in the dark) | 48 | 93.83 | 97.55 | Some unknown degradation products formed (total unknown about 2.5%) |
| Oxidation (3% $H_2O_2$ at RT in the dark) | 48 | 104.56 | 100.00 | No degradation products formed (total unknown less than 1%) |
| Thermal 60°C | 8 | 99.72 | 99.14 | No degradation products formed (total unknown less than 1%) |
| UV (254 nm) | 8 | 13.79 | 9.51 | Significant degradation; six products of degradation formed (total unknown about 90%) |

### 3.3.8 | System suitability test

A system suitability test (SST) was prepared for all separations. The parameters As USP < 2 and NTP USP > 3000 were determined. All separation passed SST. The average of the tailing factor for **3b** separations was equal to 1.36, and the average number of theoretical plates was equal to 7757.

## 3.4 | Stability of solutions

A standard solution with a concentration of 0.1 mg/mL was analyzed thrice on day 1 and thrice after 48 h. The sample was stored at RT in the dark. The standard solution was stable after 48 h because no degradation products were detected and the average recovery% was found to be 100.38%.

No relevant degradation peaks were observed for high temperature and oxidation conditions. Hydrogen peroxide reacted with methanol in the sample, which caused interference in detection, but no unknown peaks were detected barring the large solvent peak (likely formic acid derived from the oxidation of methanol) and slightly increased height of the baseline. This interference was unavoidable due to the solubility of **3b**. Base hydrolysis and acid hydrolysis caused weak degradation. About 6% of the degradation products were detected in the sample with base addition and about 5% in the sample with acid addition. Four degradation products were detected for acid and base hydrolysis conditions. UV irradiation caused serious degradation of **3b**. The average recovery% was found to be 13.79%. In addition, two main and four secondary products of degradation were detected (Figure 4). The results are presented in Table 8.

Abbreviation: RT, room temperature.

## 4 | CONCLUSIONS

The results of the physicochemical assays provided information about the huge impact the iodine atom has on the properties of aromatic rings. The position of iodine atoms affects $pK_a$ and log *P* values to a greater extent than the number of carbon atoms in the carbon chain. This may be explained by iodine's high atomic weight, large size, and relative weak atomic bond with carbon because of small electronegativity difference between it (2.66) and the carbon (2.55), as well as the distribution of charge in aromatic rings and whole structures, but the exact reasons warrant more advanced study (Lyday, 2000). All experimental values of $pK_a$ and log *P* were compared with the calculated properties using ChemAxon software. The experimental values were always smaller than the calculated values, except the $pK_{a1}$ values for which the computer algorithm–estimated values were very close to the experimental results. All compounds in the series have log *P* values smaller than 5, which is ideal for use as a medicine due to their ability to permeate through biological barriers.

The HPLC method was developed and completely validated according to the ICH guidelines Q2(R1). All validation parameters, that is, RSD < 2%, RS USP > 1, and $R^2 > 0.99$, for the calibration curve were fulfilled. The method is linear in our range and robust. Intermediate precision measurements provided information that confirmed the optimal parameters for the measurement of precision. The parameters of this analytical method can therefore be the basis for further HPLC assays on this series of compounds.

Compound **3b** is stable in the dark at RT, in high temperature (60°C), and in an oxidative environment (3% $H_2O_2$). Acidic and basic environments cause weak hydrolysis of compounds. The results of the stability test indicate the photosensitivity of the most biologically active compound due to significant degradation after 8 h of UV irradiation. It can also be explained by the weak iodine binding with carbon. After the stability test, the conclusions can be drawn that pure active compounds should be stored in the dark, and potential ready form of the drug should ensure no access to light for the active compound, and medicine should be stored in nontransparent package.

The results gathered in this study are an important addition to the physicochemical and pharmaceutical profile of a series of tetrahydroacridine derivatives conjugated with iodobenzoic acid. Crucial physicochemical properties in terms of pharmacokinetics were determined, which allow for the expansion of knowledge regarding pharmacokinetic properties of this series of compounds. Information

about stability, storage requirements, and validated HPLC method will facilitate further assays.


## FUNDING INFORMATION

Financial support by the National Science Centre, Poland (Grant number: 2015/19/B/NZ7/02847) is gratefully acknowledged.



## ORCID

*Paweł Kręcisz* https://orcid.org/0000-0003-2951-0867
*Kamila Czarnecka* https://orcid.org/0000-0002-6497-1565
*Paweł Szymański* https://orcid.org/0000-0003-3438-7509


## REFERENCES


Clark, D. E. (2003). In silico prediction of blood-brain barrier permeation. *Drug Discovery Today*, *8*(20), 927–933. https://doi.org/10.1016/s1359-6446(03)02827-7

Gleeson, M. P. (2008). Generation of a set of simple, interpretable ADMET rules of thumb. *Journal of Medicinal Chemistry*, *51*(4), 817–834. https://doi.org/10.1021/jm701122q

Hamulakova, S., Poprac, P., Jomova, K., Brezova, V., Lauro, P., Drostinova, L., … Valko, M. (2016). Targeting copper (II)-induced oxidative stress and the acetylcholinesterase system in Alzheimer's disease using multifunctional tacrine-coumarin hybrid molecules. *Journal of Inorganic Biochemistry*, *161*, 52–62. https://doi.org/10.1016/j.jinorgbio.2016.05.001

Hansch, C., Leo, A., & Hoekman, D. (1995). *Exploring QSAR: Hydrophobic, electronic, and steric constants*. Washington DC: American Chemical Society.

ICH. (2005). Q2(R1) validation of analytical procedures: Text and methodology. Paper presented at the International Conference of Harmonization, Geneve.

Liang, C., Qiao, J. Q., & Lian, H. Z. (2017). Determination of reversed-phase high performance liquid chromatography based octanol-water partition coefficients for neutral and ionizable compounds: Methodology evaluation. *Journal of Chromatography a*, *1528*, 25–34. https://doi.org/10.1016/j.chroma.2017.10.064

Lipinski, C. A., Lombardo, F., Dominy, B. W., & Feeney, P. J. (1997). Experimental and computational approaches to estimate solubility and permeability in drug discovery and development settings. *Advanced Drug Delivery Reviews*, *23*(1–3), 3–25. https://doi.org/10.1016/s0169-409x(96)00423-1

Lyday, P. A. (2000). Iodine and Iodine Compounds. In *Ullmann's encyclopedia of industrial chemistry*. Weinheim, Germany: Wiley-VCH Verlag GmbH & Co. KGaA. https://doi.org/10.1002/14356007.a14_381

Manallack, D. T. (2007). The pK(a) Distribution of Drugs: Application to Drug Discovery. *Perspectives in Medicinal Chemistry*, *1*, 25–38.

Manallack, D. T., Prankerd, R. J., Yuriev, E., Oprea, T. I., & Chalmers, D. K. (2013). The significance of acid/base properties in drug discovery. *Chemical Society Reviews*, *42*(2), 485–496. https://doi.org/10.1039/c2cs35348b

Mazak, K., & Noszal, B. (2014). Drug delivery: A process governed by species-specific lipophilicities. *European Journal of Pharmaceutical Sciences*, *62*, 96–104. https://doi.org/10.1016/j.ejps.2014.05.017

Meanwell, N. A. (2011). Improving Drug Candidates by Design: A Focus on Physicochemical Properties As a Means of Improving Compound Disposition and Safety. *Chemical Research in Toxicology*, *24*(9), 1420–1456. https://doi.org/10.1021/tx200211v

Musil, K., Florianova, V., Bucek, P., Dohnal, V., Kuca, K., & Musilek, K. (2016). Development and validation of a FIA/UV-vis method for pK(a) determination of oxime based acetylcholinesterase reactivators. *Journal of Pharmaceutical and Biomedical Analysis*, *117*, 240–246. https://doi.org/10.1016/j.jpba.2015.09.010

Perrin, D. D. (1972). *Dissociation constants of organic bases in aqueous solution. IUPAC chemical data series: Supplement 1972*. London: Butterworths.

Sangster, J. (1997). *Octanol-water partition coefficients: Fundamentals and physical chemistry*. Chichester, UK: Wiley.

Scheltens, P., Blennow, K., Breteler, M. M. B., de Strooper, B., Frisoni, G. B., Salloway, S., & Van der Flier, W. M. (2016). Alzheimer's disease. *Lancet*, *388*(10043), 505–517. https://doi.org/10.1016/s0140-6736(15)01124-1

Skibinski, R., Czarnecka, K., Girek, M., Bilichowski, I., Chufarova, N., Mikiciuk-Olasik, E., & Szymanski, P. (2018). Novel tetrahydroacridine derivatives with iodobenzoic acid moiety as multifunctional acetylcholinesterase inhibitors. *Chemical Biology & Drug Design*, *91*(2), 505–518. https://doi.org/10.1111/cbdd.13111

Sulochana, S. P., Sharma, K., Mullangi, R., & Sukumaran, S. K. (2014). Review of the validated HPLC and LC-MS/MS methods for determination of drugs used in clinical practice for Alzheimer's disease. *Biomedical Chromatography*, *28*(11), 1431–1490. https://doi.org/10.1002/bmc.3116

Tetko, I. V., Gasteiger, J., Todeschini, R., Mauri, A., Livingstone, D., Ertl, P., … Prokopenko, V. V. (2005). Virtual computational chemistry laboratory - design and description. *Journal of Computer-Aided Molecular Design*, *19*(6), 453–463. https://doi.org/10.1007/s10822-005-8694-y

The Merck Index: An Encyclopedia of Chemicals, Drugs, and Biologicals, 14th ed. (2006). In M. J. O'Neil, P. E. Heckelman, C. B. Koch, & K. J. Roman (*Eds.*). Whitehouse Station, NJ: Merck and Co., Inc.

Wager, T. T., Hou, X. J., Verhoest, P. R., & Villalobos, A. (2010). Moving beyond Rules: The Development of a Central Nervous System Multiparameter Optimization (CNS MPO) Approach To Enable Alignment of Druglike Properties. *ACS Chemical Neuroscience*, *1*(6), 435–449. https://doi.org/10.1021/cn100008c

Zhang, C., Du, Q. Y., Chen, L. D., Wu, W. H., Liao, S. Y., Yu, L. H., & Liang, X. T. (2016). Design, synthesis and evaluation of novel tacrine-multialkoxybenzene hybrids as multi-targeted compounds against Alzheimer's disease. *European Journal of Medicinal Chemistry*, *116*, 200–209. https://doi.org/10.1016/j.ejmech.2016.03.077

Zhang, F. L., Xue, J. P., Shao, J. W., & Jia, L. (2012). Compilation of 222 drugs' plasma protein binding data and guidance for study designs. *Drug Discovery Today*, *17*(9–10), 475–485. https://doi.org/10.1016/j.drudis.2011.12.018



**How to cite this article:** Kręcisz P, Czarnecka K, Szymański P. Physicochemical evaluation of new tetrahydroacridine and iodobenzoic acid hybrids as the next step in the design of potential drugs for treating Alzheimer's disease. *Biomedical Chromatography*. 2020;34:e4906. https://doi.org/10.1002/bmc.4906

## Publikacja 2

Journal of Chromatographic Science, 2021, 1–6
https://doi.org/10.1093/chromsci/bmab097
Article

Article

# Thin-Layer Chromatography Gradient Optimization Strategy for Wet Load Adsorption Flash Chromatography

**Paweł Kręcisz[1], Kamila Czarnecka[1,2], and Paweł Szymański[1,2,*]**

[1]Department of Pharmaceutical Chemistry, Drug Analysis and Radiopharmacy, Medical University of Lodz, ul. Muszyńskiego 1, 90-151 Łódź, Poland, and [2]Department of Radiobiology and Radiation Protection, Military Institute of Hygiene and Epidemiology, 4 Kozielska St., 01-163 Warsaw, Poland

*Author to whom correspondence should be addressed. Email: pawel.szymanski@umed.lodz.pl

Received 11 November 2020; Editorial Decision 5 July 2021

**Abstract**

Chromatography is one of the most popular methods for the separation of compounds in modern pharmaceutical industry and science. Despite the extensive use of the reversed phase chromatography in analytical and preparative applications, the normal phase adsorption chromatography has a special place in purifying post-reaction mixtures or the separation of natural extracts, especially in wet load mode, because of simplicity and high velocity of preparation. Complex mixtures, more difficult to separate, require gradient methods to obtain better results of separations. These methods can be developed by external software, but the automatic methods are often not very accurate and the negative impact of wet load application on separation quality is considerable in them. Therefore, we present the thin-layer chromatography (TLC) gradient optimization strategy for wet load separations to obtain repeatable results of separations for different compounds without worrying about negative impact of wet loading on separation quality. The strategy provides information about an elution model of desired compound, which is used to develop the gradient method. The strategy also allows to standardize the separation length, because gradient methods performed by the TLC gradient optimization strategy have a very similar duration time in column volumes. The method can also be simply scaled because of using the column volume as a base unit in calculations.

## Introduction

Chromatography is a widely used technique in modern pharmaceutical industry. Despite the fact that reversed phase mode chromatography is the technique of choice for analytical and very often preparative separations, the normal phase mode has several practical advantages for preparative separations in pharmaceutical chemistry. Normal phase chromatography is most suitable for separation of high hydrophobic substances, for example, medicine structures that are very lipophilic and are not in hydrochloride form just after synthesis. Normal phase chromatography allows to simplify the purification procedure because it is not required to extract the results of synthesis and pretreat them to solute into a polar solvent, which is suitable for reverse phase chromatography. Moreover, sometimes it is nearly impossible to perform the purification procedure without creating additional impurities because numerous medicine structures are insoluble in water without any modifications. In the normal phase condition, the sample can only be initially purified by crystallization or simple extraction and injected directly on a normal phase column in preferably a nonpolar solvent. Normal phase chromatography is a technique of choice for natural extract analysis and preparations (1–3). This technique is also applicable for separation of small peptide compounds, but preparative reverse phase high performance liquid chromatography (RP HPLC) or hydrophilic interaction liquid chromatography are techniques of choice in peptide separations because of the hydrophilic character of peptide structures (4).

Normal phase adsorption chromatography is the oldest liquid chromatography mode. The first description of gradient elution theory was presented by Snyder in 1964 (5). Jandera developed the Snyder theory in 1974 and derived a formula of model of the gradient elution in binary normal phase adsorption chromatography (Eq. 1).

$$k' = k'_0 x_b^{-m} \quad (1)$$

Where $k'$ is a retention factor in the mixture of two solvents, $k'_0$ is a retention factor in pure strong solvent B, $x_b$ is the mole fraction of the strong solvent B in the mixture and $m$ is a stoichiometric coefficient characterizing the number of molecules of the strong solvent B necessary to displace one adsorbed molecule of the eluted compound. $k'_0$ and $m$ are unique for any compound. This formula provides information about the shape of elution in normal phase conditions and is very useful for method development (6, 7).

Normal phase chromatography is a method where two modes of applying the sample on the column, wet load and dry load, can be used. Both methods have some advantages and disadvantages. Wet loading is a very fast and simple method of sample loading, but too large amounts of solvent can result in band broadening and loss of resolution (8). Moreover, when a compound is barely soluble in a weak solvent and the addition of strong solvent is needed, the problems can be more challenging. Dry loading provides very good separations and eliminates problems with an amount and type of sample solvents, but the procedure of sample preparation is more complex and longer. It can also lead to some loss of the sample mass or even structure decomposition during drying sample/adsorbent mix. Samples are most commonly wet loaded on columns in pharmaceutical chemistry, but dry load technique is irreplaceable in some cases (9).

The TLC optimization of flash separation is a well-known and recommended procedure to obtain successful separations and pure chemical compounds. The calculations for the development of the isocratic adsorption chromatography method are very simple and based on the relationship between the retention factor ($R_f$) and column volume (CV) (Eq. 2). It is also recommended by producers of flash chromatography equipment in their guidelines. The separations of complex mixtures are very difficult using the simple isocratic chromatography method because it is not possible to determine the solvent system in which most of the components of the mixture will obtain $R_f$ between 0.1 and 0.3 with appropriate resolution, especially if there are many components of the mixture. In this case, the gradient method is recommended and the development of gradient method is most commonly performed by software of apparatuses, which are not precise in complex and difficult separations. Therefore, the studies about the TLC optimization of gradient flash method have been started. In this study, we present the TLC optimization strategy to develop a gradient adsorption method in normal phase using wet loading technique, which can be successfully used for separations of complex mixtures including those containing alkaline compounds, such as drug structures containing an amine moiety or natural extracts. The strategy is based on the combination of a gradient elution model developed by Jandera and $R_f$/CV relationship used in the TLC optimization of isocratic method. The strategy is also available to be applied without external commercial software and does not require any additional equipment to be performed.

## Materials and Methods

### Reagents and equipment

Methanol, chloroform, water solution of ammonia 30% (ChemSolve) were used as components of the mobile phase. Strong solvent was a mixture of methanol and water solution of ammonia 30% (10:0.5, v/v). Weak solvent was a pure chloroform. PuriFlash 430 with software version V5.0b.09 (Interchim) was used to perform all flash separations. Interchim SIHP 4G 15U, 30U columns and SIHC 4G 50U columns were used. Varian DASI 12G module with empty DASI columns was used for dry load separations. RV 10 Digital and HB 10 digital (IKA) rotavap set were used to prepare a sample for dry load. Silica gel 60 for column chromatography (Aldrich) was used for dry load sample preparation. TLC Silica gel 60 F254 plates (Merck) were used for the TLC optimization. UV 4 cabinet (Camag) was used to visualize TLC plates. All TLC plate measurements and calculations were performed by GIMP 2.0 (free license) and MS Excel (Microsoft).

### Methodology

The standard TLC optimization of isocratic flash method recommended by the Interchim Purification Guide requires finding the proper composition of the mobile phase to obtain $R_f$ value of the tested compound about 0.1–0.3. $R_f$ is calculated to CV using the formula:

$$CV = \frac{1}{R_f} \quad (2)$$

CV is a predicted number of column volumes required to elute the tested compound. Flash technique is a method of separations of mixtures; therefore, it is important to calculate the quality of planned separation. Therefore, $R_f$ and CV values for all components of mixture should be calculated and obtained $\Delta R_f$ and $\Delta$CV using formulas:

$$\Delta R_f = R_{fB} - R_{fA} \quad (3)$$

$$\Delta CV = CV_B - CV_A \quad (4)$$

Where $R_{fA}$ and $R_{fB}$ or $CV_A$ and $CV_B$ are values calculated for particular components of mixtures. Acceptance criteria of $\Delta$CV value for possible separation is no less than 1. A bigger value of $\Delta$CV predicts an easier and better separation. The TLC optimization should be done by using the same type of stationary phase, for example silica or alumina for normal phase separations.

The first step of the TLC optimization of the gradient wet load flash method is in line with the Interchim Purification Guide. The basic optimization should be done for the most important compound in the mixture. $\Delta$CV between the most important compound and the nearest substances should be greater than 1. If the separation procedure predicts wet load, the weak solvent should not be able to elute the most important component of mixture. Analysis of minimum five TLC plates, where the percentage amount of strong solvent increases, should provide the information about the elution model of mixture components (Figure 1).

TLC plates provide data about $R_f$ and CV of the most important compound. CV values and the percentage amount of strong solvent should be plotted. The function formula was calculated by MS Excel regression tools. Function CV versus percentage amount of strong solvent shows the properties of a power function:

$$\varphi = \varphi_0 x^d \quad (5)$$

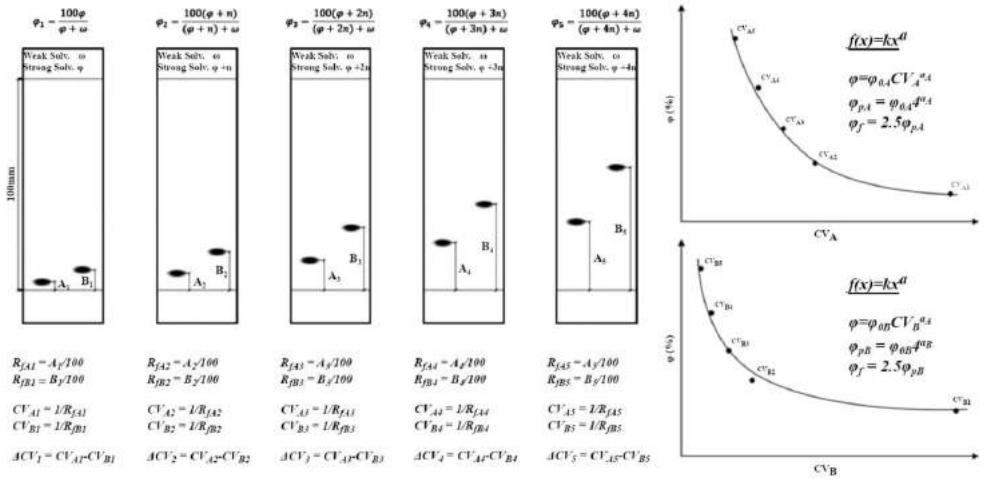


**Figure 1.** Scheme of the TLC gradient strategy optimization methodology.

Where $\varphi$ is the percentage amount of strong solvent, $x$ is a number of CV, $\varphi_0$ is the percentage amount of strong solvent that elutes the compound in 1 CV in isocratic conditions, $a$ is an exponent and it is always a negative number. $\varphi_0$ and $a$ value are unique for any compound. The obtained formula strongly corresponds with the Jandera model of linear elution adsorption chromatography in the normal phase mode (Eq. 1). Our formula corresponds to the shape of Jandera elution model (power function) and the character of constants—$k'_0$, $m$ in the Jandera model and $\varphi_0$, $a$ in our formula are unique for any compound and both constants $m$ and $a$ have to be negative numbers in both formulas. In the same time, our formula strongly corresponds to the isocratic TLC optimization and the $R_f$/CV relationship because CV is one of the variables. The second variable is $\varphi$, which has a very similar relationship to $\varphi_0$ as $k'$ to $k'_0$ in the Jandera model, despite the fact that our formula does not consider the calculation of retention factors but the percentage amount of strong solvent.

The perfect percentage amount of strong solvent ($\varphi_P$) in the mobile phase (for CV = 4.00 and $R_f$ = 0.25) can be calculated using the formula (5). The obtained $\varphi_P$ value should be multiplied by 2.5 resulting in the final percentage amount of strong solvent ($\varphi_f$) in the gradient method to obtain a chromatographic peak about 15 CV–20 CV.

The gradient should be started from 0% of strong solvent for 2 CV, than the gradient from 0% to calculated $\varphi_f$ should be set from CV = 2 to CV = 20. If it is necessary, the $\varphi_f$ value or gradient can be extended to elute difficult substances completely.

### Sample preparation

Sample dry mass was equal 1% of silica in a flash column—about 40 mg. The samples were mixtures of carbamazepine and tacrine HCl or carbamazepine and thioridazine HCl. Experiments were performed by using the wet load and dry load techniques. The dry mass was solved in a 200 µL mixture of chloroform/methanol (150 µL + 50 µL) for wet load, because of weak solubility of compounds in pure chloroform. The dry mass was solved in a small amount chloroform/methanol mixture, four times greater mass of dry silica gel was added and dried using rotavap for dry load. Dry silica with the absorbed sample was put in the empty DASI column and prepared for separation.

### Separation conditions

Three separation conditions were performed. The first one was developed according to our methodology where $\varphi_f$ was calculated for thioridazine HCl:carbamazepine (1:1) mix and tacrine HCl:carbamazepine (1:1) mix. The second separation was an automatic method for wet load performed by apparatus software. The third separation was an automatic method for dry load performed by apparatus software. Two detection wavelengths were set, each one for the specific maximum absorption value of compounds in the sample: 240 nm/285 nm for tacrine HCl:carbamazepine mix and 265 nm/285 nm for thioridazine HCl:carbamazepine mix. The threshold was set at 50 mAu. The flowrate was set at 7 mL/min according to the producer's guidelines. Column conditioning was performed with pure chloroform for 6 CV before each separation.

## Results

### Analysis of previous collected data and development of theoretic methodology

Analysis of preparative separations performed during work on previous studies provided a lot of chromatographic data, which were used for the development of our methodology (10, 11). A series of TLC separations indicated that all compounds among a series of derivatives elute in a very similar manner. The result of analysis of these collected data was the formula shown in Methodology section (Eq. 5) While working on the purification of a series of homologous tetrahydroacridine and 3,5-dichlorobenzoic acid derivatives to our previous study (12), we developed linear gradient methods based on our experience with work on tacrine derivatives, which allowed us

**Table I.** The Comparison of $\varphi_f^{exp}$ with $\varphi_P$ to Calculate the Multiplier Factor Allowing the Development of Reliable Separation Methods

| Compound name (IUPAC) | $\varphi_P$ (%) | *Rt* (CV) | $\varphi_f^{exp}$ (%) | $\varphi_f^{exp}/\varphi_P$ |
|---|---|---|---|---|
| 3,5-dichloro-N-{5-[(1,2,3,4-tetrahydroacridin-9-yl)amino]pentyl}benzamide | 15.70 | 15.65 | 42.00 | 2.67 |
| 3,5-dichloro-N-{6-[(1,2,3,4-tetrahydroacridin-9-yl)amino]hexyl}benzamide | 15.36 | 15.75 | 35.00 | 2.30 |
| 3,5-dichloro-N-{7-[(1,2,3,4-tetrahydroacridin-9-yl)amino]heptyl}benzamide | 14.42 | 14.75 | 35.00 | 2.43 |
| 3,5-dichloro-N-{8-[(1,2,3,4-tetrahydroacridin-9-yl)amino]octyl}benzamide | 13.36 | 14.70 | 32.00 | 2.39 |
| | | Average | | 2.44 |

to obtain relatively similar separations in terms of elution time and separation quality. Each separation lasted about 20 CV and started by 2 CV of a pure weak solvent. The next step was performing the procedure according to our methodology and comparing calculated values of $\varphi_P$ with the experimental maximum gradient value of strong solvent ($\varphi_f^{exp}$). The comparison was shown in Table I.

The comparison of $\varphi_f^{exp}$ with $\varphi_P$ indicates that $\varphi_P$ multiplied by 2.5 should allow to obtain a suitable value of $\varphi_f$; therefore, the multiplier 2.5 was added as the last factor used in our TLC gradient optimization strategy. The whole homologous series was successfully purified using the TLC gradient optimization strategy (12).

### Examination of the TLC methodology

The next step was the analysis of this strategy on different known compounds, not belonging to the homologous series, to check whether the method can be applied in different separation procedures. Three substances were chosen (tacrine HCl, carbamazepine and thioridazine HCl) because of their specific elution pattern in our solvent system and weak solubility in pure chloroform of hydrochloride form of compounds to simulate difficult samples for the separation using the wet load technique. Mixtures of tacrine HCl + carbamazepine and thioridazine HCl + carbamazepine were performed to examine our optimization strategy. The series of TLC plates (Figure 2) for both mixtures was performed. Both mixtures did not elute in pure chloroform. ΔCV between tacrine HCl and carbamazepine is always great, and this mix simulates the situation, in which a real post-reaction mixture would be composed of a few widely spread components on TLC plate. ΔCV between thioridazine HCl and carbamazepine is suitable for flash separation in this system solvent, but these compounds are very sensitive to very small changes in the amount of strong solvent. This mix was designed to examine the wet load impact on separation quality. The analysis of TLC plates performed in accordance with our strategy showed that the result was always a power function with various values of $\varphi_0$ and $a$. Results of five TLC plates were sufficient to obtain a formula that can be successfully used, but more TLC separations can improve the accuracy of calculations. The results of these calculations are shown in Figure 3. Both regression lines obtained from TLC results had $R^2$ value greater than 0.95. $\varphi_P$ was determined experimentally according to our methodology. $\varphi_f$ for the mixture was calculated for the compound which elutes slower, i.e., tacrine HCl and thioridazine HCl. Obtained curve for thioridazine HCl increased significantly faster than curve for tacrine HCl, that means thioridazine HCl is more sensitive for small changes of strong solvent content in mobile phase than tacrine HCl. This knowledge about the elution pattern allows to develop a very precise gradient separation.

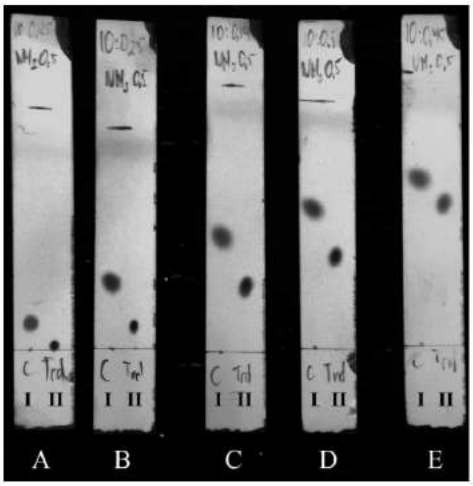


**Figure 2.** TLC plates of separations of carbamazepine and thioridazine with an increasing percentage amount of strong solvent. I—carbamazepine, II—thioridazine. Strong solvent %: A—1%; B—2%; C—4%; D—5%; E—7%.

### Examination of the strategy on flash chromatography columns

The second step in the examination of the strategy concerned the procedure of performing wet load separations on 4G silica columns with different particle sizes (15U, 30U, 50U) and the comparison of the results with automatic wet load method separation on 4G 30U silica column. Columns were changed and conditioned with chloroform for 6 CV, before each run. All separations performed according to TLC gradient optimization strategy were successful. Both compounds were well separated with good resolution and sharp peak shapes. Tacrine HCl peak was localized always about $CV = 16 \pm 1.5$, as the method predicted. Very light peak tailing can be noticed on all chromatographs. 30U column separation indicates the greatest peak tailing, but this fact may be due to the properties of the column being used, because 15U and 50U chromatograms are very similar (Supplementary Figures S1–S3). The automatic wet load

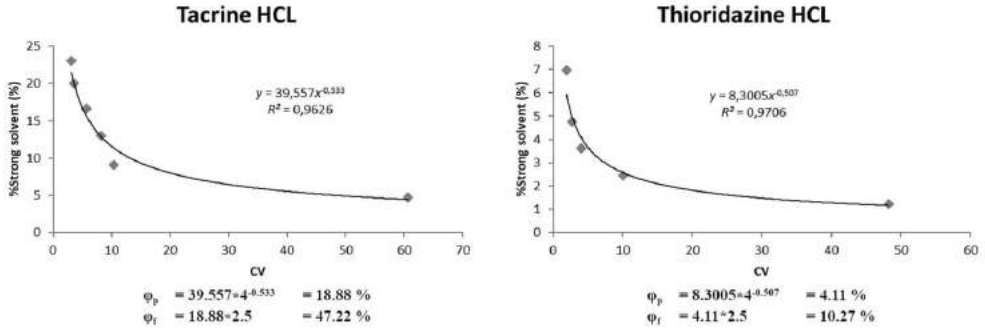


**Figure 3.** Calculation plots of slower eluted compounds in the tested mixtures.

method also provides quite a sharp peak of tacrine HCl and high resolution separation between mix components, but very advanced tailing of carbamazepine peak indicates probable problems in the separation of more complex mixtures (Supplementary Figure S4). The same compound mix was used to examine the TLC gradient optimization strategy in the dry load technique. In this case, the separation was performed in the same conditions on 4G 30U silica column, but load method was changed and the results were compared to results of the automatic dry load method separation. Samples of both separations were prepared according to the same procedure. The results of both separations were satisfactory, the resolution was acceptable and peaks were sharp. Moreover, the experiment provided information about unexpected decomposition of tacrine HCl. Both separation methods revealed the additional peak before tacrine HCl peak, but the automatic method provided a better resolution between these two peaks. However, the TLC gradient optimization strategy provided a better resolution between tacrine HCl and carbamazepine, which is promising for complex mixtures (Supplementary Figures S5 and S6).

### *Examination of wet load impact*

The last phase of the examination of the TLC gradient optimization strategy was the study of wet load impact on separation quality. In this case, thioridazine HCl + carbamazepine mix (1:1) was used as a sample for wet load separation. The separation was performed on 4G 30U silica column and according to the previously calculated gradient pattern. The result revealed a small wet load impact on separation quality. Thioridazine HCl + carbamazepine mix (1:1) was a sample which should be separated by the isocratic method, due to its sensitivity to changes of strong solvent amount, but the gradient method separated both components with acceptable resolution (Supplementary Figure S7). The shape of carbamazepine peak was symmetric and sharp, but the peak of thioridazine HCl showed significant tailing and the retention time of this substance is greater than suspected. It may be caused due to specificity of this mixture in our solvent system (fast elution in small amount of strong solvent); therefore, our experimentally determined factor of the maximum gradient (2.5) may need to be modified in gradients with low maximum percentage of strong solvent.

Finally, the TLC gradient optimization strategy was also used in purifying compounds after synthesis in our previous articles (12–14). The flash purifying procedure performed according to this method provided pure compounds, which has been confirmed by HPLC, NMR and LC–MS analysis.

## Conclusion

In this study, the methodology was examined on two mixtures of compounds, on flash silica columns with different particle sizes and with two different load methods. The TLC gradient optimization strategy allows to obtain the peak of the most important compound in $CV = 17.50 \pm 2.5$ with appropriate resolution. Test results have shown that the method can be used to separate complex mixtures, such as natural extracts or post-reaction mixtures. Separation quality is comparable between wet and dry load technique, which allows to apply the wet load technique for sensitive compounds or substance with low solubility in pure weak solvent without worrying about separation quality. Moreover, the gradient method allows to obtain peaks of other components of the mixture performing single separation and standardize the separation length without using any additional licensed software. The results of experiments have proven a high correspondence to the normal phase elution theory proposed by Jandera, which is the evidence of reliability of this optimization strategy and which could be successfully used in separation procedures in pharmaceutical science.

## Supplementary data

Supplementary data are available at *Journal of Chromatographic Science* online.

## Conflict of interest statement

The authors have declared no conflict of interests.

## References

1. Jandera, P.; Can the theory of gradient liquid chromatography be useful in solving practical problems? *Journal of Chromatography A*, (2006); 1126(1–2): 195–218. 10.1016/j.chroma.2006.04.094.
2. de Araujo, D.R.C., da Silva, T.D., Harand, W., Lima, C.S.D., Neto, J.P.F., Ramos, B.D. *et al.*; Bioguided purification of active compounds from leaves

of *Anadenanthera colubrina* var. cebil (Griseb.) Altschul; *Biomolecules*, (2019); 9(10): 14. 10.3390/biom9100590.

3. Diaz, J.G., Tuenter, E., Arranz, J.C.E., Maury, G.L., Cos, P., Pieters, L.; Antimicrobial activity of leaf extracts and isolated constituents of *Croton linearis*; *Journal of Ethnopharmacology*, (2019); 236: 250–257. 10.1016/j.jep.2019.01.049.
4. Lawton, L.A., McElhiney, J., Edwards, C.; Purification of closely eluting hydrophobic microcystins (peptide cyanotoxins) by normal-phase and reversed-phase flash chromatography; *Journal of Chromatography A*, (1999); 848(1–2): 515–522. 10.1016/s0021-9673(99)00462-8.
5. Synder, L.R.; Linear elution adsorption chromatography. 7. Gradient elution theory; *Journal of Chromatography*, (1964); 13: 415–434.
6. Jandera, P., Churacek, J.; Gradient elution in liquid-chromatography. 1. Influence of composition of mobile phase on capacity ratio (retention volume, band width, and resolution) in isocratic elution - theoretical considerations; *Journal of Chromatography*, (1974); 91: 207–221. 10.1016/s0021-9673(01)97901-4.
7. Jandera, P., Churacek, J.; Gradient elution in liquid-chromatography. 2. Retention characteristics (retention volume, band width, resolution, plate number) in solvent-programmed chromatography - theoretical considerations; *Journal of Chromatography*, (1974); 91: 223–235. 10.1016/s0021-9673(01)97902-6.
8. Jin, G.W., Guo, Z.M., Xiao, Y.S., Yan, J.Y., Dong, X.F., Shen, A.J. *et al.*; Practical method for the definition of chromatographic peak parameters in preparative liquid chromatography; *Journal of Separation Science*, (2016); 39(20): 3917–3926. 10.1002/jssc.201600579.
9. Stevens, W.C., Hill, D.C.; General methods for flash chromatography using disposable columns; *Molecular Diversity*, (2009); 13(2): 247–252. 10.1007/s11030-008-9104-x.
10. Czarnecka, K., Lisiecki, P., Szewczyk, E., Chufarova, N., Wójtowicz, P., Kręcisz, P. *et al.*; New acridine derivatives as promising agents against methicillin-resistant staphylococci – From tests to in silico analysis; *Computational Biology and Chemistry*, (2020); 88: 107321. 10.1016/j.compbiolchem.2020.107321.
11. Czarnecka, K., Girek, M., Krecisz, P., Skibinski, R., Latka, K., Jonczyk, J. *et al.*; Discovery of new Cyclopentaquinoline analogues as multifunctional agents for the treatment of Alzheimer's disease; *International Journal of Molecular Sciences*, (2019); 20(3): 22. 10.3390/ijms20030498.
12. Czarnecka, K., Girek, M., Wójtowicz, P., Kręcisz, P., Skibiński, R., Jończyk, J. *et al.*; New tetrahydroacridine hybrids with dichlorobenzoic acid moiety demonstrating multifunctional potential for the treatment of Alzheimer's disease; *International Journal of Molecular Sciences*, (2020); 21(11): 3765. 10.3390/ijms21113765.
13. Zawada, K., Czarnecka, K., Girek, M. *et al.*; New hybrids of tacrine and indomethacin as multifunctional acetylcholinesterase inhibitors; *Chemical Papers*, (2021); 75: 249–264. https://doi.org/10.1007/s11696-020-01295-y.
14. Krecisz, P., Czarnecka, K., Szymanski, P.; Physicochemical evaluation of new tetrahydroacridine and iodobenzoic acid hybrids as the next step in the design of potential drugs for treating Alzheimer's disease; *Biomedical Chromatography*, (2020); 34(10): e4906. 10.1002/bmc.4906.

Supplementary materials

# Thin layer chromatography gradient optimization strategy for wet load adsorption flash chromatography

Paweł Kręcisz[1], Kamila Czarnecka[1], Paweł Szymański*[1]

[1] Department of Pharmaceutical Chemistry, Drug Analysis and Radiopharmacy, Medical University of Lodz, ul. Muszyńskiego 1, 90-151 Łódź, Poland

* Corresponding author

Email address: pawel.szymanski@umed.lodz.pl

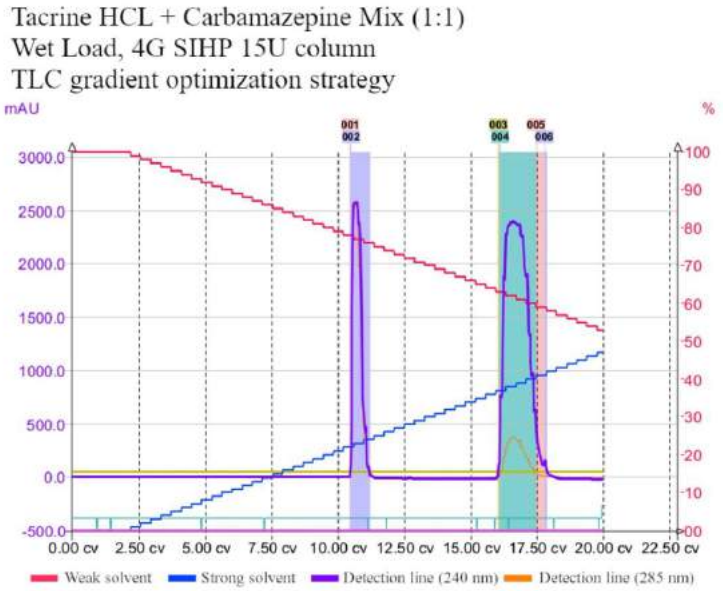


**Figure S1.** Chromatogram of Tacrine HCl and Carbamazepine mixture using wet load method optimized with TLC gradient optimization strategy on a 4G, 15U, SIHP flash column.

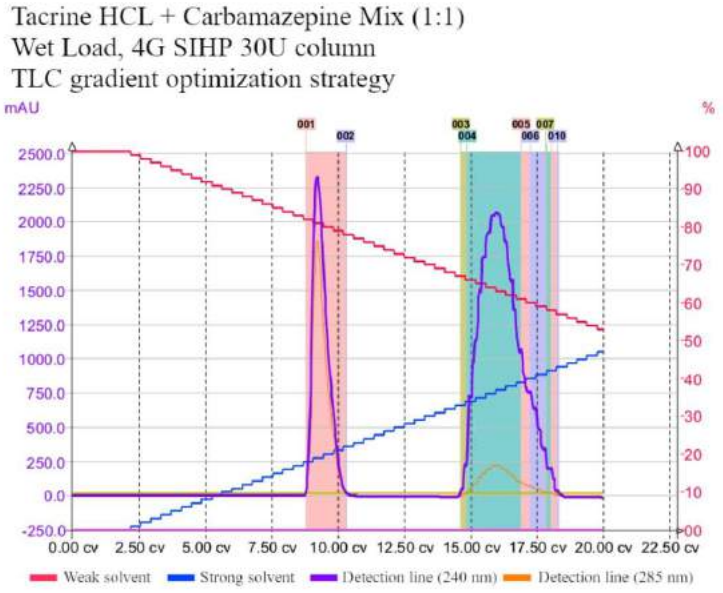


**Figure S2.** Chromatogram of Tacrine HCl and Carbamazepine mixture using wet load method optimized with TLC gradient optimization strategy on a 4G, 30U, SIHP flash column.

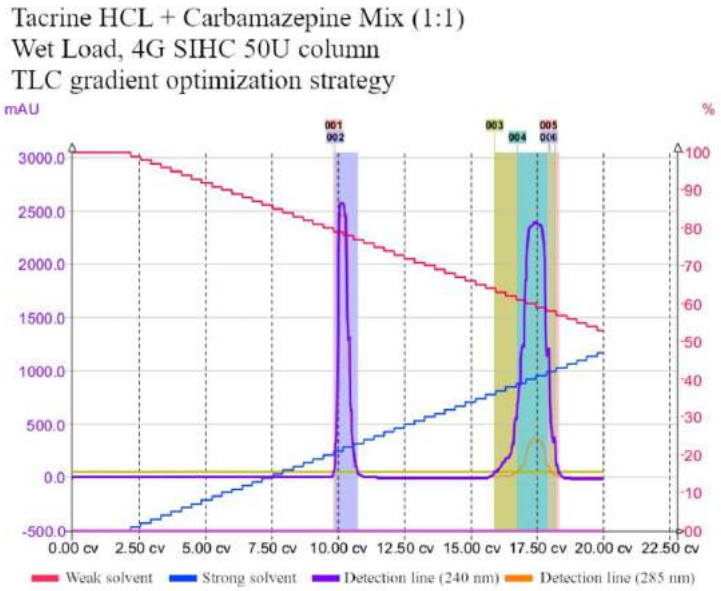


**Figure S3.** Chromatogram of Tacrine HCl and Carbamazepine mixture using wet load method optimized with TLC gradient optimization strategy on a 4G, 50U, SIHP flash column.

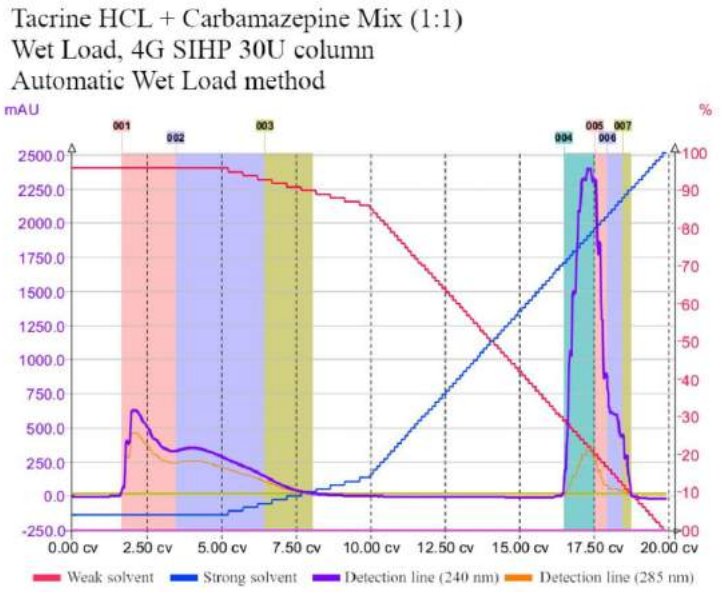


**Figure S4.** Chromatogram of Tacrine HCl and Carbamazepine mixture using wet load method optimized with apparatus software on a 4G, 30U, SIHP flash column.

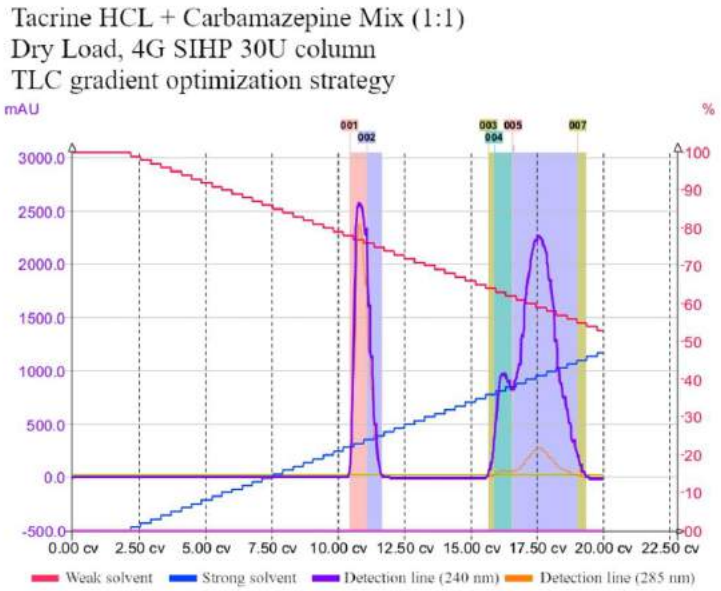


**Figure S5.** Chromatogram of Tacrine HCl and Carbamazepine mixture using dry load method optimized with TLC gradient optimization strategy on a 4G, 30U, SIHP flash column.

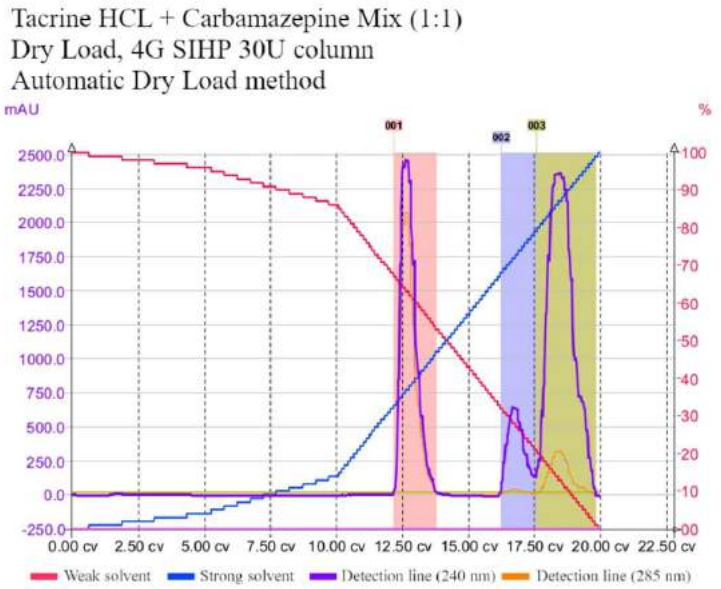


**Figure S6.** Chromatogram of Tacrine HCl and Carbamazepine mixture using dry load method optimized with apparatus software on a 4G, 30U, SIHP flash column.

## Publikacja 3

Bioconjugate Chemistry

pubs.acs.org/bc

Review

# Radiolabeled Peptides and Antibodies in Medicine

Paweł Kręcisz, Kamila Czarnecka, Leszek Królicki, Elżbieta Mikiciuk-Olasik, and Paweł Szymański*

Cite This: *Bioconjugate Chem.* 2021, 32, 25−42

Read Online

ACCESS | Metrics & More | Article Recommendations | Supporting Information

**ABSTRACT:** Radiolabeled peptides are a relatively new, very specific radiotracer group, which is still expanding. This group is very diverse in terms of peptide size. It contains very small structures containing several amino acids and whole antibodies. Moreover, radiolabeled peptides are diverse in terms of the binding aim and therapeutic or diagnostic applications. The majority of this class of radiotracers is utilized in oncology, where the same structure can be used in therapy and diagnostic imaging by varying the radionuclide. In this study, we collected new reports of radiolabeled peptide applications in diagnosis and therapy in oncology and other fields of medicine. Radiolabeled peptides are also increasingly being used in rheumatology, cardiac imaging, or neurology. The studies collected in this review concern new therapeutic and diagnostic procedures in humans and new structures tested on animals. We also performed an analysis of clinical trials, which concerns application of radiolabeled peptides and antibodies that were reported in the clinicaltrials.gov database between 2008 and 2018.

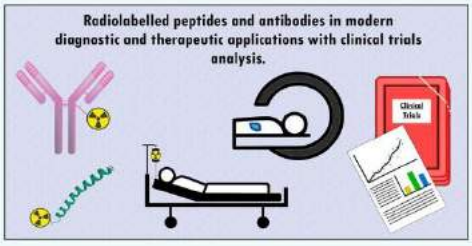


## INTRODUCTION

Peptides are one of the principal element of all known living systems. They are responsible for many biological functions including, but not limited to, neurotransmission, ion-channel regulation, and regulation of cell growth. The special place in the group of amino acid structures is occupied by antibodies, which are characterized by exceptional selectivity and precision of targeting with the ability to determine biological activity. The wide-ranging applications of peptides and antibodies in medicine are well-known. Because of its multifunctionality, common-ness in the human body, and precise targeting to a specific place of bonding in an organism, peptides and antibodies were considered very promising diagnostic and therapeutic agents or carriers of structures that fulfill these roles. Therefore, radiolabeling of peptides and antibodies was the natural direction for improvement of diagnostic techniques and medical procedures.

The first radiolabeled peptide used in humans was the somatostatin analogue $^{123}$I-204-090 developed by Krenning et al. in 1989,[1,2] and the first radiolabeled peptide approved by US Food and Drug Administration (FDA) was $^{111}$In-DTPA-octreotide ($^{111}$In-pentetreotide, $^{111}$In-DTPA-octreotide, OctreoScan). OctreoScan has been used in the diagnosis of neuroendocrine tumors since its approval in 1994. The next diagnostic radiolabeled peptide compound approved by the FDA was $^{111}$In-capromab pendetide (ProstaScint) in 1996. It is an $^{111}$indium radiolabeled murine monoclonal antibody (7E11-C5.3) with Prostate Specific Membrane Antigen (PSMA) affinity, and it was used in prostate cancer patients with a high risk of pelvic lymph node metastases. ProstaScint was the first approved agent for use in radioimmunoscintigraphy as well as a key milestone in the development of radioimmunotherapy (RIT). The FDA first approved small synthetic radiolabeled peptides for use in receptor imaging in 1997—$^{99m}$Tc-Apcitide ($^{99m}$Tc-P280, AcuTect). AcuTect is a small technetium-$^{99m}$Tc-labeled peptide composed of two identical cyclic peptide monomers.[3] The compound binds with high affinity to the $GPII_b/III_a$ receptor on activated platelets, which in turn provide information about localization of thrombi anywhere in the body.[4] Therefore, AcuTect is used for scintigraphic imaging of acute venous thrombosis in the lower extremities of patients with symptoms of acute venous thrombosis. After 2000, the European Medicines Agency (EMA) approved the next radioimmunodiagnostic agent as well as the first radioimmunotherapeutic compound. $^{99m}$Tc-Besilesomab (Scintimun) is a murine anti-granulocyte antibody used for radionuclide imaging for determining the location of inflammation/infections in the peripheral bone of adults with suspected osteomyelitis. $^{90}$Y-Ibritumomab Tiuxetan (Zevalin ) is a murine $IgG_1$ antibody used in RIT of adult patients with rituximab relapsed or refractory CD20+ follicular B-cell in non-Hodgkin's lymphoma. The National Center For Nuclear Research POLATOM achieved in 2014 a local Polish approval

Received: November 11, 2020
Revised: December 2, 2020
Published: December 16, 2020







https://dx.doi.org/10.1021/acs.bioconjchem.0c00617
*Bioconjugate Chem.* 2021, 32, 25−42

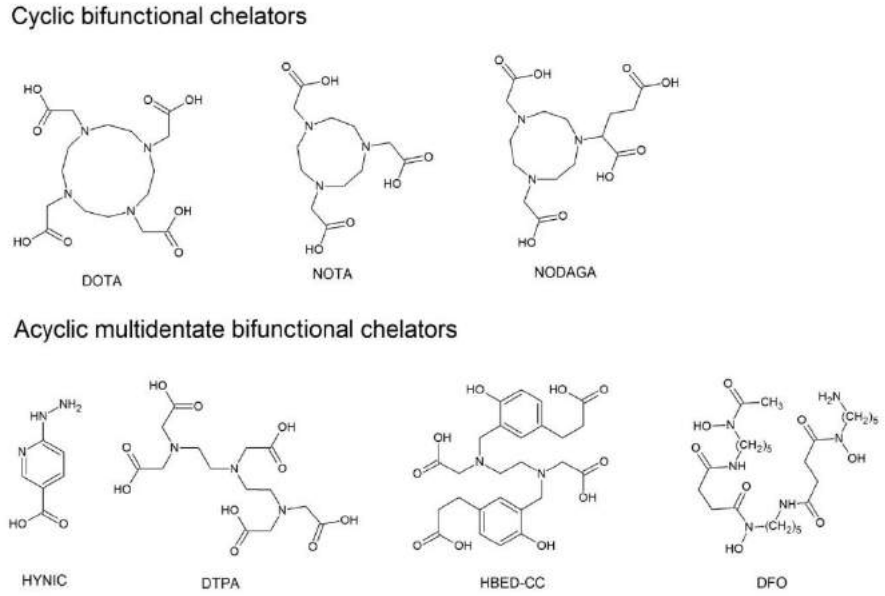


**Figure 1.** Basic structures of the most commonly BFCs used to radiolabeling peptides.

of diagnostic usage their $^{99m}$Tc-Human Immunoglobin ($^{99m}$Tc-HIG, Techimmuna) only in Poland. This agent is used to detect the location of inflammatory lesions and in semi-quantitative evaluations of inflammatory activity, particularly in the case of rheumatoid arthritis. In the past 3 years, the EMA has approved one diagnostic and one therapeutic radiolabeled somatostatin analogue. POLATOM—$^{99m}$Tc-HYNIC-octreotide ($^{99m}$Tc-HYNIC-[D-Phe$^1$,Tyr$^3$-octreotide]TFA, Tektreotyd)—has been nationally approved in 17 European countries in 2018. It is used in diagnosis and supports the therapy of tumors which overexpress somatostatin receptors as in the case of gastroenteropancreatic neuroendocrine tumors (GEP-NET). Another GEP-NET diagnostic agent was approved in 2016. It was $^{68}$Ga-edotreotide ($^{68}$Ga-DOTA$^0$-Phy$^1$-Tyr$^3$-octreotide, $^{68}$Ga-DOTA-TOC, SomaKit) and is the only approved radiolabeled peptide PET agent in Europe today. The newest therapeutic agent approved by both the FDA and EMA is $^{177}$Lu-oxodotreotide ($^{177}$Lu-DOTA-Tyr$^3$-octreotate, $^{177}$Lu-DOTA-TATE, Lutathera). It is used in the therapy of well differentiated neuroendocrine tumors.

**Peptides.** Radiolabeled peptides used in medicine are often modified variants of naturally occurring peptides, because the natural peptides are sensitive to peptidases, which rapidly break them down in blood and other tissues. Nowadays, it is possible to apply two main targeting strategies: peptide−receptor radionuclide therapy (PRRT), peptide−receptor scintigraphy (PRS), radioimmunoimaging (RII), and radioimmunotherapy (RIT). The first strategy is based on overexpression of various receptors in human cancer cells, which are attractive targets for imaging and therapy. Particularly interesting targets are somatostatin receptors (SSTRs), gastrin-release peptide receptors (GRPRs), $\alpha_V\beta_3$ integrin receptors, chemokine receptors 4 (CXCR4), or glucagon-like peptide 1 (GLP-1) receptors. A multiplicity of targets implies that the PRRT/PRS strategy has a wide spectrum of applications.[5] The second strategy is based on stable *in vivo* monoclonal antibodies (Mabs), or fragments of Mabs as ligands.[6,7]

**Methods of Labeling.** All ligands listed above require the addition of a radionuclide to achieve therapeutic or diagnostic goals. The labeling of peptides can be performed by direct labeling, addition of a prosthetic group, or with bifunctional chelators (BFCs). Direct labeling is the method used to label proteins without using intermediates such as BFCs. It can also be reduced to a one-step labeling protocol, which is an advantage for development of radiopharmaceutical kits and for short-lived radionuclide labeling. An example of this procedure is one-step direct $^{18}$F labeling by displacing a nitro group in an arene that is activated toward nucleophilic aromatic substitution by an ortho trifluoromethyl group.[8] Direct labeling technique nowadays involves mostly radioiodination and in some cases technetium-labeling.[9,10] Technetium direct labeling requires a specific structure of labeled agent coordination sphere, for example, with thiol groups, and reducing agents like phosphines.[11] The disadvantage of this method is that it necessitates a specific protocol for each radioligand as well as difficulty of developing accurate protocols to obtain highly specific products from each applied radionuclides.

Prosthetic groups are small molecules able to bind with radionuclides in one site of the structure, and simultaneously with a peptide at a second site. Radiolabeling peptides by using prosthetic groups is usually a two-step protocol—incorporation of the radionuclide in the prosthetic group structure, followed by binding the prosthetic group to peptide. Each step can be performed according to various methods. A review


https://dx.doi.org/10.1021/acs.bioconjchem.0c00617
Bioconjugate Chem. 2021, 32, 25−42

article published by Wilbur[12] provides an excellent overview of methods for labeling proteins by radiohalogens. Prosthetic groups allow us to label various peptides, because of the occurrence of multiple reactive functional groups incorporated into amino acid structures. Alcohols, amines, carboxylic acids, and thiols may be paired with the reactive site of a prosthetic group conjugated with a radionuclide to achieve the complete radiolabeled peptide.[13−15] A very effective method of $^{18}$F radiolabeling peptides by using prosthetic groups is the automated "fluorination on the Sep-Pak" method. This method was used in production 6-$^{18}$F Fluoronicotinic acid *N*-hydroxysuccinimide ester (6-[$^{18}$F]SFPy) and then radiolabeling T140 peptide−CXCR4 PET imaging ligand.[16] Another possible method for binding the prosthetic group to a peptide is modification of the peptide to bear unnatural bioorthogonal functional groups like an azide and then by using "click" chemistry to achieve the radiolabeled biomolecule.[17,18] Tolmachev et al. presented a large number of methods for binding prosthetic groups carrying various radionuclides to peptides in their review article.[9]

Despite many advantages, direct labeling and prosthetic groups have limits. These methods of labeling are the most suitable for diagnostic and therapeutic radiohalogens or $^{11}$C, given the reactivity of these nuclides. Radiometals, including $^{99m}$Tc, $^{68}$Ga, $^{64}$Cu, $^{177}$Lu, $^{111}$In, or $^{90}$Y, require BFCs to obtain the best conjugation of radionuclides with peptides. The bifunctional nature of the chelators means that they are capable of coordinating a metal ion and can also be attached to the peptide. Pendant labeling is the most commonly used method of labeling peptides in the present day. There are two main types of BFCs—cyclic BFCs and acyclic multidentate BFCs (Figure 1). 1,4,7,10-Tetraazacylododecane-1,4,7,10-tetraacetic acid (DOTA), 1,4,7,-triazacylononane-1,4,7-triacetic acid (NOTA), and 2-[4,7-bis(carboxymethyl)-1,4,7-triazonan-1-yl]-pentanedioic acid (NODAGA) are widely used cyclic BFCs to coordinate $^{111}$In, $^{67/68}$Ga, $^{64}$Cu, and $^{99m}$Tc, among others. Moreover, the most successful $^{18}$F labeling strategy was developed by McBride et al., which involves using an aluminum-[$^{18}$F]fluoride NOTA derivatives chelator system.[19] Cyclic BFCs are particularly interesting for scientists and medical practioners because of their universal usage. Peptides conjugated with cyclic BFC can be labeled by various radionuclides which, depending on the applied radionuclide, can provide structures used for therapeutic or diagnostic purposes. This allows for use of the same peptide compound in various imaging technique. Acyclic BFCs are less common than cyclic BFCs, but are still developed due to their selective high affinity for individual radionuclides and their ability to conjugate metal ions at room temperature, which is impossible when using only cyclic BFCs.[20,21] *N*,*N*′-Bis[2-hydroxy-5-(carboxyethyl)benzyl]ethylenediamine-*N*,*N*′-diacetic acid (HBED-CC) has high affinity to $Ga^{3+}$ ions.[22] 1,1,4,7,7-Diethylene triaminepentaacetic acid (DTPA) is applicable in $^{111}$In, $^{90}$Y, and $^{68}$Ga radiolabeling of thermosensitive peptides.[20,23−25] Desferoxamine (1-amino-6,17-dihydroxy-7,10,18,21-tetraoxo-27-(*N*-acetylhydroxylamino)-6,11,17,22-tetraazaheptaeicosane, DFO) is originally an iron and aluminum chelator, but DFO also complexes $Ga^{3+}$ ions rapidly[23] and is one of the best $^{89}$Zr carriers for labeling intact Mabs.[26] 2-Hydrazinonicotinic acid (HYNIC) is a well-known and commonly used $^{99m}$Tc carrier.[27,28] BFCs also have some disadvantages. BFC moieties are generally bulky, and as a result are usually located far away from the binding region of peptides to avoid steric interactions. BFCs are often placed at the N- or C-terminus of the peptide. Often, additional spacers are used, which increases the molecular weight of whole structure, an adverse fact especially for small peptides.[29] The labeling can influence charge or lipophilicity of the compound, which in turn may change its biodistribution or excretion, particularly for small ligands. The right selection of labeling method is therefore crucial to obtain appropriate resolution of images, concentration in tumors cells, and excretion methods with efficient clearance.[30]

**Radionuclides.** The type of radionuclide used is the third most important property of radiolabeled peptides. The radionuclides can be used for therapeutic or diagnostic purposes, and a small group of radionuclides may be used for both. Examples of these include theranostic radionuclides, $^{177}$Lu, $^{67}$Cu, and $^{111}$In.[31] Diagnostic radionuclides are used in molecular imaging modalities applied in nuclear medicine: SPECT and PET. Because of different mechanisms of action, each imaging method requires different radionuclides. Both modalities require the emission of photons in the form of radiation, which can be detected and processed into an image. However, this radiation has to originate from positron annihilation for PET imaging, while SPECT imaging require radionuclides that emit a direct gamma array with approximately 100−250 keV gamma energy, which is detected by scintillation detectors. Lower gamma energy produces too much scatter, but greater gamma energy than this range results in poor imaging quality due to difficulty in collimating the rays.[25] SPECT has an additional advantage in that it is possible to simultaneously image multiple radiometals emitting $\gamma$ rays with different energies.[32] PET imaging requires radionuclides which emit positrons. A single positron is formed during $\beta^+$ decay. The annihilation of positrons is pivotal for this modality of imaging, because this process generate two photons, each of 511 keV, in opposite directions. This phenomenon allows for determination of the location of annihilation in three dimensions by calculating the time difference between both photons reaching the detectors. Additional simultaneously emitted $\gamma$ rays from radionuclides are also filtrated, because only two precisely opposed rays—an interesting result of annihilation are used to image generation. The mean free path of a positron is one of the most important properties of radionuclides used in PET imaging. Short mean free paths provide increased image resolution. Mean free energy emitted from positron emission can influence on resolution; therefore, radionuclides with small positron energy produce higher resolution. In addition, mean free energy affects the surrounding tissues.[21] The half-life of radionuclides is the most significant property to be understood, independent from the radionuclide's purpose. Half-lives should be long enough to allow the peptide to accumulate in the target and clear from other compartments. Short-lived radionuclides are usually used in imaging especially because using small peptides tends to show fast biodistribution and clearance. Longer-lived radionuclides are used in imaging with peptides with long biodistribution and clearance and in therapy.[9] The most common in radionuclides are shown in Table 1.

## NEW REPORTS OF RADIOLABELED AMINO ACID BASED MOLECULES USED IN NUCLEAR MEDICINE

**SSTR.** Somatostatin receptors (SSTR) are neuroreceptors at the cell membrane, which may be used for diagnostic and


https://dx.doi.org/10.1021/acs.bioconjchem.0c00617
Bioconjugate Chem. 2021, 32, 25−42

**Table 1. Physical Characterization of Radionuclides Used in Radiolabeling Peptides**[21,33−36]

| nuclide | half-life | decay mode | mean free path (mm) | mean free energy (keV) | gamma energy (keV) |
|---|---|---|---|---|---|
| | | PET imaging isotopes | | | |
| $^{18}$F | 109.8 min | $\beta^+$ (97%) | 0.6 | 250 | - |
| $^{76}$Br | 16.2 h | $\beta^+$ (54%) EC (46%) | 1.2 | 633.9 | - |
| $^{68}$Ga | 67.7 min | $\beta^+$ (87%) | 3.5 | 844 | - |
| $^{64}$Cu | 12.7 h | $\beta^+$ (17%) $\beta^-$ (39%) EC (44%) | 0.7 | 278 | - |
| $^{11}$C | 20.4 min | $\beta^+$ (100%) | 1.2 | 386 | - |
| $^{89}$Zr | 3.3 d | $\beta^+$ (23%) EC (77%) | 1.3 | 396 | - |
| $^{124}$I | 4.2 d | $\beta^+$ (23%) EC (77%) | 0.9 | 819 | 603 |
| | | Radiotherapeutic isotopes | | | |
| $^{90}$Y | 64 h | $\beta^-$ (100%) | 2.5 | 935 | - |
| $^{131}$I | 8 d | $\beta^-$ (100%) | - | 970.8 | - |
| $^{177}$Lu | 6.7 d | $\beta^-$ (79%) | 0.7 | 130 | 208 and 113 |
| $^{211}$At | 7.2 h | $\alpha$ (100%) | 0.06 | 6790 | - |
| $^{225}$Ac | 10 d | $\alpha$ (100%) | 0.06 | 6830 | - |
| | | Gamma imaging isotopes | | | |
| $^{111}$In | 2.8 d | EC (100%) | - | - | 171 and 245 |
| $^{123}$I | 13.2 h | EC (97%) | - | - | 159 |
| $^{99m}$Tc | 6 h | EC (98%) | - | - | 140 |

therapeutic purposes. Their occurrence is common in GEP NETs. This fact have been used for more than 20 years for precise GEP NETs imaging and therapy by application as SSTR analogues.[37] A cohort study of North American patients with metastatic well-differentated NETs indicate that PRRT with SSTR analogues resulted long overall survival (over 40 months from first PRRT) and time to progression (the median was 23.9 months).[38]

Recent studies in human models are often focused on optimization and individualization of therapy. Velikyan et al. performed a pilot study to discover the impact of peptide mass on the binding of $^{68}$Ga-DOTATOC (Figure 2) to neuroendocrine tumor somatostatin receptors in 9 patients with GEP NETs in 2010. The peptide mass was considered as the peptide mass of SSTR analogue required to occupy the natural SSTRs in the body during the imaging process to obtain the best image contrast and higher tumor-to-normal tissue ratio. They were looking for the optimal unlabeled peptide mass administrated a short time before the tracer. Their study demonstrated that individual patient uptake of radiolabeled ligand in tumor and normal organs exhibited peptide mass dose dependence.[39] Hardiansyah et al. investigated PET-based treatment planning by using the physiologically based pharmacokinetic (PBPK) model with mathematical patient phantoms and Bayesian parameters or dynamic PET. Their aim was to investigate the accuracy of predicting the time-integrated activity coefficients (TIACs). TIACs are the accumulated activities in source organs per administered activity and are also called residence times. They proved that $^{68}$Ga-DOTATATE PET measurements could be used to predict the therapeutic biodistribution of $^{90}$Y-DOTATATE with acceptable accuracy if all available information is integrated in PBPK.[40−42]

$^{177}$Lu-DOTATATE is also one of the most common compounds applied in recent publications because of recent approval of Lutathera. Researchers report possible side effects, quality of life changes, and effects of the therapy. $^{177}$Lu-DOTATATE as a PRRT agent may induce long-term toxicity to the bone marrow, but a study performed on 274 GEP-NET

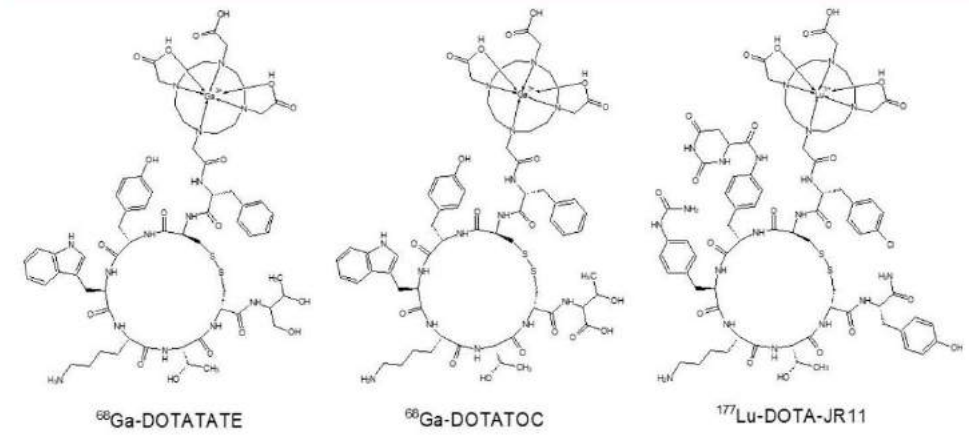


**Figure 2.** Schemes of SSTR analogues applied in new PRRT and PRS strategies.


https://dx.doi.org/10.1021/acs.bioconjchem.0c00617
Bioconjugate Chem. 2021, 32, 25−42

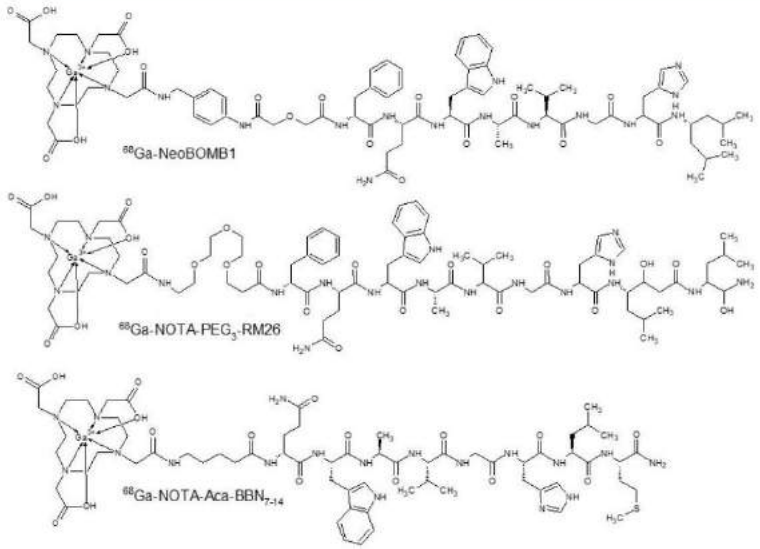


**Figure 3.** Schemes of GRPR analogues applied in new PRS strategies.

patients confirms that $^{177}$Lu-DOTATATE therapy has no risk factors for developing persistent hematological dysfunction in GEP-NET patients.[43] Furthermore, two independent studies confirm that $^{177}$Lu-DOTATATE therapy increases the quality of life of GEP-NET patients.[44,45] Hervas et al. performed a summary of experience with $^{177}$Lu-DOTATATE. They evaluated the biochemical response, imaging methods, toxicity, and quality of life of treatment for 7 patients with metastatic NET. Results of this study indicate the efficacy and safety of $^{177}$Lu-DOTATATE.[45] Ashley et al. reported a case in which they applied a $^{177}$Lu-DOTATATE neoadjuvant therapy before multivisceral transplantation in patients with metastatic small intestinal neuroendocrine neoplasm. The result of their therapy protocol is the lack of biochemical and radiological disease recurrence over 4 years after the intervention.[46] $^{177}$Lu-DOTATATE was also used to develop a PBPK model of $^{177}$Lu peptide therapy of patients with NET. It can be used for accurate calculation of biodistribution and absorbed doses of patients during individual planning of therapy.[45] Zemczak et al. studied the therapeutic effect of a mixture of $^{177}$Lu and $^{90}$Y DOTATATE. 75 patients with histopathologically proven NET G1 and G2 and after $^{18}$F-FDG PET/CT imaging were included in the study. Results of the therapy were in line with similar procedures with single isotope $^{177}$Lu DOTATATE, but they discovered that $^{18}$F-FDG positive patients have higher risk of progression in the two year follow-up.[47] A similar study was performed by Kunikowska et al. They included 103 patients with NET G1/G2 and also applied $^{177}$Lu/$^{90}$Y DOTATATE treatment. Their results are also very promising. Moreover, the study proved low hematological and renal toxicity.[48]

Imaging techniques with radiolabeled SSTR ligands have also improved. Nowadays, medicine uses PET-MRI and PET-CT scanners to image tumors and metastasis by using $\beta^+$ decay-type radionuclides, where PET-CT is a clinical routine in practice. Nevertheless, PET-MRI is able to obtain superior soft-tissue contrast and functional information. Furthermore, the dynamic contrast enhanced imaging with hepatocellular contrast agents is able to detect liver metastases. Therefore, whole-body PET-CT and PET-MRI imaging with $^{68}$Ga-DOTANOC was compared in patients with well-differentiated neuroendocrine tumors. The results indicate that PET-MRI is comparable with PET-CT. In addition, the application of the gadoxetate contrast protocol allows for detection of the liver metastasis, but the PET-CT technique was more effective in detecting lung lesions.[49]

Researchers focused on SSTRs agonists first. The most common radiolabeled structures as DOTATOC or DOTA-TATE are agonists, but nowadays the new points of interest are SSTR antagonists. Despite the internalization of the radionuclide into tumor cells, which is achievable by application of SSTR agonists, antagonists are capable of interacting with more binding sites. This fact may be more important than internalization of SSTR agonists.[50−52] Recent studies report on the effectiveness of use OPS201 (DOTA-JR11). JR11 is SSTR antagonist. Conjunction with DOTA allows for radiolabeling with for example $^{177}$Lu, $^{90}$Y, and $^{111}$In. Nicolas et al. investigated OPS201 labeled with $^{177}$Lu, $^{90}$Y, and $^{111}$In and compared it with $^{177}$Lu-DOTATATE on cell lines and a mouse model. Their results indicate that $^{177}$Lu-OPS201 exhibits a higher tumor uptake, longer tumor residence time, and improved tumor-to-kidney dose ratio than $^{177}$Lu-DOTA-TATE or $^{90}$Y-OPS201. Moreover, they confirmed that $^{111}$In should not be used as a surrogate for $^{90}$Y radiolabeled OPS201. Recommendations for nephroprotective agents which may be used in PRRT with $^{177}$Lu-OPS201 (Figure 2) are also a valuable conclusion of this study.[53] A similar study was performed by Dalm et al. They focused on usage of $^{111}$In-


https://dx.doi.org/10.1021/acs.bioconjchem.0c00617
Bioconjugate Chem. 2021, 32, 25−42

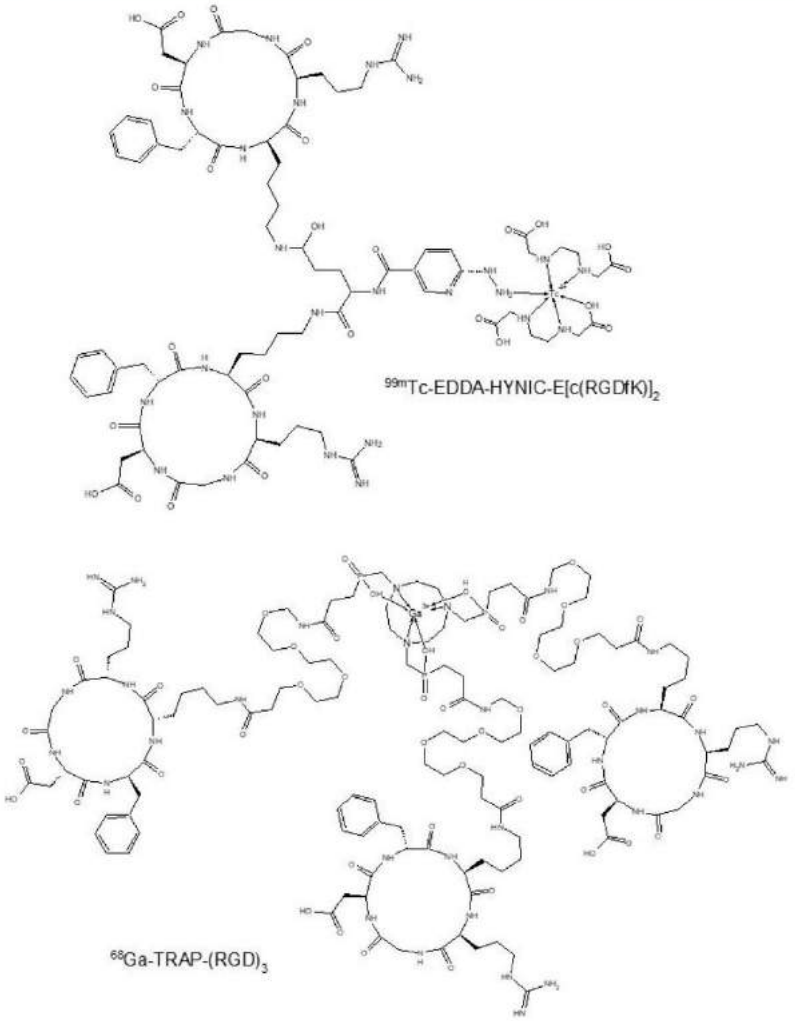


**Figure 4.** Schemes of RGD derivatives applied in new PRS strategies.

OPS201 in breast cancer imaging. This study also confirmed that OPS201 is a promising candidate for usage in medicine.[54]

**GRPR.** The gastrin-releasing peptide receptor (GRPR) is one of the bombesin receptors and a G-protein coupled receptor. Overexpression of GRPR was found in small cell lung cancer for the first time. Scientist found it later in many different tumors including breast, pancreatic, or prostate cancer.[55,56] Morgat et al. studied the GRPR overexpression in breast cancer patients. They found the GRPR overexpression in 75.8% of 1432 tumors studied, of which 83.2% were estrogen receptor (ER) positive. Besides the association of GRPR overexpression and ER positivity, scientists also found GRPR expression in metastatic lymph nodes in 94.6% of cases with overexpressed GRPR tumor. Results led to conclusion that GRPR targeting is good strategy for imaging and treatment in patients with ER positive breast cancer.[57] Recent studies report GRPR antagonist research in human models. Despite the internalization in cancer cells, GRPR agonists may cause undesirable effects after induced GRPR activation.[58] Therefore, novel GRPR antagonist peptide radiotracers are developed. Berthold et al. developed Neo-BOMB1 and conjugated it with $^{177}$Lu, $^{68}$Ga, and $^{111}$In. They performed a biologic profile resulting in all radiolabeled NeoBOMB1 conjugating to GRPR-expressing cells as well as


https://dx.doi.org/10.1021/acs.bioconjchem.0c00617
Bioconjugate Chem. 2021, 32, 25−42

mouse models, and first prostate cancer lesion visualization in human patients using $^{68}$Ga-NeoBOMB1 and PET/CT. Results indicate that NeoBOMB1 binds to GRPR with high affinity and with low internalization. Mouse model study provided information about good metabolic stability in peripheral mouse blood, high and specific uptake, and clearing from background via the kidneys. PET/CT scans of two patients showed that using $^{68}$Ga-NeoBOMB1 provides high-contrast imaging of pathologic lesions in humans. Scientists intend to continue research to investigate theranostic value of NeoBOMB1 in nuclear oncology.[59]

NeoBOMB1 was investigated also on animal models. Two independent teams performed studies about the theranostic use of $^{68/67}$Ga-NeoBOMB1 in breast and prostate cancer. Kaloudi et al. investigated $^{68}$Ga-NeoBOMB1 and $^{67}$Ga-NeoBOMB1 profiles on GRPR expressing T-47D cells as well as mice bearing human T-47D xenografts. $^{67}$Ga-NeoBOMB1 showed high affinity for GRPR on T-47D cell membranes with poor internalization. Mice models provided biodistribution data. >90% intact of dose was detected in mice peripheral blood at 30 min post-injection. $^{67}$Ga-NeoBOMB1 localized tumor in mice bearing T-47D xenografts. Increasing the dose of NeoBOMB1 to 200 pmol reduced the unfavorably high pancreatic uptake without change in tumor uptake.[60] Dalm et al. investigated the biodistribution of $^{68}$Ga-NeoBOMB1 and $^{177}$Lu-NeoBOMB1 on PC-3 xenograft BALB/c mice. They obtained similar results, indicating a good pharmacokinetic profile of NeoBOMB1. The improvement of the tumor/pancreas uptake ratio was also observed by increasing the dose of peptide.[61] Another $^{68}$Ga labeled GRPR antagonist RM26 (Figure 3) was compared with GRPR agonist $BBN_{7-14}$ by using PC-3 cells and PC-3 tumor xenografted mice. Both compounds indicated similar affinity to GRPR, but biodistribution data obtained from in vivo studies show a better profile for RM26. $BBN_{7-14}$ demonstrated rapid elimination after injection, high background signal, and high level of degradation in mice serum in comparison to RM26. Antagonists offer improved tumor to organ ratios as well as better image results due to lower accumulation in the pancreas and intestines.[62] Improved profiles of GRPR antagonists were also confirmed by Liolios et al. They developed four $^{68}$Ga labeled analogues of bombesin connected with HBED-CC chelator—two agonists and two antagonists. Due to the presence of two connectable carboxylic moieties in the structure of HBED-CC, one of the antagonist structures was a homodimer. All compounds were investigated by using PC-3 and T-47D cell lines to obtain information about cell-bound radioactivity. The best results were obtained for the homodimeric antagonist structure in both cell lines. In vivo assays with PC-3 tumor bearing mice and $\mu$PET imaging provided information about better quality imaging by using antagonist structures. Despite exceptionally good results with respect to cell bonding and imaging quality of dimeric antagonists, the monomeric structure had a superior pharmacokinetic profile as a result of lower AUC values for nontarget organs and blood relative to the dimeric form.[63]

**$\alpha_V\beta_3$ Integrin Receptors.** $\alpha_V\beta_3$ and $\alpha_V\beta_5$ integrins are used as indicators in breast cancer as they signal cell growth, including malignancy, metastasis, and cancer induced angiogenesis. They are overexpressed in tumor and endothelial cells of breast cancer.[64,65] Small peptide sequence Arg-Gly-Asp (RGD) has been reported as a structure that is recognized by integrins. Therefore, radiolabeled structures with an RGD core were used as radiopharmaceuticals with high affinity and selectivity for the $\alpha_V\beta_3$ and $\alpha_V\beta_5$ integrins.[66] The research performed on the RGD sequence has provided many new structures such as dimeric compounds, that offer much greater affinity to $\alpha_V\beta_3$ integrins than the monomer. Ortiz et al. developed a biokinetic model for $^{99m}$Tc-EDDA/HYNIC-E-[c(RGDfK)]$_2$ (Figure 4) from a lyophilized formulation kit. Ethylenediamine-*N*,*N*′-diacetic acid (EDDA) was used as a coligand in radiolabeling of HYNIC-peptides to complete the technetium coordination sphere. In addition, the scientists chose EDDA as a coligand because of its hydrophilic properties that improved renal excretion and allowed it to combine in lyophilized formulation. Scientists obtained 96 ± 2% purity after labeling, and biodistribution studies in mice showed renal and hepatobiliary excretion. $^{99m}$Tc-EDDA/HYNIC-E-[c-(RGDfK)]$_2$ has high affinity and showed highly specific uptake to MCF7, T47-D, and MDA-MB-231 cell lines. The imaging in three breast cancer patients localized lesions with high contrast. In addition, ten heathy patients took part in this study. None of patients reported any adverse reactions after $^{99m}$Tc-EDDA/HYNIC-E-[c(RGDfK)]$_2$ administration. It was observed that thyroid and kidneys were the organs which received the highest absorbed dose, but these amount of absorbed doses were comparable to different $^{99m}$Tc radiopharmaceutical studies.[67,68] Zhang et al. performed a study in which they evaluated imaging of breast cancer and metastasis with a dual targeting tracer $^{68}$Ga-BBN-RGD PET/CT. Twenty-two female patients with suspected breast cancer who underwent radical mastectomy were sampled to take part in this study. $^{68}$Ga-BBN-RGD showed high tumor to organ ratios, which in turn provided high contrast in PET/CT image. According to Morgat et al., higher maximum standardized uptake values were observed in patients with ER-positive tumors because of higher overexpression of GRPR in tumor cells. In addition, $^{68}$Ga-BBN-RGD was compared with $^{68}$Ga-BBN. Results of this comparison indicated that dual targeting tracer localized more pathological lesions than $^{68}$Ga-BBN.[69] Kazmierczak et al. investigated the $^{68}$Ga-TRAP-(RGD)$_3$ (Figure 4) for in vivo monitoring of a $\alpha_V\beta_3$ integrin expression as a biomarker of anti-angiogenic therapy effects by using PET/CT. They used 25 mice bearing MDA-MB-231 xenografts which were divided into two cohorts. The first cohort was subject to imaging tests and the second to immunohistochemistry tests. Either anti VEGF antibody bevacizumab or a placebo was administrated for a week in the experimental protocol. Imaging with $^{68}$Ga-TRAP-(RGD)$_3$ at the beginning and at the end of study allowed for observation of reductions in $\alpha_V\beta_3$ integrin expression in xenografts. Immunohistochemistry assays confirmed that bevacizumab therapy caused reduction of $\alpha_V\beta_3$ integrin expression, microvascular density proliferation, and increase of tumor cell apoptosis. Therefore, $^{68}$Ga-TRAP-(RGD)$_3$PET/CT allows for monitoring of anti-angiogenic therapeutic effects which scientists will continue to explore.[70]

**GLP-1 Receptors.** Glucagon-like peptide 1 (GLP-1) is an incretin secreted from intestinal L cells. It is able to activate GLP-1 receptors which play a significant role in glucose metabolism. Scientists also reported positive effects from activation of GLP-1 receptors on decrease of pancreatic $\beta$-cell apoptosis and even increased differentiation of $\beta$-cell precursor cells in the pancreas.[71,72] Overexpression of GLP-1 receptors was found in a number of cancers such as gastrinomas or insulinomas. GLP-1 receptors in insulinomas are expressed in


https://dx.doi.org/10.1021/acs.bioconjchem.0c00617
Bioconjugate Chem. 2021, 32, 25−42

the highest incidence and density among any other peptide receptors in this type of tumor; therefore, GLP-1 receptors offer great potential as a diagnostic target. Azad et al. investigated the GPL-1 receptors through optical and PET imaging. They synthesized and evaluated GLP-1 analogues with a DOTA bifunctional chelator and one analogue combined with fluorescein. Two of these analogues were radiolabeled by $^{68}$Ga and administered to normal CD1 and C57BL/6 mice for biodistribution evaluation and Balb/c$^{nu/nu}$ mice harboring insulinomas for imaging tests. The pancreatic uptake in CD1/C57BL/6 mice observed after 30 min post injection was low and stable. Imaging tests provide clearly visualized tumor after 90 min post injection. Scientists compared results of radiolabeled GLP-1 analogues with radiolabeled exendin-3 and exendin-4. Radiolabeled GLP-1 analogues indicated faster overall clearance rate than exendin-3 and exendin-4, but also a lower tumor uptake.[73] Bauman et al. had a similar goal in their study, but they investigated $^{68}$Ga and $^{89}$Zr radiolabeled exendin-4. Exendin-3 and exendin-4 are reptilian agonists of GLP-1 receptors. Exedin-4 is especially interesting, because it is not degraded by dipeptidylpeptidase 4, and exhibits a 10-fold-increase in affinity toward human GLP-1 receptor. Because of the low spatial resolution of SPECT images obtained by $^{111}$In radiolabeled exendin-4 reported in earlier studies,[74,75] Bauman et al. developed an exendin-4 derivative conjugated to desferoxamine (DFO). Utilization of DFO allowed for radiolabeling of one derivative by both $^{68}$Ga and $^{89}$Zr radionuclides. PET imaging results indicate that [Lys$^{40}$(AHX-DFO-$^{68}$Ga)NH$_2$]exendin-4 developed by Bauman et al. on nude mice bearing RIN-m5F xenografts is a promising candidate for clinical translation. A comparison of results with [Lys$^{40}$(AHX-DTPA-$^{111}$In)NH$_2$]exendin-4 showed that novel radiotracers exhibit comparable or even superior targeting of GLP-1 receptors.[76] Antwi et al. used $^{68}$Ga-DOTA-exendin-4 to localize benign insulinoma lesions in 52 human patients by PET/CT. They compared imaging results with $^{111}$In-DOTA-exendin-4 SPECT/CT and MRI. The highest values of accuracy, impact for surgery planning, and percentage reading agreement were obtained for PET/CT imaging.[77] Parihar et al. reported a case study which used the same radiolabeled tracer on a 31-year-old patient to localize pathological lesions on the pancreas. The patient suffered from gradually increasing lethargy and multiple episodes of dizziness. Biochemical examinations raised suspicions of insulinoma. PET/CT imaging with $^{68}$Ga-DOTA-exendin-4 allowed for identification of localized lesions and surgical intervention. The patient underwent surgical enucleation, after which he experienced an uneventful and complete postoperative recovery.[78]

The GLP-1 receptor is also a target for imaging of $\beta$ cells of intact pancreatic islets in monitoring type II diabetes or transplanted islets in monitoring type I diabetes therapy. Mikkola et al. performed a study measuring stability, affinity, biodistribution, and PET imaging quality of $^{64}$Cu and $^{68}$Ga labeled [Nle$^{14}$,Lys$^{40}$(Ahx-NODAGA)NH$_2$]-exendin-4 in rats. Results indicate better image properties for $^{64}$Cu labeled tracer, but high radiation doses observed in the kidneys may be the limitation of application of this structure in the future.[79] Li et al. evaluated $^{68}$Ga-DO3A-VS-Cys$^{40}$-exendin-4 as a tracer for imaging human transplanted islets in the mouse liver. They chose the liver as it offers the best target to background contrast. Additional examinations confirmed the number and function of transplanted islets, and the imaging tests provided information about high contrast in images. Biodistribution tests revealed that the uptake in livers with transplanted islets was 6-fold higher than in the livers of mock transplanted mice. Scientists are working on the application of $^{68}$Ga-DO3A-VS-Cys$^{40}$-exendin-4 in PET quantification of human islet mass and function in clinical applications.[80]

Wang et al. focused on the presence of GLP-1 receptors in the brain, and examined the influences of age on GLP-1 receptors expression using NOTA-MAL-Cys$^{39}$-exendin-4 radiolabeled with aluminum $^{18}$F fluoride and uPET imaging. uPET imaging provided data about the variable uptake of $^{18}$F-AlF-NOTA-MAL-Cys$^{39}$-exendin-4 with respect to regions of the brain. They compared images of nine aged and nine normal rat brains and concluded that the expression of GLP-1 receptors in rat brains decreased with age. Researchers noted the differences in uptake, based on rat ages and regions of brain. They justified this by the fact that variable distribution depended on both brain region as well as and differential expression of GLP-1 receptors in each rat. Therefore, they predicted unique $^{18}$F-AlF-NOTA-MAL-Cys$^{39}$-exendin-4 uptake patterns for different neurological diseases. Biodistribution studies indicated that $^{18}$F-AlF-NOTA-MAL-Cys$^{39}$-exendin-4 is primarily excreted from the renal system due to high uptake in kidneys. The second organ indicating significantly increased higher uptake relative to others was the pancreas. Scientists noted also that this method required further work in part because a small group of rats was used in this study to obtain reliable results, the yield of radiotracer was also not satisfactory, and kidney uptake was too high, which may cause renal damage.[81]

**CXCR4.** The chemokine receptor 4 (CXCR4) is widely expressed throughout the human body G protein-coupled receptor. Together with chemokine CXCL12, which is produced mainly in the bone marrow, lymph nodes, lung, heart, thymus, and liver, CXCR4 forms a CXCL12-CXCR4 signaling axis.[82] This pathway is involved in the homeostasis of the adult hematopoietic system and adequate response of the immune system.[83] CXCR4 has also been found to be involved in a numerous diseases: HIV-1 infection,[84] rheumatoid arthritis,[85] atherosclerosis,[86] chronic inflammation,[87] and even neurodegenerative diseases.[88] In oncology, CXCR4 plays a pivotal role in tumor development and metastasis, which has been proven for breast, prostate, lung, colorectal cancer, or primary brain tumors such as glioblastoma.[83] Therefore, CXCR4 is an attractive target for imaging and therapeutic purposes.

Nowadays, two radiolabeled peptide imaging molecules, which are CXCR4 ligands, were already tested on human patients—$^{68}$Ga-Pentixafor and $^{68}$Ga-NOTA-NFB. $^{68}$Ga-Pentixafor is an FC-131 based cyclic pentapeptide radiolabeled with DOTA chelator conjugated with amino acid structure via 4-(aminomethyl) benzoic acid.[89] In 2015, Wester et al. for the first time investigated the effectiveness of the imaging properties of this agent in patients with lymphoproliferative diseases. $^{68}$Ga-Pentixafor bound with high affinity and selectivity to human CXCR4. PET scan with this agent provided images with good specificity and contrast. Dosimetry studies have provided data with even better properties than $^{68}$Ga-DOTATOC or $^{68}$Ga-DOTATATE for absorbed doses in organs. $^{68}$Ga-Pentixafor also showed very good pharmacokinetic profile and fast clearance kinetics.[90] Similar results and conclusions were obtained by Breun et al., who investigated the use of PET/CT $^{68}$Ga-Pentixafor scan in patients with vestibular schwannomas.[91] The second mentioned agent was


https://dx.doi.org/10.1021/acs.bioconjchem.0c00617
Bioconjugate Chem. 2021, 32, 25−42

$^{68}$Ga-NOTA-NFB. $^{68}$Ga-NOTA-NFB is a derivative of 14-amino-acid peptide, CXCR4 inhibitor—T140. Peptide structure was modified by changing the binding site of the disulfide bridge and conjugating NOTA chelator for radionuclide labeling. Wang et al. investigated this agent in healthy volunteers and patients with glioma. $^{68}$Ga-NOTA-NFB was safe and well-tolerated, and it displayed a rapid activity clearance from blood circulation. Imaging studies proved to be more sensitive glioma detecting results than $^{18}$F-FDG PET/CT. Unfortunately, the clearance pattern of $^{68}$Ga-NOTA-NFB exhibited very high splenic and liver uptake, which challenged the application of $^{68}$Ga-NOTA-NFB PET/CT in high contrast clinical imaging of CXCR4 expression.[92] Despite moderate results of $^{68}$Ga-NOTA-NFB, other modifications to the T140 derivatives are under development.[16,93]

There are also other radiolabeled amino acid structures under development that are able to imaging CXCR4. Li et al. reported a $^{64}$Cu radiolabeled modified ubiquitin molecule. Ubiquitin is a small regulatory protein and natural CXCR4 ligand. Li et al. modified ubiquitin structure by addition a C-terminal GGCGG sequence and functionalized the whole structure with trans-cyclooctane (TCO) moiety via thiol-maleimide click reaction. The obtained structure (UbCG4-TCO) was $^{64}$Cu-radiolabeled through TCO/tetrazine-based Diels−Alder click reaction. The obtained molecule was $^{64}$Cu-Cb-1K1P-UBCG4. The molecule was investigated as imaging agent on mice with 4T1 breast cancer xenografts. The results indicate good quality of imaging 4T1 cells with low backgrounds. Dosimetry studies results indicate relatively low accumulation in normal tissues and organs.

CXCR4 is also a good therapeutic and theranostic aim. The therapeutic peptide CXCR4 agent is Pentixather (3-iodo-D-Tyr$^1$-Pentixafor). This Pentixafor derivative was labeled by $^{177}$Lu and investigated on Daudi-lymphoma veering SCID mice and patients with multiple myeloma by Schottelius et al. Tests results on mice and patients indicated very promising CXCR4 targeting characteristics (total cellular tracer uptake is improved compared to $^{68}$Ga-Pentifaxor, but internalization at time point ≥15 min was lower than reference) and suitable pharmacokinetic profile (rapidly cleared from stomach, intestines, and kidneys, but slow excretion from the liver, which can be controlled by coinjection of an excess of unlabeled competitor). The dose-limiting organ for $^{177}$Lu-Pentixather agent are kidneys.[94] Lau et al. reported a theranostic pair $^{68}$Ga/$^{177}$Lu-BL01. BL01 is a modified derivative of LY2510924 (cyclic peptide, CXCR4 inhibitor) by conjugating DOTA chelator with lysine residue at the C terminus of peptide. Because of its structure, BL01 can be radiolabeled by $^{68}$Ga as well as $^{177}$Lu; therefore, it was a very promising candidate to develop a pair of theranostic agents. $^{68}$Ga/$^{177}$Lu-BL01 was investigated on mice bearing Daudi Burkitt's lymphoma xenografts. PET/CT scan shows significant radioactivity in the tumor, liver, kidneys, and bladder. Image contrast was improved at 2 h post injection. Tumor uptake also increased with continued clearance from nontarget tissues. The uptake of $^{177}$Lu-BL01 was the highest in tumor, urinary bladder, liver, spleen, and skeleton. The spleen may be the dose-limiting organ for PRRT.[95]

**Other PRRT and PRS Mechanisms.** The imaging and therapy strategies described above are the most commonly applied in the present day, but scientists are still searching for new peptide tracers or targets which may provide unique insights on certain diseases or provide better results for modern diagnostic methods and therapies. Zoghi et al. reported the new peptide tracer for PET imaging of gonadotropin-releasing hormone receptors (GnRH-R). These receptors are localized in normal and human cancer tissues including breast cancer. In addition, it was observed that GnRH-R are localized to a high percentage of estrogen receptor-negative breast cancers.[96,97] It is also known that GnRH-R agonists show an antiproliferative effect on breast cancer cells.[98] All this data was purposed for developing $^{68}$Ga-DOTA-triptorelin by Zoghi et al. as a novel radiolabeled peptide tracer in breast cancer diagnostic. They obtained 99% HPLC purity of the radiolabeled product after the full synthesis protocol. The biodistribution tests on normal rats provided data showing significant uptake in the kidney, stomach, and testicles, as well as fast kidney clearance. Furthermore, tests with T41 tumor-bearing mice provide information about significant tumor uptake 1 h after injection with a high value of tumor−blood and tumor−muscle ratios (28 and >50, respectively).[99] Another, less common radiotargeting strategy, is urokinase-type plasminogen receptors (uPARs) imaging. uPAR is a cell membrane protein responsible for proteolysis, but it also activates many intracellular signaling pathways, including proliferation through cooperation with transmembrane receptors. uPAR expression is limited in normal tissues, but uPAR overexpression was detected in cancer tissues, for example, in urinary bladder cancer and breast cancer. Moreover, it was reported that high uPAR expression is associated with cancer invasion and metastases. Therefore, uPAR is considered a biomarker for aggressive diseases and poor prognoses.[100,101] Skovsgaard et al. are working on the development of radioligands based on peptide uPAR antagonist AE105 for PET imaging. They reported the results of phase 1 clinical trial of $^{68}$Ga-NOTA-AE105, where they investigated its safety and biodistribution in normal tissues, as well as its uptake in tumor lesions. Ten patients with breast, prostate, and urinary bladder cancer took part in the trial. No patient experienced adverse events or clinically detectable pharmacologic effects due to administration of $^{68}$Ga-NOTA-AE105. Results indicated high in vivo stability, fast clearance from tissues, and primarily renal excretion of the radioligand. Image tests provided images with satisfactory contrast and allowed for identification of primary tumors and metastases. The most promising results were obtained for breast cancer patients, where the administration of $^{68}$Ga-NOTA-AE105 provided an image of localization of metastatic axillary lymph nodes, which has not been previously detected by preoperative workup with ultrasound, fine-needle aspiration, and contrast-enhanced CT. However, the scientist reported the failure of $^{68}$Ga-NOTA-AE105 PET in imaging liver metastasis in a patient with disseminated urinary bladder cancer.[102]

**RIT and RII Strategy.** Targeting radionuclides using monoclonal antibodies (Mabs) has been well studied in the literature. Identification of the acceptable antigen and selection of the proper MAB are paramount for obtaining successful therapies or diagnostic results. Antigens should be highly expressed in the targeted tissue, but not in other tissues, as this may affect the quality of imaging or therapy. In addition, they should be localized on the cell surface for accessibility to circulating Mabs. The properly selected antibody should be highly specific for the target antigen, while uptake in other tissues or cross activity with nonspecific antigens should be



https://dx.doi.org/10.1021/acs.bioconjchem.0c00617
Bioconjugate Chem. 2021, 32, 25−42

low, because of the probability of occurrence of toxicity or excessively fast clearance.[103]

Nowadays there are a few kinds of Mabs used in medicine and a few methods of Mabs classification. In this review, we want to mention origin structure-type classification and include some information about production of these Mabs. The first type is murine Mabs produced by hybridoma cell lines. These are intact whole murine Mabs. It is the oldest and very widely used Mabs production technique. Names of these Mabs have several specific endings, e.g., −omab for mice antibodies, −emab for hamster antibodies, or −amab for rat antibodies, which makes these types of antibodies easy to recognize in praxis.[104] The second type are whole murine recombinant Mabs or Mabs fragments produced by cloning the genetic material responsible for expression of specific Mab fragments, creating a recombinant DNA chain, and using it in, for example, in yeast display or phage display system technology to obtain a specific product.[105] In addition, the recombinant Mabs can be basically divided into three subtypes. First subtype are chimeric Mabs. These are constructed mostly from human proteins (usually heavy chains, sometimes with light chain fragments) and murine proteins (light chains or only variable regions of light chains). All chimeric Mabs names ended in −ximab. The second subtype are humanized Mabs, where only the hypervariable region of human antibody has murine origin. These antibodies show reduced immunogenicity, because of reducing the human anti-mouse antibody production effect. Names of humanized Mabs end in −zumab.[106] The third subtype are human Mabs, which are constructed only from human proteins. Human Mabs are better tolerated by patients, and they eliminate the human anti-mouse antibody production effect. This type can be produced by recombinant techniques or by transgenic mice (specific modification of hybridoma cell lines technique). Human Mabs can be recognized by the −umab ending in the agent name.[107]

By analyzing recently reported studies, it is evident that scientists are focused on improving of immuno-PET technique in human therapy. This technique allows for the utilization of high specificity Mabs with the high sensitivity and resolution offered by PET imaging to perform noninvasive quantification of Mab uptake in normal and tumor tissues for therapy development. For example, it may be applied for the selection of targeted therapies or to choose the appropriate dose of radioimmunotherapy. Radiolabeling with positron emitting nuclides of therapeutic antitumor affibodies allows us to achieve theranostic goals such as the evaluation of responses to therapy.[108,109] ImmunoPET was utilized for evaluation of the impact of preloading with unlabeled rituximab on $^{89}$Zr/$^{90}$Y-rituximab radioimmunotherapy of CD20+ B-cell lymphoma. This study provided information about the impairment of radioconjugate tumor targeting in the majority of patients, which suggests the reconsideration and further evaluation of the preloading strategy in rituximab or $^{90}$Y-ibritumomab tiuxetan therapy.[110] Pitalua-Cortez et al. successfully identified the overexpression of human epidermal growth factor receptor 2 (HER2) in lung metastases in a 43-year-old breast cancer patient by using immunoPET technique with $^{68}$Ga radiolabeled trastuzumab. They compared the obtained image results with $^{18}$F-FDG imaging. In conclusion, they confirmed that $^{68}$Ga-trastuzumab provides information as a specific metastasis biomarker, but the higher uptake of $^{18}$F-FDG and significant background activity of the liver and heart were caused by fast imaging after injection, because of the usage of a short-life radionuclide, are the reasons for research continuation. Nevertheless, scientists pointed out that conjugation of Mabs with long-life radionuclides, which together have the capacity to improve image quality, may provide an excessively high radiation dose for the patient, because of slow blood clearance and the long residence time of Mabs.[111] One of the solutions to the biodistribution problem presented in the study performed by Pitalua-Cortez et al. is the modification of the peptide structure. Honarvar et al. developed a nonapeptide A9 derived from the trastuzumab-Fab portion, radiolabeled it with $^{111}$In by using bifunctional chelator DTPA, and studied its affinity to HER2-expressing BT474 cells as well as biodistribution in NMRI mice. Binding to HER2-expressing cells study provided information about two interactions of $^{111}$In-DTPA-A9 with HER2, specific for HER2 and nonspecific to characteristics for similar peptide structures. The biodistribution profile was also promising due to the substance's rapid clearance from blood and insignificant binding to any tissues.[112]

Another solution to solve pharmacokinetic problems was proposed by Xu et al. They modified a cysteinylated ZHER$_{2:342}$ anti-HER2 affibody with a hydrophilic linker and labeled it by the $^{18}$FAl-NOTA method. Affibodies are a small size engineered scaffold protein binders (~6.5 kDa), originally based on the protein A domain. They are characterized by high affinity and very fast clearance of unbound molecules via the kidneys, because of their small size. A new tracer was developed named $^{18}$FAl-NOTA-MAL-MZHER$_{2:342}$. uPET imaging probes on mice provide very high image quality as confirmed by biodistribution studies. Results indicated rapid localization to HER2-positive tumors, quick elimination from blood and normal tissues, and low accumulation in liver or bones. $^{18}$FAl-NOTA-MAL-MZHER$_{2:342}$ was excreted mainly through the kidney, and as a result, kidneys are the major dose-limiting organ. Scientists pointed out that renal protection could be used in future studies, and they declared an active investigation into the possible effects of these compounds.[113] Tolmachev et al. met with a different problem with renal excretion. They evaluated anti-HER2 affibody ZHER$_{2:S1}$ conjugated with NOTA and NODAGA chelators and radiolabeled with $^{64}$Cu. These were compared with $^{68}$Ga-NODAGA-ZHER$_{2:S1}$ to obtain information about which radionuclide is more favorable in immunoPET imaging of HER2-expressed tumors in mice. Results from biodistribution evaluation provided evidence of renal redistribution of the radiotracer. The renal uptake was reduced 6 and 24 h post injection and radioactivity increased in blood, lung, liver, spleen, and intestines at the same time. This resulted in a decrease of the tumor to organ ratio. In conclusion, Tolmachev et al. suggested avoiding the combination of radiocopper and NOTA/NODAGA amido derivatives with proteins displaying high renal reabsorption.[114] Sandberg et al. investigated a novel affibody, ABY-025, conjugated with $^{68}$Ga and $^{111}$In. ABY-025 is an affibody capable of identifying HER2 expression in breast cancer metastases. The radiolabeled molecule has successfully passed the first and second phases of clinical trials. In their study, Sandberg et al. successfully performed an intraimage normalization using tumor to reference tissue ratio by administration of $^{68}$Ga-ABY-025 to 16 patients and $^{111}$In-ABY-025 to 7 patients with prediagnosed HER2 positive/negative metastasized breast cancer and PET/CT or SPECT/CT scan, respectively.[115]


https://dx.doi.org/10.1021/acs.bioconjchem.0c00617
Bioconjugate Chem. 2021, 32, 25−42

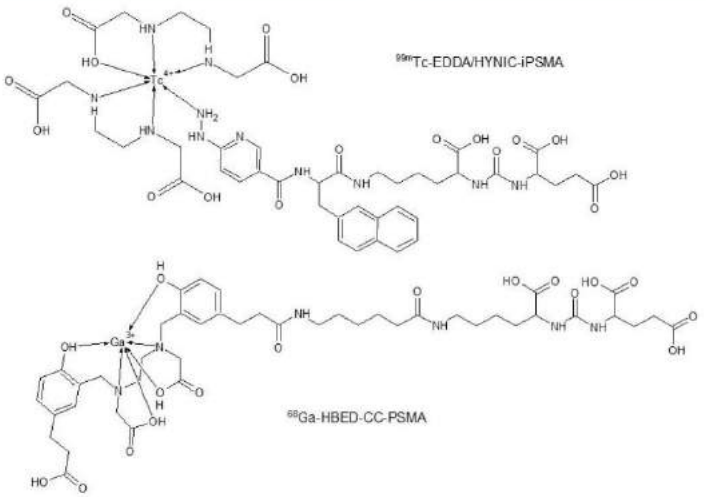


**Figure 5.** Schemes of PSMA derivatives applied in new diagnostic strategies.

The RIT or RII strategy is often associated with cancer, but not always. $^{99m}$Tc-labeled murine anti-human CD4 IgG1-Fab fragment were investigated by Steinhoff in patients with active synovitis due to rheumatoid arthritis to evaluate this compound as a potential marker of inflammatory activity. Study confirmed that scintigraphy with $^{99m}$Tc-anti-CD4-Fab is a promising technique.[116]

Recent immunoPET reports relate also to a new target—programed death-ligand 1 (PD-L1). It is an immune checkpoint in the negative regulation of T cells. Overexpression of PD-L1 was found in a variety of cancers and it is upregulated by tumors in the presence of infiltrating lymphocytes. Antibody blockage of PD-L1 was utilized to design therapeutic antibodies like the FDA-approved pembrolizumab, ipilimumab, and nivolumab. Mayer et al. developed four PD-L1 ligands radiolabeled with $^{64}$Cu and two radiolabeled with $^{68}$Ga. They used a small high-affinity consensus (HAC) PD1 peptide and its aglycosylated derivative (HACA) as a scaffold to design their radiotracers. They also evaluated the influence of chelators in their study. They used DOTA and NOTA chelators to conjugate the radionuclides in various structures. Results from immunoPET indicated that aglycolyzation was the most prominent design affecting tracer uptake, specificity, and clearance. $^{64}$Cu-NOTA-HACA-PD1 was an agent that visualized human PD-L1 expression as the most accurate in tumor bearing mice. $^{68}$Ga-DOTA-HACA-PD1 and $^{68}$Ga-NOTA-HACA-PD1 also exhibited a very promising tumor to background ratio 1 h post injection.[117]

Therapeutic application of radiolabeled antibodies has also been reported in recent literature. J591 is an murine Mab that has affinity to prostate-specific membrane antigen (PSMA) and has the property of internalization once bound to PSMA. PSMA is one of the most recognizable targets for management of castration-resistant prostate cancer (CRPC), and J591 was investigated for this application. Niaz at al. gathered the published clinical trials results of $^{177}$Lu-J591 in the treatment of CRPC. $^{177}$Lu-J591 application has shown promising results. The agent targeted tumor accurately, gave biochemical and radiographical response, and increased overall survival among CRPC patients. Authors indicated that ongoing studies of $^{177}$Lu-J591 focus on improving the therapeutic index because of myelosuppression due $^{177}$Lu-J591 application.[118]

**Other Radiotargeting Strategies.** There are a number of strategies that cannot be assigned to PRRT or RIS, which are very widespread and are the mainstream in modern nuclear medicine science. The most popular technique in this division is prostate-specific membrane antigen (PSMA) imaging. PSMA is an integral membrane glycosylated metalloenzyme, and it is also known as glutamate carboxypeptidase II. It was found on the apical membrane of the epithelium lining the prostatic ducts in the heathy prostate, but it is also expressed in kidneys, liver, colon, and the nervous system. PSMA is of interest to the field of nuclear medicine because of its overexpression on prostate cancer cells. In addition, PSMA levels correlate well with the Gleason score, which makes PSMA a phenomenal target for identifying and monitoring the progression of prostate cancer.[21] Other tumors like gliomas or breast cancer are able to express PSMA also, and PSMA is then an angiogenesis marker.[119]

At present, the most common method for targeting PSMA is administration of the radiolabeled small urea-linked diamino acid ligand—the PSMA inhibitors (iPSMA). iPSMA may be radiolabeled with various radionuclides. Santos-Cuevas et al. evaluated the biokinetics of the conjugated iPSMA with $^{99m}$Tc by using the HYNIC/EDDA method as a SPECT or SPECT/CT, SPECT/MRI imaging agent in prostate cancer patients. They obtained high-resolution images of tumor and metastases through the use of SPECT/CT imaging, due to the high $^{99m}$Tc-EDDA/HYNIC-iPSMA (Figure 5) uptake in the prostate cancer tissue and metastases. Biokinetic studies on healthy volunteers confirmed the usefulness of this compound in human patients due to high patient tolerance after administration and a similar profile to the previously examined $^{99m}$Tc-iPSMA compounds. In addition, $^{99m}$Tc-EDDA/HYNIC-


https://dx.doi.org/10.1021/acs.bioconjchem.0c00617
Bioconjugate Chem. 2021, 32, 25−42

iPSMA showed fast blood clearance and urinary excretion. Therefore, the scientists were able to perform the prostate cancer gland imaging 3 h after administration.[120] Advanced research on human patients was performed with $^{68}$Ga-iPSMA-HBED-CC (Figure 5), also known as $^{68}$Ga-PSMA11. Schmidt-Hegemann et al. performed a retrospective study of 129 prostate cancer patients in which $^{68}$Ga-iPSMA-HBED-CC was used to visualize neoplastic lesions. Their aim was to define a pattern of positive lesion detection by using $^{68}$Ga-iPSMA-HBED-CC PET/CT imaging. A few potential influencing factors were evaluated, and it was found that the level of prostate specific antigen in blood before PSMA−PET scan was significantly correlated with positive detection of lesions.[121] $^{68}$Ga-iPSMA-HBED-CC is also considered as a potentially useful radiotracer in visualization of breast cancer metastasis, because of the reported PSMA expression on human solid tumors.[122] Minamimoto et al. compared the effectiveness of visualizing pathological lesions by PET/MRI and PET/CT with $^{68}$Ga-RM (GRPR antagonist) and $^{68}$Ga-iPSMA-HBED-CC, respectively, in patients with biochemically recurrent prostate cancer. Both radiotracers showed characteristic physiological uptake to specific organs. Uptake outside the expected physiologic biodistribution indicated a difference between agents. Administration of each agent allowed visualization of some lesions in bone marrow, retroperitoneal lymph nodes, mediastinal lymph nodes, seminal vesicle, and subclavian lymph nodes. However, $^{68}$Ga-RM2 uptake was low in the pelvic lymph node and vas deferens, where $^{68}$Ga-iPSMA-HBED-CC uptake was significantly higher. This phenomenon occurred twice in the same patients. Researchers also found lesions where $^{68}$Ga-iPSMA-HBED-CC uptake was low in comparison to $^{68}$Ga-RM2. In conclusion, studies by Minamimoto et al. indicate the need for advanced performance studies to understand the heterogeneous expression of PSMA and GRPRs in different types of prostate cancer.[123] In addition to many studies with $^{68}$Ga-iPSMA-HBED-CC, the new radiolabeled iPSMA structures are reported. Liu et al. reported the synthesis and preclinical evaluation of $^{68}$Ga-PSMA-BCH for prostate cancer imaging. It is a NOTA conjugated iPSMA structure and showed high affinity to 22Rv1 tumor cells expressing PSMA. Bouvet et al. evaluated the influence of prosthetic groups containing $^{18}$F on tumor uptake in PSMA targeting. They investigated three new iPSMA structures conjugated with succinimidyl-4-[$^{18}$F]fluorobenzoate ($^{18}$F-SFB), 4-[$^{18}$F]fluorobenzaldehyde ($^{18}$F-FBA), and 2-deoxy-2-[$^{18}$F]fluoro-D-glucose ($^{18}$F-FDG) prosthetic groups. In vitro and in vivo studies indicated the iPSMA structure conjugated with $^{18}$F-SFB prosthetic group as the most potent agent in future PSMA−PET imaging research.[124] iPSMA are also in interest of therapeutic applications. $^{177}$Lu-iPSMA was reported as the beta emitting agent used in prostate cancer therapy and a good alternative to $^{177}$Lu-J591, which is still being investigated and improved.[125] $^{225}$Ac-iPSMA is new approach because of the usage of the alpha emitter. Alpha particles have greater destructive power against malignant cells than beta particles. Azorin-Vega et al. compared the effectiveness of $^{177}$Lu-iPSMA and $^{225}$Ac-iPSMA in a bone microenvironment model. Their studies proved that $^{225}$Ac-iPSMA produced doses to prostate cancer calls almost 3 orders of magnitude greater than $^{177}$Lu-iPSMA. Moreover, they indicated that $^{225}$Ac-iPSMA could be the best option for treatment of the bone metastases in prostate cancer because of very high doses of radiation to prostate cancer cells in bone metastases.[126]

Another mechanism of tumor targeting was reported by Ahmadpour et al. They used a small synthetic tumor cell-binding peptide FROP-1 primarily reported by Zitzmann et al.[127] FROP-1 has an ability to bind specifically to MCF-7 breast tumor; therefore, Ahmadpour et al. conjugated FROP-1 peptide with HYNIC structure and radiolabeled it with $^{99m}$Tc by using tricine and EDDA as a coligand. Planar gamma imaging in MCF-7 female tumor-bearing nude mice was acquired at 15 min after the administration of $^{99m}$Tc-HYNIC-FROP. Tumors were clearly localized by SPECT imaging at 15 post injection also. Biodistribution studies indicated rapid blood clearance and renal excretion. Therefore, scientists observed a high radiation dose in kidneys and urinary bladder and found that radiolabeled FROP derivatives needed further studies in order to improve in vivo tumor targeting.[128]

## ■ CLINICAL TRIAL ANALYSIS

For the purposes of this publication, a review of clinical trials on the use of new radiolabeled peptide structures in therapy or diagnostics was performed. The review refers to studies reported on www.clinicaltrials.gov in the period from 2008 to November 31, 2018, and it includes 146 trials involving the use of radiolabeled peptide structures in medicine. The complete list of analyzed clinical trials is presented in Table S1. Among them, 28 had the status of terminated, withdrawn, or unknown. Out of the 50 trials completed, three trials concerned phase 3 of clinical trials. They were the safety and efficacy study of $^{111}$In pentetreotide in high doses in treatment of neuroendocrine tumors (NCT00442533), the comparison of rituximab versus tositumomab and $^{131}$I tositumomab in patients with relapsed follicular nonhodgkins lymphoma (NCT00268983), and a study on the impact of adding $^{90}$Y ibritumomab tiuxetan to BEAM chemotherapy and autologous stem-cell transplantation in patients with aggressive lymphoma (NCT00491491). Other completed trials concerned phase 1 and phase 2, and included 23 and 24 trials, respectively. A significant majority of the trials concerned the RIT strategy (86.00%) and pretargeted RIT strategy (8.00%) where bispecific antibodies are used. Only one completed clinical trial was performed for diagnostic purposes, and this was phase 2 of a clinical trial study on the use $^{68}$Ga-DOTA-RM2 PET/MRI in diagnostic imaging in patients with prostate cancer (NCT02440308). Seventeen active clinical trials were found. No active phase 3 trials were found; however, one phase 0 of a clinical trial was reported. This was the pilot clinical trial study on the use $^{99}$Tc HYNIC/Tricine Interleukin-2 in SPECT imaging in patients with stage IV skin melanoma (NCT01789827). This study also was the only active clinical trial performed for diagnostic purposes. In this group of trials, RIT (76.47%) and pretargeted RIT (11.76%) were also the most often studied strategy of therapy. Forty-seven clinical trials have a recruiting status, of which five trials concerned phase 3 clinical trials. The goal of the diagnostic phase 3 trial was to determine the effectiveness of PET/MRI imaging in detection of prostate cancer cells with $^{68}$Ga DOTA-RM2 in patients with negative CT scan and elevated prostate-specific antigen levels after surgical treatment or radiation (NCT02624518). Two phase 3 clinical trials concerned PRRT strategy. They were studies of the efficacy and safety of use $^{177}$Lu-DOTATOC in patients with inoperable, progressive, somatostatin receptor-positive GEP-NET (NCT03049189) and studies of the use of $^{111}$In pentetreotide-based adjuvant therapy in patients with digestive neuro-


https://dx.doi.org/10.1021/acs.bioconjchem.0c00617
Bioconjugate Chem. 2021, 32, 25−42

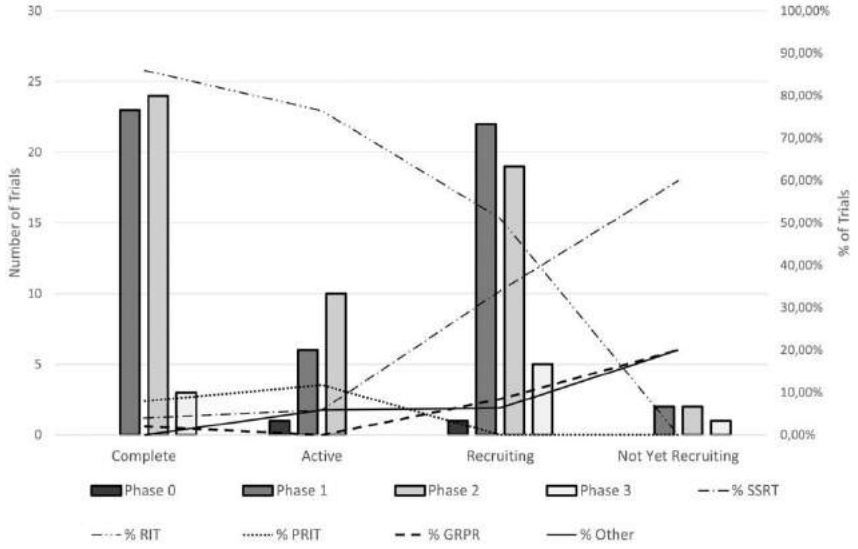


**Figure 6.** Summary of clinical trial analysis.

endocrine tumors after complete surgical resection of liver metastases (NCT02465112). The last two phase 3 clinical trials with a recruiting status concerned RIT strategy. Those were studies on the use of intracerebroventricular treatment with $^{131}$I omburtamab in children with diagnosed neuroblastoma and central nervous system/leptomeningeal metastases (NCT03275402) and studies of the comparison of $^{90}$Y ibritumomab tiuxetan RIT to autologous stem cell transplantation in patients with relapsed or refracted follicular lymphoma (NCT01827605). One pilot phase 0 clinical trial was reported as a trial at a recruitment stage. It concerned evaluation of the use $^{64}$Cu anticarcinoembryonic (CEA) antigen monoclonal antibody MSA in PET imaging of CEA positive cancer (NCT02293954). Clinical trials with a recruiting status mainly concerned treatment procedures; only ten trials were reported as studies with a diagnostic primary purpose. RIT strategy was also the most common strategy of studies in this group of trials (51.06%); however, PRRT was the second most frequently reported treatment strategy (34.04%). Four trials were reported as clinical trials in a prerecruitment stage. One of them was a phase 3 diagnostic clinical trial, where the examination of the performance of the LightPath Imaging System combined with $^{68}$Ga DOTA-RM2 as PET tracer was planned (NCT03731026). A two-phase diagnostic clinical trial involving studies of $^{68}$Ga DOTA-TATE as PET/MRI tracer of hepatocellular carcinoma (NCT03648073) was also identified as a trial in a prerecruitment stage. Graphical summary of clinical trial analysis is shown in Figure 6.

## ■ SUMMARY

In conclusion, the most actively studied therapy with radiolabeled peptides in the period from 2008 to November 31, 2018 was radioimmunotherapy. The majority of completed and active clinical trials performed in that period were aimed at application of radiolabeled antibodies. New clinical trials that will commence soon or in which the recruitment process will begin are also concerned with radiolabeled antibodies. Nevertheless, the number of studies with somatostatin and bombesin analogues has increased. It is noteworthy that these new phase 3 clinical trials were more than complete and active, which brings hope for new radiolabeled peptide agents in modern therapy and diagnosis.

## ■ ASSOCIATED CONTENT

### Supporting Information

The Supporting Information is available free of charge at https://pubs.acs.org/doi/10.1021/acs.bioconjchem.0c00617.

List of clinical trials (PDF)

## ■ AUTHOR INFORMATION

### Corresponding Author

**Paweł Szymański** − *Department of Pharmaceutical Chemistry, Drug Analyses and Radiopharmacy, Faculty of Pharmacy, Medical University of Lodz, 90-151 Lodz, Poland;* orcid.org/0000-0003-3438-7509; Email: pawel.szymanski@umed.lodz.pl

### Authors

**Paweł Kręcisz** − *Department of Pharmaceutical Chemistry, Drug Analyses and Radiopharmacy, Faculty of Pharmacy, Medical University of Lodz, 90-151 Lodz, Poland;* orcid.org/0000-0003-2951-0867

**Kamila Czarnecka** − *Department of Pharmaceutical Chemistry, Drug Analyses and Radiopharmacy, Faculty of Pharmacy, Medical University of Lodz, 90-151 Lodz, Poland;* orcid.org/0000-0002-6497-1565



https://dx.doi.org/10.1021/acs.bioconjchem.0c00617
Bioconjugate Chem. 2021, 32, 25−42

Leszek Królicki – *Department of Nuclear Medicine, Medical University of Warsaw, 02-097 Warsaw, Poland;* orcid.org/0000-0002-7117-9621

Elżbieta Mikiciuk-Olasik – *Department of Pharmaceutical Chemistry, Drug Analyses and Radiopharmacy, Faculty of Pharmacy, Medical University of Lodz, 90-151 Lodz, Poland;* orcid.org/0000-0002-7171-4524

Complete contact information is available at: https://pubs.acs.org/10.1021/acs.bioconjchem.0c00617

### Author Contributions

All authors have given approval to the final version of the manuscript.

### Notes

The authors declare no competing financial interest.

## REFERENCES

(1) Richter, S., and Wuest, F. (2014) F-18-Labeled Peptides: The Future Is Bright. *Molecules 19* (12), 20536−20556.

(2) Krenning, E. P., Breeman, W. A. P., Kooij, P. P. M., Lameris, J. S., Bakker, W. H., Koper, J. W., Ausema, L., Reubi, J. C., and Lamberts, S. W. J. (1989) LOCALIZATION OF ENDOCRINE-RELATED TUMORS WITH RADIOIODINATED ANALOG OF SOMATOSTATIN. *Lancet* 333 (8632), 242−244.

(3) Muto, P., Lastoria, S., Varrella, P., Vergara, E., Salvatore, M., Morgano, G., Listerjames, J., Bernardy, J. D., Dean, R. T., Wencker, D., et al. (1995) Detecting Deep Venous Thrombosis with Tc-99m-Labeled Synthetic Peptide P280. *J. Nucl. Med. 36* (8), 1384−1391.

(4) ListerJames, J., Knight, L. C., Maurer, A. H., Bush, L. R., Moyer, B. R., and Dean, R. T. (1996) Thrombus imaging with a technetium-99m-labeled, activated platelet receptor-binding peptide. *J. Nucl. Med. 37* (5), 775−781.

(5) de Visser, M., Verwijnen, S. M., and de Jong, M. (2008) Improvement strategies for peptide receptor scintigraphy and radionuclide therapy. *Cancer Biother.Radiopharm. 23* (2), 137−157.

(6) Goldenberg, D. M., Sharkey, R. M., Paganelli, G., Barbet, J., and Chatal, J. F. (2006) Antibody pretargeting advances cancer radioimmunodetection and radioimmunotherapy. *J. Clin. Oncol. 24* (5), 823−834.

(7) Leaman Alcibar, O., Candini, D., Lopez-Campos, F., Albert Antequera, M., Morillo Macias, V., Conde, A. J., Rodriguez Perez, A., Hervas Moron, A., Contreras Martinez, J., Ferrer Albiach, C., Navarro Aguilar, S., Rodriguez-Ruiz, M. E., et al. (2019) Time for radioimmunotherapy: an overview to bring improvements in clinical practice. *Clin. Transl. Oncol. 21* (8), 992−1004.

(8) Jacobson, O., Zhu, L., Ma, Y., Weiss, I. D., Sun, X. L., Niu, G., Kiesewetter, D. O., and Chen, X. Y. (2011) Rapid and Simple One-Step F-18 Labeling of Peptides. *Bioconjugate Chem. 22* (3), 422−428.

(9) Tolmachev, V., and Stone-Elander, S. (2010) Radiolabelled proteins for positron emission tomography: Pros and cons of labelling methods. *Biochim. Biophys. Acta, Gen. Subj. 1800* (5), 487−510.

(10) Marek, M. J., Lambert, C. R., and Rhodes, B. A. (1994) TECHNIQUES FOR DIRECT RADIOLABELING OF MONOCLONAL-ANTIBODIES. *Radiolabeled Blood Elements: Recent Advances in Techniques and Applications* 262, 207−220.

(11) Greenland, W. E. P., and Blower, P. J. (2005) Water-soluble phosphines for direct labeling of peptides with technetium and rhenium: Insights from electrospray mass spectrometry. *Bioconjugate Chem. 16* (4), 939−948.

(12) Wilbur, D. S. (1992) Radiohalogenation of Proteins - an Overview of Radionuclides, Labeling Methods, And Reagents for Conjugate Labeling. *Bioconjugate Chem. 3* (6), 433−470.

(13) Kiesewetter, D. O., Jacobson, O., Lang, L. X., and Chen, X. Y. (2011) Automated radiochemical synthesis of F-18 FBEM: A thiol reactive synthon for radiofluorination of peptides and proteins. *Appl. Radiat. Isot. 69* (2), 410−414.

(14) Vaidyanathan, G., and Zalutsky, M. R. (1992) Labeling proteins with fluorine-18 using N-succinimidyl 4-[18F]fluorobenzoate. *International Journal of Radiation Applications and Instrumentation. Part B. Nuclear Medicine and Biology 19* (3), 275−281.

(15) Guhlke, S., Coenen, H. H., and Stöcklin, G. (1994) Fluoroacylation agents based on small n.c.a. [18F]fluorocarboxylic acids. *Appl. Radiat. Isot. 45* (6), 715−727.

(16) Basuli, F., Zhang, X., Phelps, T. E., Jagoda, E. M., Choyke, P. L., and Swenson, R. E. (2020) Automated Synthesis of Fluorine-18 Labeled CXCR4 Ligand via the Conjugation with Nicotinic AcidN-Hydroxysuccinimide Ester (6- F-18 SFPy). *Molecules 25* (17), 3924.

(17) Meyer, J. P., Adumeau, P., Lewis, J. S., and Zeglis, B. M. (2016) Click Chemistry and Radiochemistry: The First 10 Years. *Bioconjugate Chem. 27* (12), 2791.

(18) Sachin, K., Jadhav, V. H., Kim, E. M., Kim, H. L., Lee, S. B., Jeong, H. J., Lim, S. T., Sohn, M. H., and Kim, D. W. (2012) F-18 Labeling Protocol of Peptides Based on Chemically Orthogonal Strain-Promoted Cycloaddition under Physiologically Friendly Reaction Conditions. *Bioconjugate Chem. 23* (8), 1680−1686.

(19) McBride, W. J., D'Souza, C. A., Sharkey, R. M., Karacay, H., Rossi, E. A., Chang, C. H., and Goldenberg, D. M. (2010) Improved F-18 Labeling of Peptides with a Fluoride-Aluminum-Chelate Complex. *Bioconjugate Chem. 21* (7), 1331−1340.

(20) Schibli, R., and Schubiger, P. A. (2002) Current use and future potential of organometallic radiopharmaceuticals. *Eur. J. Nucl. Med. Mol. Imaging 29* (11), 1529−1542.

(21) Jackson, I. M., Scott, P. J. H., and Thompson, S. (2017) Clinical Applications of Radiolabeled Peptides for PET. *Semin. Nucl. Med. 47* (5), 493−523.

(22) Eder, M., Krivoshein, A. V., Backer, M., Backer, J. M., Haberkorn, U., and Eisenhut, M. (2010) ScVEGF-PEG-HBED-CC and scVEGF-PEG-NOTA conjugates: comparison of easy-to-label recombinant proteins for Ga-68 PET imaging of VEGF receptors in angiogenic vasculature. *Nucl. Med. Biol. 37* (4), 405−412.

(23) Maecke, H. R., and André, J. P. (2007) *68Ga-PET Radiopharmacy: A Generator-Based Alternative to 18F-Radiopharmacy, Berlin, Heidelberg*, pp 215−242, Springer Berlin Heidelberg, Berlin, Heidelberg.

(24) Brouwers, A. H., van Eerd, J. E. M., Frielink, C., Oosterwijk, E., Oyen, W. J. G., Corstens, F. H. M., and Boerman, O. C. (2004) Optimization of radioimmunotherapy of renal cell carcinoma: Labeling of monoclonal antibody cG250 with I-131, Y-90, Lu-177, or Re-186. *J. Nucl. Med. 45* (2), 327−337.

(25) Psimadas, D., Georgoulias, P., Valotassiou, V., and Loudos, G. (2012) Molecular Nanomedicine Towards Cancer: In-111-Labeled Nanoparticles. *J. Pharm. Sci. 101* (7), 2271−2280.

(26) Borjesson, P. K. E., Jauw, Y. W. S., Boellaard, R., de Bree, R., Comans, E. F. I., Roos, J. C., Castelijns, J. A., Vosjan, M., Kummer, J. A., Leemans, C. R., et al. (2006) Performance of immuno-positron emission tomography with zirconium-89-labeled chimeric monoclonal antibody U36 in the detection of lymph node metastases in head and neck cancer patients. *Clin. Cancer Res. 12* (7), 2133−2140.

(27) Meszaros, L. K., Dose, A., Biagini, S. C. G., and Blower, P. J. (2010) Hydrazinonicotinic acid (HYNIC) - Coordination chemistry and applications in radiopharmaceutical chemistry. *Inorg. Chim. Acta* 363 (6), 1059−1069.

(28) Meszaros, L. K., Dose, A., Biagini, S. C. G., and Blower, P. J. (2011) Synthesis and evaluation of analogues of HYNIC as bifunctional chelators for technetium. *Dalton Transactions 40* (23), 6260−6267.

(29) Charron, C. L., Hickey, J. L., Nsiama, T. K., Cruickshank, D. R., Turnbull, W. L., and Luyt, L. G. (2016) Molecular imaging probes derived from natural peptides. *Nat. Prod. Rep. 33* (6), 761−800.

(30) Decristoforo, C., and Mather, S. J. (1999) 99m-technetium-labelled peptide-HYNIC conjugates: Effects of lipophilicity and stability on biodistribution. *Nucl. Med. Biol. 26* (4), 389−396.

(31) Qaim, S. M. (2019) Theranostic radionuclides: recent advances in production methodologies. *J. Radioanal. Nucl. Chem. 322* (3), 1257−1266.

(32) Berman, D. S., Kiat, H., Van Train, K., Friedman, J. D., Wang, F. P., and Germano, G. (1994) Dual-Isotope Myocardial Perfusion Spect with Rest Thallium-201 and Stress Tc-99m Sestamibi. *Cardiology Clinics 12* (2), 261−270.
(33) Rangger, C., and Haubner, R. (2020) Radiolabelled Peptides for Positron Emission Tomography and Endoradiotherapy in Oncology dagger. *Pharmaceuticals 13* (2), 22.
(34) Feijtel, D., de Jong, M., and Nonnekens, J. (2020) Peptide Receptor Radionuclide Therapy: Looking Back, Looking Forward. *Curr. Top. Med. Chem. 20*, 2959.
(35) Vaidyanathan, G., and Zalutsky, M. R. (2008) Astatine Radiopharmaceuticals: Prospects and Problems. *Curr. Radiopharm. 1* (3), 177−177.
(36) Sharifi, M., Jalilian, A. R., Yousefnia, H., Alirezapour, B., Bahrami-Samani, A., and Zolghadri, S. (2018) Production, quality control, biodistribution and imaging studies of Lu-177-PSMA-617 in breast adenocarcinoma model. *Radiochim. Acta 106* (6), 507−513.
(37) Fani, M., Nicolas, G. P., and Wild, D. (2017) Somatostatin Receptor Antagonists for Imaging and Therapy. *J. Nucl. Med. 58*, 61S−66S.
(38) Sharma, N., Naraev, B. G., Engelman, E. G., Zimmerman, M. B., Bushnell, D. L., O'Dorisio, T. M., O'Dorisio, M. S., Menda, Y., Muller-Brand, J., Howe, J. R., et al. (2017) Peptide Receptor Radionuclide Therapy Outcomes in a North American Cohort With Metastatic Well-Differentiated Neuroendocrine Tumors. *Pancreas 46* (2), 151−156.
(39) Velikyan, I., Sundin, A., Eriksson, B., Lundqvist, H., Sorensen, J., Bergstrom, M., and Langstrom, B. (2010) In vivo binding of Ga-68 -DOTATOC to somatostatin receptors in neuroendocrine tumours - impact of peptide mass. *Nucl. Med. Biol. 37* (3), 265−275.
(40) Hardiansyah, D., Attarwala, A. A., Kletting, P., Mottaghy, F. M., and Glatting, G. (2017) Prediction of time-integrated activity coefficients in PRRT using simulated dynamic PET and a pharmacokinetic model. *Physica Medica-European Journal of Medical Physics 42*, 298−304.
(41) Hardiansyah, D., Maass, C., Attarwala, A. A., Muller, B., Kletting, P., Mottaghy, F. M., and Glatting, G. (2016) The role of patient-based treatment planning in peptide receptor radionuclide therapy. *Eur. J. Nucl. Med. Mol. Imaging 43* (5), 871−880.
(42) Hardiansyah, D., Guo, W., Kletting, P., Mottaghy, F. M., and Glatting, G. (2016) Time-integrated activity coefficient estimation for radionuclide therapy using PET and a pharmacokinetic model: A simulation study on the effect of sampling schedule and noise. *Med. Phys. 43* (9), 5145−5154.
(43) Bergsma, H., van Lom, K., Konijnenberg, M., Kam, B., Teunissen, J., de Herder, W., Krenning, E., and Jkwekkeboom, D. (2018) Therapy-related hematological malignancies after peptide receptor radionuclide therapy with 177 Lu-DOTA-Octreotate: Incidence, course & predicting factors in patients with GEP-NETs. *J. Nucl. Med. 59*, 452.
(44) Hervas, I., Bello, P., Falgas, M., del Olmo, M. I., Torres, I., Olivas, C., Vera, V., Olivan, P., and Yepes, A. M. (2017) Lu-177-DOTATATE treatment in neuroendocrine tumours. A preliminary study. *Revista Espanola De Medicina Nuclear E Imagen Molecular 36* (2), 91−98.
(45) Gospavic, R., Knoll, P., Mirzaei, S., and Popov, V. (2016) Physiologically Based Pharmacokinetic (PBPK) Model for Biodistribution of Radiolabeled Peptides in Patients with Neuroendocrine Tumours. *Asia Oceania journal of nuclear medicine & biology 4* (2), 90−97.
(46) Clift, A. K., Giele, H., Reddy, S., Macedo, R., Al-Nahhas, A., Wasan, H. S., Gondolesi, G. E., Vianna, R. M., Friend, P., Vaidya, A., et al. (2017) Neoadjuvant peptide receptor radionuclide therapy and modified multivisceral transplantation for an advanced small intestinal neuroendocrine neoplasm: an updated case report. *Innovative Surgical Sciences 2* (4), 247.
(47) Zemczak, A., Kołodziej, M., Gut, P., Królicki, L., Kos-Kudła, B., Kamiński, G., Ruchała, M., Pawlak, D., and Kunikowska, J. (2020) Effect of Peptide Receptor Radionuclide Therapy (PRRT) with tandem isotopes - [90Y]Y/[177Lu]Lu-DOTATATE in patients with disseminated neuroendocrine tumours depending on qualification [18F]FDG PET/CT in Polish multicenter experience - do we need [18F]FDG. *Endokrynol. Pol.*, 1 DOI: 10.5603/EP.a2020.0014.
(48) Kunikowska, J., Zemczak, A., Kolodziej, M., Gut, P., Lon, I., Pawlak, D., Mikolajczak, R., Kaminski, G., Ruchala, M., Kos-Kudla, B., and Krolicki, L. (2020) Tandem peptide receptor radionuclide therapy using Y-90/Lu-177-DOTATATE for neuroendocrine tumors efficacy and side-effects-polish multicenter experience. *Eur. J. Nucl. Med. Mol. Imaging 47* (4), 922−933.
(49) Berzaczy, D., Giraudo, C., Haug, A. R., Raderer, M., Senn, D., Karanikas, G., Weber, M., and Mayerhoefer, M. E. (2017) Whole-Body 68Ga-DOTANOC PET/MRI Versus 68Ga-DOTANOC PET/CT in Patients With Neuroendocrine Tumors: A Prospective Study in 28 Patients. *Clinical Nuclear Medicine 42* (9), 669−674.
(50) Ginj, M., Zhang, H. W., Waser, B., Cescato, R., Wild, D., Wang, X. J., Erchegyi, J., Rivier, J., Macke, H. R., and Reubi, J. C. (2006) Radiolabeled somatostatin receptor antagonists are preferable to agonists for in vivo peptide receptor targeting of tumors. *Proc. Natl. Acad. Sci. U. S. A. 103* (44), 16436−16441.
(51) Dalm, S. U., Nonnekens, J., Doeswijk, G. N., de Blois, E., van Gent, D. C., Konijnenberg, M. W., and de Jong, M. (2016) Comparison of the Therapeutic Response to Treatment with a Lu-177-Labeled Somatostatin Receptor Agonist and Antagonist in Preclinical Models. *J. Nucl. Med. 57* (2), 260−265.
(52) Wild, D., Fani, M., Fischer, R., Del Pozzo, L., Kaul, F., Krebs, S., Rivier, J. E. F., Reubi, J. C., Maecke, H. R., and Weber, W. A. (2014) Comparison of Somatostatin Receptor Agonist and Antagonist for Peptide Receptor Radionuclide Therapy: A Pilot Study. *J. Nucl. Med. 55* (8), 1248−1252.
(53) Nicolas, G. P., Mansi, R., McDougall, L., Kaufmann, J., Bouterfa, H., Wild, D., and Fani, M. (2017) Biodistribution, Pharmacokinetics, and Dosimetry of Lu-177-, Y-90-, and In-111-Labeled Somatostatin Receptor Antagonist OPS201 in Comparison to the Agonist Lu-177-DOTATATE: The Mass Effect. *J. Nucl. Med. 58* (9), 1435−1441.
(54) Dalm, S. U., Haeck, J., Doeswijk, G. N., de Blois, E., de Jong, M., and van Deurzen, C. H. M. (2017) SSTR-Mediated Imaging in Breast Cancer: Is There a Role for Radiolabeled Somatostatin Receptor Antagonists? *J. Nucl. Med. 58* (10), 1609−1614.
(55) Morgat, C., Mishra, A. K., Varshney, R., Allard, M., Fernandez, P., and Hindie, E. (2014) Targeting Neuropeptide Receptors for Cancer Imaging and Therapy: Perspectives with Bombesin, Neurotensin, and Neuropeptide-Y Receptors. *J. Nucl. Med. 55* (10), 1650−1657.
(56) Ramos-Alvarez, I., Moreno, P., Mantey, S. A., Nakamura, T., Nuche-Berenguer, B., Moody, T. W., Coy, D. H., and Jensen, R. T. (2015) Insights into bombesin receptors and ligands: Highlighting recent advances. *Peptides 72*, 128−144.
(57) Morgat, C., MacGrogan, G., Brouste, V., Velasco, V., Sevenet, N., Bonnefoi, H., Fernandez, P., Debled, M., and Hindie, E. (2017) Expression of Gastrin-Releasing Peptide Receptor in Breast Cancer and Its Association with Pathologic, Biologic, and Clinical Parameters: A Study of 1,432 Primary Tumors. *J. Nucl. Med. 58* (9), 1401−1407.
(58) Bodei, L., Ferrari, M., Nunn, A., Llull, J., Cremonesi, M., Martano, L., Laurora, G., Scardino, E., Tiberini, S., Bufi, G., et al. (2007) Lu-177-AMBA Bombesin analogue in hormone refractory prostate cancer patients: A phase I escalation study with single-cycle administrations. *European Journal of Nuclear Medicine and Molecular Imaging 34*, S221−S221.
(59) Nock, B. A., Kaloudi, A., Lymperis, E., Giarika, A., Kulkarni, H. R., Klette, I., Singh, A., Krenning, E. P., de Jong, M., Maina, T., et al. (2017) Theranostic Perspectives in Prostate Cancer with the Gastrin Releasing Peptide Receptor Antagonist NeoBOMB1: Preclinical and First Clinical Results. *J. Nucl. Med. 58* (1), 75−80.
(60) Kaloudi, A., Lymperis, E., Giarika, A., Dalm, S., Orlandi, F., Barbato, D., Tedesco, M., Maina, T., de Jong, M., and Nock, B. A. (2017) NeoBOMB1, a GRPR-Antagonist for Breast Cancer Theragnostics: First Results of a Preclinical Study with Ga-67

NeoBOMB1 in T-47D Cells and Tumor-Bearing Mice. *Molecules 22* (11), 1950.
(61) Dalm, S. U., Bakker, I. L., de Blois, E., Doeswijk, G. N., Konijnenberg, M. W., Orlandi, F., Barbato, D., Tedesco, M., Maina, T., Nock, B. A., and de Jong, M. (2017) Ga-68/Lu-177-NeoBOMB1, a Novel Radiolabeled GRPR Antagonist for Theranostic Use in Oncology. *J. Nucl. Med. 58* (2), 293−299.
(62) Cheng, S. Y., Lang, L. X., Wang, Z. T., Jacobson, O., Yung, B., Zhu, G. Z., Gu, D. Y., Ma, Y., Zhu, X. H., Niu, G., et al. (2018) Positron Emission Tomography Imaging of Prostate Cancer with Ga-68-Labeled Gastrin-Releasing Peptide Receptor Agonist BBN7−14 and Antagonist RM26. *Bioconjugate Chem. 29* (2), 410−419.
(63) Liolios, C., Buchmuller, B., Bauder-Wust, U., Schafer, M., Leotta, K., Haberkorn, U., Eder, M., and Kopka, K. (2018) Monomeric and Dimeric Ga-68-Labeled Bombesin Analogues for Positron Emission Tomography (PET) Imaging of Tumors Expressing Gastrin-Releasing Peptide Receptors (GRPrs). *J. Med. Chem. 61* (5), 2062−2074.
(64) Taherian, A., Li, X. L., Liu, Y. Q., and Haas, T. A. (2011) Differences in integrin expression and signaling within human breast cancer cells. *BMC Cancer 11*, 15.
(65) Jin, H., and Varner, J. (2004) Integrins: roles in cancer development and as treatment targets. *Br. J. Cancer 90* (3), 561−565.
(66) Li, Z. B., Chen, K., and Chen, X. (2008) Ga-68-labeled multimeric RGD peptides for microPET imaging of integrin alpha(v)beta(3) expression. *Eur. J. Nucl. Med. Mol. Imaging 35* (6), 1100−1108.
(67) Ortiz-Arzate, Z., Santos-Cuevas, C. L., Ocampo-Garcia, B. E., Ferro-Flores, G., Garcia-Becerra, R., Estrada, G., Gomez-Argumosa, E., and Izquierdo-Sanchez, V. (2014) Kit preparation and biokinetics in women of Tc-99m-EDDA/HYNIC-E- c(RGDfK) (2) for breast cancer imaging. *Nucl. Med. Commun. 35* (4), 423−432.
(68) Janssen, M., Oyen, W. J. G., Massuger, L., Frielink, C., Dijkgraaf, I., Edwards, D. S., Radjopadhye, M., Corstens, F. H. M., and Boerman, O. C. (2002) Comparison of a monomeric and dimeric radiolabeled RGD-peptide for tumor targeting. *Cancer Biother.Radiopharm. 17* (6), 641−646.
(69) Zhang, J. J., Mao, F., Niu, G., Peng, L., Lang, L. X., Li, F., Ying, H. Y., Wu, H. W., Pan, B. J., Zhu, Z. H., et al. (2018) Ga-68-BBN-RGD PET/CT for GRPR and Integrin alpha(v)beta(3) Imaging in Patients with Breast Cancer. *Theranostics 8* (4), 1121−1130.
(70) Kazmierczak, P. M., Todica, A., Gildehaus, F. J., Hirner-Eppeneder, H., Brendel, M., Eschbach, R. S., Hellmann, M., Nikolaou, K., Reiser, M. F., Wester, H. J., et al. (2016) Ga-68-TRAP-(RGD)(3) Hybrid Imaging for the In Vivo Monitoring of alpha(v)beta(3)-Integrin Expression as Biomarker of Anti-Angiogenic Therapy Effects in Experimental Breast Cancer. *PLoS One 11* (12), 19.
(71) Brubaker, P. L., and Drucker, D. J. (2004) Minireview: Glucagon-like peptides regulate cell proliferation and apoptosis in the pancreas, gut, and central nervous system. *Endocrinology 145* (6), 2653−2659.
(72) Willard, F. S., and Sloop, K. W. (2012) Physiology and Emerging Biochemistry of the Glucagon-Like Peptide-1 Receptor. *Exp. Diabetes Res. 2012*, 12.
(73) Azad, B. B., Rota, V., Yu, L. H., McGirr, R., Amant, A. H. S., Lee, T. Y., Dhanvantari, S., and Luyt, L. G. (2015) Synthesis and Evaluation of Optical and PET GLP-1 Peptide Analogues for GLP-1R Imaging. *Mol. Imaging 14*, 16.
(74) Wild, D., Macke, H., Christ, E., Gloor, B., and Reubi, J. C. (2008) Glucagon-like peptide 1-receptor scans to localize occult insulinomas. *N. Engl. J. Med. 359* (7), 766−768.
(75) Christ, E., Wild, D., Forrer, F., Brandle, M., Sahli, R., Clerici, T., Gloor, B., Martius, F., Maecke, H., and Reubi, J. C. (2009) Glucagon-Like Peptide-1 Receptor Imaging for Localization of Insulinomas. *J. Clin. Endocrinol. Metab. 94* (11), 4398−4405.
(76) Bauman, A., Valverde, I. E., Fischer, C. A., Vomstein, S., and Mindt, T. L. (2015) Development of Ga-68- and Zr-89-Labeled Exendin-4 as Potential Radiotracers for the Imaging of Insulinomas by PET. *J. Nucl. Med. 56* (10), 1569−1574.
(77) Antwi, K., Fani, M., Heye, T., Nicolas, G., Rottenburger, C., Kaul, F., Merkle, E., Zech, C. J., Boll, D., Vogt, D. R., et al. (2018) Comparison of glucagon-like peptide-1 receptor (GLP-1R) PET/CT, SPECT/CT and 3T MRI for the localisation of occult insulinomas: evaluation of diagnostic accuracy in a prospective crossover imaging study. *Eur. J. Nucl. Med. Mol. Imaging 45* (13), 2318−2327.
(78) Parihar, A. S., Vadi, S. K., Kumar, R., Mittal, B. R., Singh, H., Bal, A., Walia, R., Shukla, J., and Sinha, S. K. (2018) 68Ga DOTA-Exendin PET/CT for Detection of Insulinoma in a Patient With Persistent Hyperinsulinemic Hypoglycemia. *Clinical Nuclear Medicine 43* (8), E285−E286.
(79) Kirsi, M., Cheng-Bin, Y., Veronica, F., Tamiko, I., Viki-Veikko, E., Johan, R., Jori, J., Tiina, S., Tuula, T., Marko, T., Eleni, G., Martin, B., Martin, G., Claude, R. J., Helmut, M., Anne, R., Olof, S., Pirjo, N., et al. (2014) Cu-64- and Ga-68-Labelled Nle(14),Lys(40)(Ahx-NODAGA)NH2 -Exendin-4 for Pancreatic Beta Cell Imaging in Rats. *Molecular Imaging and Biology 16* (2), 255−263.
(80) Li, J. F., Rawson, J., Chea, J., Tang, W., Miao, L., Sui, F., Li, L., Poku, E., Shively, J. E., and Kandeel, F. (2019) Evaluation of Ga-68 DO3A-VS-Cys(40)-Exendin-4 as a PET Probe for Imaging Human Transplanted Islets in the Liver. *Sci. Rep. 9*, 8.
(81) Wang, L. Z., Liu, Y., Xu, Y. P., Sheng, J., Pan, D. H., Wang, X. Y., Yan, J. J., Yang, R. L., and Yang, M. (2018) Age-related change of GLP-1R expression in rats can be detected by F-18 AlF-NOTA-MAL-Cys(39)-exendin-4. *Brain Res. 1698*, 213−219.
(82) Juarez, J., Bendall, L., and Bradstock, K. (2004) Chemokines and their receptors as therapeutic targets: The role of the SDF-1/CXCR4 axis. *Curr. Pharm. Des. 10* (11), 1245−1259.
(83) Kircher, M., Herhaus, P., Schottelius, M., Buck, A. K., Werner, R. A., Wester, H. J., Keller, U., and Lapa, C. (2018) CXCR4-directed theranostics in oncology and inflammation. *Ann. Nucl. Med. 32* (8), 503−511.
(84) Feng, Y., Broder, C. C., Kennedy, P. E., and Berger, E. A. (1996) HIV-1 entry cofactor: Functional cDNA cloning of a seven-transmembrane, G protein-coupled receptor. *Science 272* (5263), 872−877.
(85) Nagafuchi, Y., Shoda, H., Sumitomo, S., Nakachi, S., Kato, R., Tsuchida, Y., Tsuchiya, H., Sakurai, K., Hanata, N., Tateishi, S., et al. (2016) Immunophenotyping of rheumatoid arthritis reveals a linkage between HLA-DRB1 genotype, CXCR4 expression on memory CD4(+) T cells, and disease activity. *Sci. Rep. 6*, 11.
(86) Galkina, E., and Ley, K. (2009) Immune and Inflammatory Mechanisms of Atherosclerosis. *Annu. Rev. Immunol. 27*, 165−197.
(87) Fang, H. Y., Munch, N. S., Schottelius, M., Ingermann, J., Liu, H. B., Schauer, M., Stangl, S., Multhoff, G., Steiger, K., Gerngross, C., et al. (2018) CXCR4 Is a Potential Target for Diagnostic PET/CT Imaging in Barrett's Dysplasia and Esophageal Adenocarcinoma. *Clin. Cancer Res. 24* (5), 1048−1061.
(88) Bonham, L. W., Karch, C. M., Fan, C. C., Tan, C., Geier, E. G., Wang, Y., Wen, N., Broce, I. J., Li, Y., Barkovich, M. J., et al. (2018) CXCR4 involvement in neurodegenerative diseases. *Transl. Psychiatry 8*, 10.
(89) Demmer, O., Gourni, E., Schumacher, U., Kessler, H., and Wester, H. J. (2011) PET Imaging of CXCR4 Receptors in Cancer by a New Optimized Ligand. *ChemMedChem 6* (10), 1789−1791.
(90) Wester, H. J., Keller, U., Schottelius, M., Beer, A., Philipp-Abbrederis, K., Hoffmann, F., Simecek, J., Gerngross, C., Lassmann, M., Herrmann, K., et al. (2015) Disclosing the CXCR4 Expression in Lymphoproliferative Diseases by Targeted Molecular Imaging. *Theranostics 5* (6), 618−630.
(91) Breun, M., Monoranu, C. M., Kessler, A. F., Matthies, C., Lohr, M., Hagemann, C., Schirbel, A., Rowe, S. P., Pomper, M. G., Buck, A. K., et al. (2019) Ga-68 -Pentixafor PET/CT for CXCR4-Mediated Imaging of Vestibular Schwannomas. *Front. Oncol. 9*, 6.
(92) Wang, Z., Zhang, M. R., Wang, L., Wang, S. J., Kang, F., Li, G. Q., Jacobson, O., Niu, G., Yang, W. D., Wang, J., et al. (2015) Prospective Study of Ga-68-NOTA-NFB: Radiation Dosimetry in Healthy Volunteers and First Application in Glioma Patients. *Theranostics 5* (8), 882−889.


https://dx.doi.org/10.1021/acs.bioconjchem.0c00617
*Bioconjugate Chem.* 2021, 32, 25−42

(93) Yan, X. F., Niu, G., Wang, Z., Yang, X. Y., Kiesewetter, D. O., Jacobson, O., Shen, B. Z., and Chen, X. Y. (2016) Al F-18 NOTA-T140 Peptide for Noninvasive Visualization of CXCR4 Expression. *Molecular Imaging and Biology 18* (1), 135−142.
(94) Schottelius, M., Osl, T., Poschenrieder, A., Hoffmann, F., Beykan, S., Hanscheid, H., Schirbel, A., Buck, A. K., Kropf, S., Schwaiger, M., et al. (2017) Lu-177 pentixather: Comprehensive Preclinical Characterization of a First CXCR4-directed Endoradiotherapeutic Agent. *Theranostics 7* (9), 2350−2362.
(95) Lau, J., Kwon, D., Rousseau, E., Zhang, Z. X., Zeisler, J., Uribe, C. F., Kuo, H. T., Zhang, C. C., Lin, K. S., and Benard, F. (2019) Ga-68 Ga/ Lu-177 Lu-BL01, a Novel Theranostic Pair for Targeting C-X-C Chemokine Receptor 4. *Mol. Pharmaceutics 16* (11), 4688−4695.
(96) Fekete, M., Wittliff, J. L., and Schally, A. V. (1989) Characteristics and Distribution of Receptors for D-Trp6 -Luteinizing Hormone-Releasing Hormone, Somatostatin, Epidermal Growth-Factor, And Sex Steroids in 500 Biopsy Samples of Human-Breast Cancer. *J. Clin. Lab. Anal. 3* (3), 137−147.
(97) Eidne, K. A., Flanagan, C. A., Harris, N. S., and Millar, R. P. (1987) Gonadotropin-Releasing-Hormone (Gnrh)-Binding Sites in Human-Breast Cancer Cell-Lines and Inhibitory Effects of Gnrh Antagonists. *J. Clin. Endocrinol. Metab. 64* (3), 425−432.
(98) Fekete, M., Zalatnai, A., Comaruschally, A. M., and Schally, A. V. (1989) Membrane-Receptors for Peptides in Experimental and Human Pancreatic Cancers. *Pancreas 4* (5), 521−528.
(99) Zoghi, M., Jalilian, A. R., Niazi, A., Johari-Daha, F., Alirezapour, B., and Ramezanpour, S. (2016) Development of a Ga-68-peptide tracer for PET GnRH1-imaging. *Ann. Nucl. Med. 30* (6), 400−408.
(100) Dohn, L. H., Pappot, H., Iversen, B. R., Illemann, M., Hoyer-Hansen, G., Christensen, I. J., Thind, P., Salling, L., von der Maase, H., and Laerum, O. D. (2015) uPAR Expression Pattern in Patients with Urothelial Carcinoma of the Bladder - Possible Clinical Implications. *PLoS One 10* (8), 15.
(101) Persson, M., and Kjaer, A. (2013) Urokinase-type plasminogen activator receptor (uPAR) as a promising new imaging target: potential clinical applications. *Clin. Physiol. Funct. Imaging* 33 (5), 329−337.
(102) Skovgaard, D., Persson, M., Brandt-Larsen, M., Christensen, C., Madsen, J., Klausen, T. L., Holm, S., Andersen, F. L., Loft, A., Berthelsen, A. K., et al. (2017) Safety, Dosimetry, and Tumor Detection Ability of Ga-68-NOTA-AE105: First-in-Human Study of a Novel Radioligand for uPAR PET Imaging. *J. Nucl. Med. 58* (3), 379−386.
(103) Carmon, K. S., and Azhdarinia, A. (2018) Application of Immuno-PET in Antibody-Drug Conjugate Development. *Mol. Imaging 17*, 10.
(104) Keenan, A. M., Harbert, J. C., and Larson, S. M. (1985) Monoclonal-Antibodies in Nuclear-Medicine. *J. Nucl. Med. 26* (5), 531−537.
(105) Siegel, D. L. (2002) Recombinant monoclonal antibody technology. *Transfusion Clinique Et Biologique 9* (1), 15−22.
(106) Benjouad, A. (2009) Antibody biotechnology. *African Journal of Biotechnology 8* (13), 2911−2915.
(107) Lonberg, N., and Huszar, D. (1995) Human Antibodies from Transgenic Mice. *Int. Rev. Immunol. 13* (1), 65−93.
(108) Bailly, C., Clery, P. F., Faivre-Chauvet, A., Bourgeois, M., Guerard, F., Haddad, F., Barbet, J., Cherel, M., Kraeber-Bodere, F., Carlier, T., et al. (2017) Immuno-PET for Clinical Theranostic Approaches. *Int. J. Mol. Sci. 18* (1), 57.
(109) Bodet-Milin, C., Bailly, C., Touchefeu, Y., Frampas, E., Bourgeois, M., Rauscher, A., Lacoeuille, F., Drui, D., Arlicot, N., Goldenberg, D. M., et al. (2019) Clinical Results in Medullary Thyroid Carcinoma Suggest High Potential of Pretargeted Immuno-PET for Tumor Imaging and Theranostic Approaches. *Front. Med. 6*, 7.
(110) Muylle, K., Flamen, P., Vugts, D., Guiot, T., Ghanem, G., Meuleman, N., Bourgeois, P., Vanderlinden, B., van Dongen, G., Everaert, H., et al. (2015) Tumour targeting and radiation dose of radioimmunotherapy with Y-90-rituximab in CD20+B-cell lymphoma as predicted by Zr-89-rituximab immuno-PET: impact of preloading with unlabelled rituximab. *Eur. J. Nucl. Med. Mol. Imaging 42* (8), 1304−1314.
(111) Pitalua-Cortes, Q. G., Garcia-Perez, F. O., Villasenor-Navarro, Y., Lara-Medina, F. U., Matus-Santos, J. A., Soldevilla-Gallardo, I., Porras-Reyes, F. I., Perez-Sanchez, V. M., Maldonado-Martinez, H. A., Perez-Baez, W., et al. (2017) Ga-68-DTPA Anti-HER2 positron emission tomography/CT successfully predicts the overexpression of human epidermal growth factor receptor in lung metastases from breast cancer. *Bjr Case Reports 3* (3), 20160136.
(112) Honarvar, H., Calce, E., Doti, N., Langella, E., Orlova, A., Buijs, J., D'Amato, V., Bianco, R., Saviano, M., Tolmachev, V., et al. (2018) Evaluation of HER2-specific peptide ligand for its employment as radiolabeled imaging probe. *Sci. Rep. 8*, 12.
(113) Xu, Y. P., Bai, Z. C., Huang, Q. H., Pan, Y. Y., Pan, D. H., Wang, L. Z., Yan, J. J., Wang, X. Y., Yang, R. L., and Yang, M. (2017) PET of HER2 Expression with a Novel (FAl)-F-18 Labeled Affibody. *J. Cancer 8* (7), 1170−1178.
(114) Tolmachev, V., Yim, C. B., Rajander, J., Perols, A., Karlstrom, A. E., Haaparanta-Solin, M., Gronroos, T. J., Solin, O., and Orlova, A. (2017) Comparative Evaluation of Anti-HER2 Affibody Molecules Labeled with Cu-64 Using NOTA and NODAGA. *Contrast Media Mol. Imaging 2017*, 1.
(115) Sandberg, D., Tolmachev, V., Velikyan, I., Olofsson, H., Wennborg, A., Feldwisch, J., Carlsson, J., Lindman, H., and Sorensen, J. (2017) Intra-image referencing for simplified assessment of HER2-expression in breast cancer metastases using the Affibody molecule ABY-025 with PET and SPECT. *Eur. J. Nucl. Med. Mol. Imaging 44* (8), 1337−1346.
(116) Steinhoff, K., Pierer, M., Siegert, J., Pigla, U., Laub, R., Hesse, S., Seidel, W., Sorger, D., Seese, A., Kuenstler, J. U., et al. (2014) Visualizing inflammation activity in rheumatoid arthritis with Tc-99 m Anti-CD4-mAb fragment scintigraphy. *Nucl. Med. Biol. 41* (4), 350−354.
(117) Mayer, A. T., Natarajan, A., Gordon, S. R., Maute, R. L., McCracken, M. N., Ring, A. M., Weissman, I. L., and Gambhir, S. S. (2017) Practical Immuno-PET Radiotracer Design Considerations for Human Immune Checkpoint Imaging. *J. Nucl. Med. 58* (4), 538−546.
(118) Niaz, M. O., Sun, M., Ramirez-Fort, M., and Niaz, M. J. (2020) Review of Lutetium-177-labeled Anti-prostate-specific Membrane Antigen Monoclonal Antibody J591 for the Treatment of Metastatic Castration-resistant Prostate Cancer. *Cureus 12* (2), 6.
(119) Nomura, N., Pastorino, S., Jiang, P. F., Lambert, G., Crawford, J. R., Gymnopoulos, M., Piccioni, D., Juarez, T., Pingle, S. C., Makale, M., et al. (2014) Prostate specific membrane antigen (PSMA) expression in primary gliomas and breast cancer brain metastases. *Cancer Cell Int. 14*, 26.
(120) Santos-Cuevas, C., Davanzo, J., Ferro-Flores, G., Garcia-Perez, F. O., Ocampo-Garcia, B., Ignacio-Alvarez, E., Gomez-Argumosa, E., and Pedraza-Lopez, M. (2017) Tc-99m-labeled PSMA inhibitor: Biokinetics and radiation dosimetry in healthy subjects and imaging of prostate cancer tumors in patients. *Nucl. Med. Biol. 52*, 1−6.
(121) Schmidt-Hegemann, N. S., Fendler, W. P., Buchner, A., Stief, C., Rogowski, P., Niyazi, M., Eze, C., Li, M. L., Bartenstein, P., Belka, C., and Ganswindt, U. (2017) Detection level and pattern of positive lesions using PSMA PET/CT for staging prior to radiation therapy. *Radiat. Oncol. 12*, 9.
(122) Sathekge, M., Lengana, T., Modiselle, M., Vorster, M., Zeevaart, J., Maes, A., Ebenhan, T., and Van de Wiele, C. (2017) Ga-68-PSMA-HBED-CC PET imaging in breast carcinoma patients. *Eur. J. Nucl. Med. Mol. Imaging 44* (4), 689−694.
(123) Minamimoto, R., Hancock, S., Schneider, B., Chin, F. T., Jamali, M., Loening, A., Vasanawala, S., Gambhir, S. S., and Iagaru, A. (2016) Pilot Comparison of Ga-68-RM2 PET and Ga-68-PSMA-11 PET in Patients with Biochemically Recurrent Prostate Cancer. *J. Nucl. Med. 57* (4), 557−562.
(124) Bouvet, V., Wuest, M., Bailey, J. J., Bergman, C., Janzen, N., Valliant, J. F., and Wuest, F. (2017) Targeting Prostate-Specific Membrane Antigen (PSMA) with F-18-Labeled Compounds: the

Influence of Prosthetic Groups on Tumor Uptake and Clearance Profile. *Molecular Imaging and Biology 19* (6), 923−932.
(125) Baum, R. P., Kulkarni, H. R., Schuchardt, C., Singh, A., Wirtz, M., Wiessalla, S., Schottelius, M., Mueller, D., Klette, I., and Wester, H. J. (2016) Lu-177-Labeled Prostate-Specific Membrane Antigen Radioligand Therapy of Metastatic Castration-Resistant Prostate Cancer: Safety and Efficacy. *J. Nucl. Med. 57* (7), 1006−1013.
(126) Azorin-Vega, E., Rojas-Calderon, E., Ferro-Flores, G., Aranda-Lara, L., Jimenez-Mancilla, N., and Nava-Cabrera, M. A. (2019) Assessment of the radiation absorbed dose produced by Lu-177-iPSMA, Ac-225-iPSMA and (RaCl2)-Ra-223 to prostate cancer cell nuclei in a bone microenvironment model. *Appl. Radiat. Isot. 146*, 66−71.
(127) Zitzmann, S., Kramer, S., Mier, W., Hebling, U., Altmann, A., Rother, A., Berndorff, D., Eisenhut, M., and Haberkorn, U. (2007) Identification and evaluation of a new tumor cell-binding peptide, FROP-1. *J. Nucl. Med. 48* (6), 965−972.
(128) Ahmadpour, S., Noaparast, Z., Abedi, S. M., and Hosseinimehr, S. J. (2018) Tc-99m-HYNIC-(tricine/EDDA)-FROP peptide for MCF-7 breast tumor targeting and imaging. *J. Biomed. Sci. 25*, 11.


https://dx.doi.org/10.1021/acs.bioconjchem.0c00617
*Bioconjugate Chem.* 2021, 32, 25−42

Supplementary data

# Radiolabeled peptides and antibodies in medicine

Paweł Kręcisz[1], Kamila Czarnecka[2*], Leszek Królicki[3**], Elżbieta Mikiciuk-Olasik[4*], Paweł Szymański[5*]

[1] ORCID: 0000-0003-2951-0867
[2] ORCID: 0000-0002-6497-1565
[3] ORCID: 0000-0002-7117-9621
[4] ORCID: 0000-0002-7171-4524
[5] ORCID: 0000-0003-3438-7509

** Department of Pharmaceutical Chemistry, Drug Analyses and Radiopharmacy, Faculty of Pharmacy, Medical University of Lodz, Muszyńskiego 1, 90-151 Lodz, Poland*

*** Department of Nuclear Medicine, Medical University of Warsaw, ul. Banacha 1 a, 02-097, Warsaw, Poland.*

Corresponding author: Paweł Szymański, e-mail: pawel.szymanski@umed.lodz.pl

| Status | Type | Strategy | Phase | Name of Compound | Combined with | Disease | Number of Clinical Trial |
|---|---|---|---|---|---|---|---|
| Complete | Diagnostic | GRPR | 2 | 68GA DOTA-RM2 | PET/MRI Scan | Prostate Carcinoma | NCT02440308 |
| Complete | Treatment | PRIT | 1 | 177Lu IMP-288 + BsMAb TF2 | 111In IMP-288 (imaging) | Colorectal Neoplasms | NCT00860860 |
| Complete | Treatment | PRIT | 1 | 177Lu IMP-288 + BsMAb TF2 | 111In IMP-288 (imaging) | Small Cell Lung Cancer, CEA-expressing Non Small Cell Lung Carcinoma (NSCLC) | NCT01221675 |
| Complete | Treatment | PRIT | 2 | 131I di-DTPA + BsMAB AntiCEA/AntiDTPA | - | Thyroid Neoplasms | NCT00467506 |
| Complete | Treatment | PRIT | 2 | 177Lu IMP-288 + BsMAb TF2 | 111In IMP-288 (imaging) | Small Cell Lung Cancer, CEA-expressing Non Small Cell Lung Carcinoma (NSCLC) | NCT01221675 |
| Complete | Treatment | PRRT | 2 | 111In pentetreotide | - | Neuroendocrine Tumors | NCT00442533 |
| Complete | Treatment | PRRT | 3 | 111In pentetreotide | - | Neuroendocrine Tumors | NCT00442533 |
| Complete | Treatment | RIT | 1 | 131I 3F8 Mab | Bevacizumab, Filgrastim | Neuroblastoma | NCT00450827 |
| Complete | Treatment | RIT | 1 | 131I BB4 MAb | - | Multiple Myeloma | NCT01296204 |
| Complete | Treatment | RIT | 1 | 131I chTNT-1/B Mab | - | Glioblastoma Multiforme | NCT00509301 |
| Complete | Treatment | RIT | 1 | 131I F16SIP | - | Cancer | NCT01240720 |
| Complete | Treatment | RIT | 1 | 131I Ibritumomab tiuxetan | bortezomib, tositumomab | Non-Hodgkin Lymphoma | NCT00777114 |
| Complete | Treatment | RIT | 1 | 131I Tositumomab | - | Follicular Lymphoma | NCT00315731 |
| Complete | Treatment | RIT | 1 | 131I Tositumomab | fludarabine phosphate | Extranodal Marginal Zone B-cell Lymphoma of Mucosa-associated Lymphoid Tissue, Nodal Marginal Zone B-cell Lymphoma, Recurrent Adult Burkitt Lymphoma, Recurrent Adult Diffuse Large Cell Lymphoma, Recurrent Adult Diffuse Mixed Cell Lymphoma, Recurrent Adult Diffuse Small Cleaved Cell Lymphoma, Recurrent Adult Immunoblastic Large Cell Lymphoma, Recurrent Adult Lymphoblastic Lymphoma, Recurrent Grade 1 Follicular Lymphoma, Recurrent Grade 2 Follicular Lymphoma, Recurrent Grade 3 Follicular Lymphoma, Recurrent Mantle Cell Lymphoma, Recurrent Marginal Zone Lymphoma, Splenic Marginal Zone Lymphoma, Waldenström Macroglobulinemia | NCT00110071 |
| Complete | Treatment | RIT | 1 | 131I Tositumomab | - | Non-Hodgkin Lymphoma | NCT00992758 |
| Complete | Treatment | RIT | 1 | 131I Tositumomab | - | Hodgkin's Disease | NCT00484874 |
| Complete | Treatment | RIT | 1 | 212Pb TCMC-Trastuzumab | trastuzumab | Breast Neoplasms, Peritoneal Neoplasms, Ovarian Neoplasms, Pancreatic Neoplasms, Stomach Neoplasms | NCT01384253 |

**Table S1.** The list of clinical trials used to clinical trials analysis. (part 1)

| Status | Type | Strategy | Phase | Name of Compound | Combined with | Disease | Number of Clinical Trial |
|---|---|---|---|---|---|---|---|
| Complete | Treatment | RIT | 2 | 131I Tositumomab | Cyclophosphamide, etoposide, rituximab, cytarabine, doxorubicin | B-cell Lymphoma | NCT00577629 |
| Complete | Treatment | RIT | 2 | 131I Tositumomab | - | Non-Hodgkin Lymphoma | NCT00996996 |
| Complete | Treatment | RIT | 2 | 131I Tositumomab | - | Hodgkin's Disease | NCT00484874 |
| Complete | Treatment | RIT | 2 | 131I Tositumomab | - | Non-Hodgkin Lymphoma | NCT01573000 |
| Complete | Treatment | RIT | 2 | 131I Tositumomab | - | Mantle Cell Lymphoma | NCT00992992 |
| Complete | Treatment | RIT | 2 | 90Y Ibritumomab tiuxetan | allogeneic hematopoietic cell transplantation | Non-Hodgkin Lymphoma | NCT00302757 |
| Complete | Treatment | RIT | 2 | 90Y Ibritumomab tiuxetan | ZBEAM (Zevalin, BCNU, Etoposide, Aracytine, Melphalan) therapy, Rituximab, allogeneic hematopoietic cell transplantation | Diffuse Large B Cell Lymphoma | NCT00689169 |
| Complete | Treatment | RIT | 2 | 90Y Ibritumomab tiuxetan | - | Mantle Cell Lymphoma | NCT00514475 |
| Complete | Treatment | RIT | 2 | 90Y Ibritumomab tiuxetan | Agatolimod Na, Rituximab, 111In ibritumomab tiuxetan (SPECT imaging) | Adult Non-Hodgkin Lymphoma, Extranodal Marginal Zone Lymphoma of Mucosa-Associated Lymphoid Tissue, Nodal Marginal Zone Lymphoma, Recurrent Adult Diffuse Large Cell Lymphoma, Recurrent Grade 1 Follicular Lymphoma, Recurrent Grade 2 Follicular Lymphoma, Recurrent Grade 3 Follicular Lymphoma, Recurrent Mantle Cell Lymphoma, Recurrent Marginal Zone Lymphoma, Recurrent Small Lymphocytic Lymphoma, Splenic Marginal Zone Lymphoma, Waldenstrom Macroglobulinemia | NCT00438880 |
| Complete | Treatment | RIT | 2 | 90Y Ibritumomab tiuxetan | - | B-cell Lymphoma | NCT00761384 |
| Complete | Treatment | RIT | 2 | 90Y Ibritumomab tiuxetan | rituximab, carmustine, cytarabine, etoposide, melphalan, ASCT | Lymphoma | NCT00695409 |
| Complete | Treatment | RIT | 2 | 90Y Ibritumomab tiuxetan | - | Non-Hodgkin Lymphoma | NCT01868035 |
| Complete | Treatment | RIT | 2 | 90Y Ibritumomab tiuxetan | rituximab, etoposide, busulfan, cyclophosphamide | Non-Hodgkin Lymphoma | NCT00336843 |
| Complete | Treatment | RIT | 2 | 90Y Ibritumomab tiuxetan | filgrastim, cyclophosphamide, etoposide, ASCT | Lymphoma | NCT00562978 |
| Complete | Treatment | RIT | 2 | Y90 ArtiCEA Mab cT84.66 | Gemcitabine HCl, Fluoridine | Liver Metastases, Recurrent Colon Cancer, Recurrent Rectal Cancer, Stage IV Colon Cancer, Stage IV Rectal Cancer | NCT00645710 |
| Complete | Treatment | RIT | 3 | 131I Tositumomab | Rituximab | Non-Hodgkin Lymphoma | NCT00268983 |

**Table S1.** The list of clinical trials used to clinical trials analysis. (part 3)

| Status | Type | Strategy | Phase | Name of Compound | Combined with | Disease | Number of Clinical Trial |
|---|---|---|---|---|---|---|---|
| Complete | Treatment | RIT | 1 | 89Zr AMG211 | PET Scan | Advanced Gastrointestinal Cancer | NCT02760199 |
| Complete | Treatment | RIT | 1 | 90Y DOTA M5A AntiCEA MAb | irinotecan HCl, Leucovorin Ca, Fluorouracil, Bevacizumab | Recurrent Colon Cancer, Recurrent Rectal Cancer, Stage IV Colon Cancer, Stage IV Rectal Cancer | NCT01205022 |
| Complete | Treatment | RIT | 1 | 90Y Ibritumomab tiuxetan | allogeneic hematopoietic cell transplantation | Non-Hodgkin Lymphoma | NCT00302757 |
| Complete | Treatment | RIT | 1 | 90Y Ibritumomab tiuxetan | Rituximab, Melphalan, Sargramostim, 111In ibritumomab tiuxetan (zevalin) | Multiple Myeloma and Plasma Cell Neoplasm | NCT00477815 |
| Complete | Treatment | RIT | 1 | 90Y Ibritumomab tiuxetan | Agatolimod Na, Rituximab, 111In ibritumomab tiuxetan (SPECT imaging) | Adult Non-Hodgkin Lymphoma, Extranodal Marginal Zone Lymphoma of Mucosa-Associated Lymphoid Tissue, Nodal Marginal Zone Lymphoma, Recurrent Adult Diffuse Large Cell Lymphoma, Recurrent Grade 1 Follicular Lymphoma, Recurrent Grade 2 Follicular Lymphoma, Recurrent Grade 3 Follicular Lymphoma, Recurrent Mantle Cell Lymphoma, Recurrent Marginal Zone Lymphoma, Recurrent Small Lymphocytic Lymphoma, Splenic Marginal Zone Lymphoma, Waldenstrom Macroglobulinemia | NCT00438880 |
| Complete | Treatment | RIT | 1 | 90Y Ibritumomab tiuxetan | - | B-cell Lymphoma | NCT00761384 |
| Complete | Treatment | RIT | 1 | 90Y Ibritumomab tiuxetan | filgrastim, cyclophosphamide, etoposide, ASCT | Lymphoma | NCT00452978 |
| Complete | Treatment | RIT | 1 | 90Y Ibritumomab tiuxetan | rituximab, fludarabine, cyclophosphamide ASCT | lymphoma, leucemia | NCT00048737 |
| Complete | Treatment | RIT | 1 | 90Y Ibritumomab tiuxetan | rituximab, fludarabine, cyclophosphamide ASCT | lymphoma, leucemia | NCT00048737 |
| Complete | Treatment | RIT | 1 | Y90 ArtiCEA Mab cT84.66 | after Radiotherapy and Chemotherapy | Lung Cancer | NCT00738452 |
| Complete | Treatment | RIT | 1 | Y90 ArtiCEA Mab cT84.66 | Gemcitabine HCl, Fluoridine | Liver Metastases, Recurrent Colon Cancer, Recurrent Rectal Cancer, Stage IV Colon Cancer, Stage IV Rectal Cancer | NCT00645710 |
| Complete | Treatment | RIT | 2 | 131I chTNT-1/B Mab | - | Glioblastoma Multiforme | NCT00677716 |
| Complete | Treatment | RIT | 2 | 131I F16SIP | - | Cancer | NCT01240720 |
| Complete | Treatment | RIT | 2 | 131I Radretumab | Whole Brain Radiation Therapy | Brain Metastases From Solid Tumors | NCT01125085 |
| Complete | Treatment | RIT | 2 | 131I Radretumab | External Beam Radiotherapy and chemotherapy | Non Small Cell Lung Cancer | NCT01125085 |
| Complete | Treatment | RIT | 2 | 131I Tositumomab | Acetaminophen, diphenhydramine, potassium iodide | Lymphoma | NCT00490009 |

**Table S1.** The list of clinical trials used to clinical trials analysis. (part 2)

| Status | Type | Strategy | Phase | Name of Compound | Combined with | Disease | Number of Clinical Trial |
|---|---|---|---|---|---|---|---|
| Complete | Treatment | RIT | 3 | 90Y Ibritumomab tiuxetan | BEAM Therapy | Non-Hodgkin Lymphoma | NCT00491491 |
| Active | Diagnostic | Other | 0 | 99mTc-HYNIC-IL2 | SPECT | Stage IV Skin Melanoma | NCT01789827 |
| Active | Treatment | PRIT | 1 | 90Y IMP-288 + BsMAb TF2 | 111In IMP-288 (imaging) | Metastatic Colorectal Cancer | NCT02300922 |
| Active | Treatment | PRIT | 2 | 90Y IMP-288 + BsMAb TF2 | 111In IMP-288 (imaging) | Metastatic Colorectal Cancer | NCT02300922 |
| Active | Treatment | PRRT | 1 | 177Lu DOTA-TATE | - | Neuroendocrine Tumors, Gastro Entero Pancreatic Neuroendocrine Tumors | NCT02736500 |
| Active | Treatment | RIT | 2 | 131I 3F8 MAb | Cisplatin, lomustine, Vincristine sulfate, radiotherapy | Brain and Central Nervous System Tumors | NCT00588370 |
| Active | Treatment | RIT | 1 | 131I BC8 Mab | cyclophosphamide, fludarabine phsphate, tacrolimus mycophenolate mofetil | Acute Myeloid Leukemia Arising From Previous Myelodysplastic Syndrome, Adult Acute Lymphoblastic Leukemia in Remission, Adult Acute Myeloid Leukemia in Remission, CD45-Positive Neoplastic Cells Present, Chronic Myelomonocytic Leukemia, Previously Treated Myelodysplastic Syndrome, Refractory Anemia With Excess Blasts, Refractory Anemia With Ring Sideroblasts, Refractory Cytopenia With Multilineage Dysplasia, Refractory Cytopenia With Multilineage Dysplasia and Ring Sideroblasts | NCT00589316 |
| Active | Treatment | RIT | 1 | 177Lu CHX-A''-DTPA-HuMab-5B1 (MVT-1075) | MVT-5873 (HuMab-5B1) | Pancreatic Carcinoma, Tumors That Express CA 19-9 | NCT03118349 |
| Active | Treatment | RIT | 1 | 177Lu J591 Mab | - | Prostate Cancer | NCT00538668 |
| Active | Treatment | RIT | 1 | 90Y Daclizumab | Auto stem cell transplant, BEAM therapy, 111In Daclizumab (Imaging) | Hodgkin Disease, Hodgkin Lymphoma | NCT01468311 |

**Table S1.** The list of clinical trials used to clinical trials analysis. (part 4)

| Status | Type | Strategy | Phase | Name of Compound | Combined with | Disease | Number of Clinical Trial |
|---|---|---|---|---|---|---|---|
| Active | Treatment | RIT | 2 | 131I BC8 Mab | fludarabine, cyclosporine, mycophenolate mofetil | Adult Acute Myeloid Leukemia With 11q23 (MLL) Abnormalities, Adult Acute Myeloid Leukemia With Del(5q), Adult Acute Myeloid Leukemia With Inv(16)(p13q22), Adult Acute Myeloid Leukemia With t(15;17)(q22;q12), Adult Acute Myeloid Leukemia With t(16;16)(p13;q22), Adult Acute Myeloid Leukemia With t(8;21)(q22;q22), Childhood Myelodysplastic Syndromes, Chronic Myelomonocytic Leukemia, Previously Treated Myelodysplastic Syndromes, Recurrent Adult Acute Myeloid Leukemia, Recurrent Childhood Acute Myeloid Leukemia, Refractory Anemia With Excess Blasts, Refractory Anemia With Excess Blasts in Transformation, Refractory Anemia With Ringed Sideroblasts, Refractory Cytopenia With Multilineage Dysplasia, Secondary Acute Myeloid Leukemia, Secondary Myelodysplastic Syndromes | NCT00119366 |
| Active | Treatment | RIT | 2 | 131I Tositumomab | cyclophosphamide, etoposide | Anaplastic Large Cell Lymphoma, Cutaneous B-cell Non-Hodgkin Lymphoma, Extranodal Marginal Zone B-cell Lymphoma of Mucosa-associated Lymphoid Tissue, Nodal Marginal Zone B-cell Lymphoma, Recurrent Adult Burkitt Lymphoma, Recurrent Adult Diffuse Large Cell Lymphoma, Recurrent Adult Diffuse Mixed Cell Lymphoma, Recurrent Adult Diffuse Small Cleaved Cell Lymphoma, Recurrent Adult Immunoblastic Large Cell Lymphoma, Recurrent Adult Lymphoblastic Lymphoma, Recurrent Grade 1 Follicular Lymphoma, Recurrent Grade 2 Follicular Lymphoma, Recurrent Grade 3 Follicular Lymphoma, Recurrent Mantle Cell Lymphoma, Recurrent Marginal Zone Lymphoma, Splenic Marginal Zone Lymphoma, Waldenström Macroglobulinemia | NCT00073918 |
| Active | Treatment | RIT | 2 | 90Y Daclizumab | Auto stem cell transplant, BEAM therapy, 111In Daclizumab (Imaging) | Hodgkin Disease, Hodgkin Lymphoma | NCT01468311 |
| Active | Treatment | RIT | 2 | 90Y Ibritumomab tiuxetan | Methylprednisolone, Etoposide, Cytarabine, Cisplatin, Rituximab, 111In Ibritumomab tiuxetan | Lymphoma | NCT00732498 |
| Active | Treatment | RIT | 2 | 90Y Ibritumomab tiuxetan | fludarabine, mitoxantrone, rituximab, dexamethasone | Lymphoma | NCT00290511 |
| Active | Treatment | RIT | 2 | 90Y Ibritumomab tiuxetan | Bendamustine, Rituximab | Follicular Lymphoma | NCT01234766 |
| Active | Treatment | RIT | 2 | 90Y Ibritumomab tiuxetan | rituximab, fludarabine phosphate, melphalan, sirolimus, tacrolimus, ASCT | Graft Versus Host Disease, Leukemia, Lymphoma | NCT00577287 |

**Table S1.** The list of clinical trials used to clinical trials analysis. (part 5)

| Status | Type | Strategy | Phase | Name of Compound | Combined with | Disease | Number of Clinical Trial |
|---|---|---|---|---|---|---|---|
| Active | Treatment | RIT | 2 | 90Y Ibritumomab tiuxetan | darbepoetin alfa, filgrastim, rituximab, cyclophosphamide, doxorubicine HCl, prednisone, vincristine Sulphate, 111In ibritumomab tuxetan (imaging) | Lymphoma | NCT00858422 |
| Recruiting | Diagnostic | GRPR | 2 | 68GA DOTA-RM2 | PET/MRI Scan | Prostate Adenocarcinoma | NCT02624518 |
| Recruiting | Diagnostic | GRPR | 2 | 68Ga NeoBOMB1 | PET Scan | Breast Cancer, Prostate Cancer, Colorectal Cancer, Non Small Cell Lung Cancer, Small Cell Lung Cancer | NCT03724253 |
| Recruiting | Diagnostic | GRPR | 2 | 68GA RM2 | PET/CT Scan | Prostate Cancer | NCT02559115 |
| Recruiting | Diagnostic | GRPR | 3 | 68GA DOTA-RM2 | PET/MRI Scan | Prostate Adenocarcinoma | NCT02624518 |
| Recruiting | Diagnostic | Other | 1 | 99mTc-Annexin V-128 | SPECT | Endocarditis, Thrombosis | NCT02459613 |
| Recruiting | Diagnostic | Other | 2 | 99mTc-Annexin V-128 | SPECT | Endocarditis, Thrombosis | NCT02459613 |
| Recruiting | Diagnostic | PRRT | 2 | 68Ga Satoreotide trizoxetan | PET Scan | Gastro-Enteropancreatic Neuroendocrine Tumors | NCT03220217 |
| Recruiting | Diagnostic | RIT | 0 | Cu 64 anti-CEA MAb M5A IV | PET Scan | Breast Cancer, Colon Cancer, Extrahepatic Bile Duct Cancer, Gallbladder Cancer, Gastrointestinal Cancer, Liver and Intrahepatic Biliary Tract Cancer, Lung Cancer, Metastatic Cancer, Pancreatic Cancer, Rectal Cancer, Thyroid Gland Medullary Carcinoma, Unspecified Adult Solid Tumor, Protocol Specific | NCT02293954 |
| Recruiting | Diagnostic | RIT | 1 | 89Zr Bevacizumab | PET-CT Scan | Pulmonary Arterial HypertensionExercise Associated Pulmonary Arterial Hypertension | NCT03166306 |
| Recruiting | Diagnostic | RIT | 2 | 89Zr Bevacizumab | PET-CT Scan | Pulmonary Arterial HypertensionExercise Associated Pulmonary Arterial Hypertension | NCT03166306 |
| Recruiting | Treatment | Other | 1 | 177Lu PP-F11N | - | Medullary Thyroid Cancer | NCT02088645 |
| Recruiting | Treatment | PRRT | 1 | 177Lu DOTA-EB-TATE | - | Neuroendocrine Tumors | NCT03308682 |
| Recruiting | Treatment | PRRT | 1 | 177Lu DOTA-EB-TATE | - | Neuroendocrine Tumors | NCT03478358 |
| Recruiting | Treatment | PRRT | 1 | 177Lu DOTA-TATE | - | Neuroendocrine Tumors | NCT03478358 |
| Recruiting | Treatment | PRRT | 1 | 212Pb DOTAMTATE | - | Neuroendocrine Tumors | NCT03466216 |
| Recruiting | Treatment | PRRT | 1 | 90Y DOTA-TOC | 68GA DOTA-TOC PET Scan | Neuroendocrine Tumors | NCT03197012 |
| Recruiting | Treatment | PRRT | 1 | 90Y DOTA-TOC | 131I MIBG | Malignant Neuroendocrine Tumor, Hormone-Secreting Neuroendocrine Tumor Gastrointestinal | NCT03044977 |
| Recruiting | Treatment | PRRT | 2 | 177Lu DOTA-TATE | - | Carcinoma, Neuroendocrine | NCT01876771 |
| Recruiting | Treatment | PRRT | 2 | 177Lu DOTA-TATE | - | Neuroendocrine Tumors | NCT03422029 |
| Recruiting | Treatment | PRRT | 2 | 177Lu DOTA-TATE | - | Neuroendocrine Tumors | NCT02125474 |

**Table S1.** The list of clinical trials used to clinical trials analysis. (part 6)

| Status | Type | Strategy | Phase | Name of Compound | Combined with | Disease | Number of Clinical Trial |
|---|---|---|---|---|---|---|---|
| Recruiting | Treatment | PRRT | 2 | 177Lu DOTA-TATE | - | Neuroendocrine Tumors<br>Carcinoid Tumor<br>Carcinoma, Neuroendocrine | NCT02754297 |
| Recruiting | Treatment | PRRT | 2 | 177Lu DOTA-TATE | - | Neuroendocrine Tumors | NCT02489604 |
| Recruiting | Treatment | PRRT | 2 | 177Lu DOTA-TOC | Sunitinib | Pancreatic Neuroendocrine Carcinoma | NCT02230176 |
| Recruiting | Treatment | PRRT | 2 | 90Y DOTA-TOC | 68Ga DOTA-TATE/ 68Ga DOTA-TOC Pet Scan | Neuroendocrine Tumors, Meningioma, Neuroblastoma, Medulloblastoma | NCT03273712 |
| Recruiting | Treatment | PRRT | 3 | 111In pentetreotide | - | Digestive Neuroendocrine Tumors, Metabolic Radiotherapy, Resection, Liver Metastases | NCT02465112 |
| Recruiting | Treatment | PRRT | 3 | 177Lu DOTA-TOC | Everolimus | Neuroendocrine Tumors | NCT03049189 |
| Recruiting | Treatment | RIT | 1 | 124I 8H9 Mab | - | Brain Cancer/Brain Stem Glioma | NCT01502917 |
| Recruiting | Treatment | RIT | 1 | 131I 8H9 Mab | - | Brain and Central Nervous System Tumors, Neuroblastoma, Sarcoma | NCT00089245 |
| Recruiting | Treatment | RIT | 1 | 131I I-8H9 MAb | - | Peritoneal Cancer | NCT01099644 |
| Recruiting | Treatment | RIT | 1 | 177Lu lilotomab | - | Non-Hodgkin Lymphoma, Follicular Lymphoma | NCT01796171 |
| Recruiting | Treatment | RIT | 1 | 177Lu lilotomab | - | Diffuse Large B-Cell Lymphoma | NCT02658968 |
| Recruiting | Treatment | RIT | 1 | 177Lu lilotomab | - | Non-Hodgkin Lymphoma | NCT02657447 |
| Recruiting | Treatment | RIT | 1 | 177Lu lilotomab | - | Non-Hodgkin Lymphoma | NCT02657447 |
| Recruiting | Treatment | RIT | 1 | 177Lu lilotomab | - | Non-Hodgkin Lymphoma, Follicular Lymphoma | NCT01796171 |
| Recruiting | Treatment | RIT | 1 | 177Lu lilotomab | - | Diffuse Large B-cell Lymphoma | NCT02658968 |
| Recruiting | Treatment | RIT | 1 | 211At BC8-B10 AntiCD45 MAb | cyclosporine, fludarabine phosphate, mycophenolate mofetil, sirolimus | Acute Lymphoblastic Leukemia in Remission, Acute Myeloid Leukemia Arising From Previous Myelodysplastic Syndrome, Acute Myeloid Leukemia in Remission, CD45-Positive Neoplastic Cells Present, Chronic Myelomonocytic Leukemia, Myelodysplastic Syndrome With Excess Blasts, Recurrent Adult Acute Myeloid Leukemia, Refractory Adult Acute Lymphoblastic Leukemia | NCT03128034 |
| Recruiting | Treatment | RIT | 1 | 227Th Epratuzumab | - | Non-Hodgkin Lymphoma | NCT02581878 |
| Recruiting | Treatment | RIT | 1 | 90Y AntiCD66 Mab | - | Acute Leukaemia, Chronic Leukaemia, Myeloma, Lymphoma | NCT01521611 |
| Recruiting | Treatment | RIT | 1 | 90Y DOTA-biotin + Anti-CD20 B9E9 scFv-Streptavidin Fusion protein | Autologous Hematopoietic Stem Cell Transplantation, carmustine, clearing agent, etoposide, melphalan, 111In DOTA-biotin (Imaging) | Burkitt Lymphoma, CD20-Positive Neoplastic Cells Present, Diffuse Large B-Cell Lymphoma, Indolent Non-Hodgkin Lymphoma, Mantle Cell Lymphoma, Recurrent B-Cell Non-Hodgkin Lymphoma, Refractory Mature B-Cell Non-Hodgkin Lymphoma | NCT02483000 |

**Table S1.** The list of clinical trials used to clinical trials analysis. (part 6)

| Status | Type | Strategy | Phase | Name of Compound | Combined with | Disease | Number of Clinical Trial |
|---|---|---|---|---|---|---|---|
| Recruiting | Treatment | RIT | 2 | 131I omburtamab | - | NeuroblastomaCNS MetastasesLeptomeningeal Metastases | NCT03275402 |
| Recruiting | Treatment | RIT | 2 | 177Lu lilotomab | - | Non-Hodgkin Lymphoma, Follicular Lymphoma | NCT01796171 |
| Recruiting | Treatment | RIT | 2 | 177Lu lilotomab | - | Non-Hodgkin Lymphoma, Follicular Lymphoma | NCT01796171 |
| Recruiting | Treatment | RIT | 2 | 211At BC8-B10 AntiCD45 MAb | cyclosporine, fludarabine phosphate, mycophenolate mofetil, sirolimus | Acute Lymphoblastic Leukemia in Remission, Acute Myeloid Leukemia Arising From Previous Myelodysplastic Syndrome, Acute Myeloid Leukemia in Remission, CD45-Positive Neoplastic Cells Present, Chronic Myelomonocytic Leukemia, Myelodysplastic Syndrome With Excess Blasts, Recurrent Adult Acute Myeloid Leukemia, Refractory Adult Acute Lymphoblastic Leukemia | NCT03128034 |
| Recruiting | Treatment | RIT | 2 | 90Y AntiCD66 Mab | - | Acute Leukaemia, Chronic Leukaemia, Myeloma, Lymphoma | NCT01521611 |
| Recruiting | Treatment | RIT | 2 | 90Y Ibritumomab tiuxetan | cyclosporine, fludarabine, ASCT, mycophenolate mofetil, rituximab, 111In ibritumomab tiuxetane (Imaging) | Post-Transplant Lymphoproliferative Disorder, Recurrent Adult Diffuse Large Cell Lymphoma, Recurrent B-Cell Non-Hodgkin Lymphoma, Recurrent Burkitt Lymphoma, Refractory B-Cell Non-Hodgkin Lymphoma, Refractory Burkitt Lymphoma, Refractory Diffuse Large B-Cell Lymphoma | NCT01434472 |
| Recruiting | Treatment | RIT | 3 | 131I omburtamab | - | NeuroblastomaCNS MetastasesLeptomeningeal Metastases | NCT03275402 |
| Recruiting | Treatment | RIT | 3 | 90Y Ibritumomab tiuxetan | BEAM therapy | Relapsed Follicular Lymphoma | NCT01827605 |
| Not Yet Recruiting | Diagnostic | GRPR | 3 | 68GA RM2 | LightPath (68Ga RM2 product), PET/CT | Breast Cancer | NCT03731026 |
| Not Yet Recruiting | Diagnostic | PRRT | 1 | 68Ga DOTA-TATE | PET/MRI Scan | Hepatocellular Carcinoma | NCT03648073 |
| Not Yet Recruiting | Diagnostic | PRRT | 2 | 68Ga DOTA-TATE | PET/MRI Scan | Hepatocellular Carcinoma | NCT03648073 |
| Not Yet Recruiting | Diagnostic | PRRT | 2 | 68Ga Satorcotide trizoxetan | PET Scan | Breast Cancer | NCT03697551 |
| Not Yet Recruiting | Treatment | Other | 1 | 177Lu PP-F11N | Sacubitril | Medullary Thyroid Cancer | NCT03647657 |
| Terminated | Treatment | PRIT | 1 | 90Y IMP-288 + BsMAb TF2 | - | Metastatic Colorectal Cancer | NCT01273402 |
| Terminated | Treatment | PRRT | 2 | 90Y DOTA-TOC | - | Diffuse Large B Cell and Mantle Cell Lymphomas | NCT02488512 |
| Terminated | Treatment | RIT | 1 | 131I Radretumab | External Beam Radiotherapy and chemotherapy | Non Small Cell Lung Cancer | NCT01124812 |

**Table S1.** The list of clinical trials used to clinical trials analysis. (part 7)

| Status | Type | Strategy | Phase | Name of Compound | Combined with | Disease | Number of Clinical Trial |
|---|---|---|---|---|---|---|---|
| Terminated | Treatment | RIT | 1 | 131I Radretumab | - | Patiens with cancer | NCT01242943 |
| Terminated | Treatment | RIT | 1 | 131I Tenatumomab | - | Breast Neoplasm, Head and Neck Neoplasm, Skin Neoplasm, Respiratory Tract Neoplasm, Urogenital Neoplasm, Digestive System Neoplasm, Pancreatic Neoplasm, Connective and Soft Tissue Neoplasm, Lymphoma, Non-Hodgkin | NCT02602067 |
| Terminated | Treatment | RIT | 1 | 90Y Epratuzumab Tetraxetan | Veltuzumab | Follicular Lymphoma | NCT01147393 |
| Terminated | Treatment | RIT | 2 | 131I Tositumomab | methotexate | Follicular Lymphoma | NCT01389076 |
| Terminated | Treatment | RIT | 2 | 90Y Epratuzumab Tetraxetan | Veltuzumab | Follicular Lymphoma | NCT01147393 |
| Terminated | Treatment | RIT | 2 | 90Y Ibritumomab tiuxetan | 111In Ibritumomab tiuxetan (Zevalin) (Imaging) | Multiple Myeloma | NCT01207765 |
| Terminated | Treatment | RIT | 2 | 90Y Ibritumomab tiuxetan | Rituximab | Primary Central Nervous System Non-Hodgkin Lymphoma | NCT01973062 |
| Terminated | Treatment | RIT | 3 | 90Y Ibritumomab tiuxetan | carmustine, etoposide, cytarabine, melphalan, ASCT, rituximab | Diffuse Large B-Cell Lymphoma | NCT02366663 |
| Terminated | Treatment | RIT | 3 | 90Y Ibritumomab tiuxetan | Comparison 90Y Ibritumomab tiuxetan vs rituximab | Follicular Lymphoma | NCT01662102 |
| Withdrawn | Treatment | PRRT | 2 | 90Y DOTA-TOC | 68Ga DOTA-TOC Pet Scan | Neuroendocrine Tumors, Meningioma, Neuroblastoma, Medulloblastoma | NCT03013387 |
| Withdrawn | Treatment | PRRT | 3 | 177Lu DOTATATE | 177Lu DOTA-TATE vs. INFalfa | Gastro-intestinal Neuroendocrine Tumors | NCT01860742 |
| Withdrawn | Treatment | RIT | 1 | 90Y DOTA-epratuzumab | Busulfan, Fludarabine, allogenic stem cell transplantation | Lymphocyte B CD22 Positive Acute Lymphoblastic Leukemia | NCT02579094 |
| Withdrawn | Treatment | RIT | 2 | 90Y DOTA-epratuzumab | Chemotherapy/immunotherapy | CD22+ Relapsed/Refractory B-ALL | NCT02844530 |
| Unknown | Diagnostic | GRPR | 1 | 68Ga NOTA-BBN-RGD | PET/CT Scan | Breast Cancer | NCT02749019 |
| Unknown | Diagnostic | GRPR | 1 | 68Ga NOTA-BBN-RGD | PET/CT Scan | Breast Cancer | NCT02747290 |
| Unknown | Diagnostic | PRIT | 1 | 131I AntiCEA/AntiHSG BsMAb T2F | Scintygraphy | Colorectal Cancer | NCT00895323 |
| Unknown | Diagnostic | PRRT | 1 | 68Ga DOTA-TATE | PET Scan | Neuroendocrine Carcinoma | NCT01879657 |
| Unknown | Diagnostic | RIT | 2 | 99m Tc EP-1645 | SPECT/CT | Carotid Stenosis | NCT00904254 |
| Unknown | Treatment | PRRT | 2 | 177Lu DOTA-TATE | - | Neuroendocrine Tumors | NCT01237457 |
| Unknown | Treatment | RIT | 1 | 90Y Epratuzumab | - | Acute Lymphoblastic Leukemia | NCT01354457 |
| Unknown | Treatment | RIT | 1 | 90Y Epratuzumab Tetraxetan | Veltuzumab | Non-Hodgkin's Lymphoma, Diffuse Large B-cell Lymphoma | NCT01101581 |
| Unknown | Treatment | RIT | 2 | 131I Rituximab | - | Relapsed or Refractory Diffuse Large B Cell Lymphoma | NCT01676558 |

**Table S1.** The list of clinical trials used to clinical trials analysis. (part 8)

| Status | Type | Strategy | Phase | Name of Compound | Combined with | Disease | Number of Clinical Trial |
|---|---|---|---|---|---|---|---|
| Unknown | Treatment | RIT | 2 | 131I Rituximab | - | Relapsed or Refractory Marginal Zone B-cell Lymphoma | NCT01678404 |
| Unknown | Treatment | RIT | 2 | 90Y Epratuzumab | - | Acute Lymphoblastic Leukemia | NCT01354457 |
| Unknown | Treatment | RIT | 2 | 90Y Ibritumomab tiuxetan | Rituximab | Follicular Lymphoma | NCT01493479 |

**Table S1.** The list of clinical trials used to clinical trials analysis. (part 9)

# Oświadczenia współautorów

UNIWERSYTET MEDYCZNY W ŁODZI

*prof. dr hab. n. farm. Paweł Szymański*

Łódź, 06.09.2021

# Oświadczenie o współautorstwie

Oświadczam, że mój udział w wymienionych publikacjach był następujący

1. Krecisz, P.; Czarnecka, K.; Szymanski, P. Physicochemical evaluation of new tetrahydroacridine and iodobenzoic acid hybrids as the next step in the design of potential drugs for treating Alzheimer's disease. Biomedical Chromatography 2020, 9, doi:10.1002/bmc.4906

- Nadzór merytoryczny oraz konsultacje dotyczące przeprowadzanych analiz HPLC oraz procesu walidacji zgodnego z normami ICH
- Korekty manuskryptu oraz współudział w jego dalszym przygotowaniu do publikacji jako autor korespondencyjny

2. Kręcisz, P.; Czarnecka, K.; Szymański, P. Thin-Layer Chromatography Gradient Optimization Strategy for Wet Load Adsorption Flash Chromatography. Journal of Chromatographic Science 2021, doi:10.1093/chromsci/bmab097

- Nadzór merytoryczny oraz konsultacje dotyczące projektowania doświadczeń chromatograficznych
- Korekty manuskryptu oraz współudział w jego dalszym przygotowaniu do publikacji jako autor korespondencyjny

3. Kręcisz, P.; Czarnecka, K.; Królicki, L.; Mikiciuk-Olasik, E.; Szymański, P. Radiolabeled Peptides and Antibodies in Medicine. Bioconjugate Chemistry 2021, 32, 25-42, doi:10.1021/acs.bioconjchem.0c00617

- Nadzór merytoryczny
- Współudział w koncepcji pracy
- Korekty manuskryptu oraz współudział w jego dalszym przygotowaniu do publikacji jako autor korespondencyjny

KIEROWNIK
Pracowni Radiofarmacji
Zakładu Chemii Farmaceutycznej, Analizy Leków i Radiofarmacji
Katedry Chemii Farmaceutycznej
Uniwersytetu Medycznego w Łodzi
Prof. dr hab. n. farm. Paweł Szymański

Zakład Chemii Farmaceutycznej, Analizy Leków i Radiofarmacji
90-151 Łódź | ul. Muszyńskiego 1
tel. (042) 677 92 90 fax. (042) 677 92 50
e-mail: pawel.szymanski@umed.lodz.pl
www.umed.pl

UNIWERSYTET MEDYCZNY W ŁODZI

*dr n. farm. Kamila Czarnecka*

Łódź, 06.09.2021

# Oświadczenie o współautorstwie

Oświadczam, że mój udział w wymienionych publikacjach był następujący

1. Krecisz, P.; Czarnecka, K.; Szymanski, P. Physicochemical evaluation of new tetrahydroacridine and iodobenzoic acid hybrids as the next step in the design of potential drugs for treating Alzheimer's disease. Biomedical Chromatography 2020, 9, doi:10.1002/bmc.4906
   - Korekta manuskryptu
   - Konsultacja merytoryczna

2. Kręcisz, P.; Czarnecka, K.; Szymański, P. Thin-Layer Chromatography Gradient Optimization Strategy for Wet Load Adsorption Flash Chromatography. Journal of Chromatographic Science 2021, doi:10.1093/chromsci/bmab097
   - Korekta manuskryptu
   - Konsultacja merytoryczna

3. Kręcisz, P.; Czarnecka, K.; Królicki, L.; Mikiciuk-Olasik, E.; Szymański, P. Radiolabeled Peptides and Antibodies in Medicine. Bioconjugate Chemistry 2021, 32, 25-42, doi:10.1021/acs.bioconjchem.0c00617
   - Korekta manuskryptu
   - Konsultacja merytoryczna

Kamila Czarnecka

ADIUNKT
Zakładu Chemii Farmaceutycznej, Analizy Leków i Radiofarmacji
Katedry Chemii Farmaceutycznej
Uniwersytetu Medycznego w Łodzi

Dr n. farm. Kamila Czarnecka

Zakład Chemii Farmaceutycznej, Analizy Leków i Radiofarmacji
90-151 Łódź | ul. Muszyńskiego 1
tel. (042) 677 92 90 fax. (042) 677 92 50
e-mail: kamila.czarnecka@umed.lodz.pl
www.umed.pl

UNIWERSYTET MEDYCZNY W ŁODZI

*Prof. dr hab. n. farm. Elżbieta Mikiciuk-Olasik*

Łódź,06.09.2021

# Oświadczenie o współautorstwie

Oświadczam, że mój udział w poniższej publikacji:

1. Kręcisz, P.; Czarnecka, K.; Królicki, L.; Mikiciuk-Olasik, E.; Szymański, P. Radiolabeled Peptides and Antibodies in Medicine. Bioconjugate Chemistry 2021, 32, 25-42, doi:10.1021/acs.bioconjchem.0c00617

był następujący:

Konsultacje i pomoc merytoryczna w trakcie opracowywania manuskryptu

KIEROWNIK
Katedry Chemii Farmaceutycznej
i Zakładu Chemii Farmaceutycznej
Analizy Leków i Radiofarmacji
Uniwersytetu Medycznego w Łodzi
Prof. dr hab. n. farm. Elżbieta Mikiciuk-Olasik

Zakład Chemii Farmaceutycznej, Analizy Leków i Radiofarmacji
90-151 Łódź | ul. Muszyńskiego 1
tel. (042) 677 92 90 fax. (042) 677 92 50
e-mail: elzbieta.mikiciuk-olasik@umed.lodz.pl
www.umed.pl

Warszawa, 06.09.2021

Prof. dr hab. n. med. Leszek Królicki

leszek.krolicki@wum.edu.pl

Warszawski Uniwersytet Medyczny

Zakład Medycyny Nuklearnej

Ul. Banacha 1A

02-097 Warszawa

# Oświadczenie o współautorstwie

Oświadczam, że mój udział w wymienionej publikacji był następujący

1. Kręcisz, P.; Czarnecka, K.; Królicki, L.; Mikiciuk-Olasik, E.; Szymański, P. Radiolabeled Peptides and Antibodies in Medicine. Bioconjugate Chemistry 2021, 32, 25-42, doi:10.1021/acs.bioconjchem.0c00617

- Konsultacje, pomoc merytoryczna oraz korekta w trakcie przygotowywania manuskryptu

# Dorobek naukowy

## Dorobek całkowity

*Suma IF:* ***37,768***

*Suma MNiSW:* ***880***

## Publikacje będące podstawą pracy doktorskiej

1. **Krecisz, P.**; Czarnecka, K.; Szymanski, P. Physicochemical evaluation of new tetrahydroacridine and iodobenzoic acid hybrids as the next step in the design of potential drugs for treating Alzheimer's disease. *Biomedical Chromatography* **2020**, 9, doi:10.1002/bmc.4906.

   IF: 1,902 (2020) MNiSW: 40

2. **Kręcisz, P.**; Czarnecka, K.; Królicki, L.; Mikiciuk-Olasik, E.; Szymański, P. Radiolabeled Peptides and Antibodies in Medicine. *Bioconjugate Chemistry* **2021**, *32*, 25-42, doi:10.1021/acs.bioconjchem.0c00617.

   IF: 4,774 (2020) MNiSW: 100

3. **Kręcisz, P.**; Czarnecka, K.; Szymański, P. Thin-Layer Chromatography Gradient Optimization Strategy for Wet Load Adsorption Flash Chromatography *Journal of Chromatographic Science* **2021**, bmab097, doi: https://doi.org/10.1093/chromsci/bmab097

   IF: 1,618 (2020) MNiSW: 40

**Łącznie:**

*Suma IF:* ***8,294***

*Suma MNiSW:* ***180***

## Pozostały dorobek naukowy

### Publikacje w czasopismach z listy filadelfijskiej

1. Czarnecka, K.; Girek, M.; **Krecisz, P.**; Skibinski, R.; Latka, K.; Jonczyk, J.; Bajda, M.; Kabzinski, J.; Majsterek, I.; Szymczyk, P.; et al. Discovery of New Cyclopentaquinoline Analogues as Multifunctional Agents for the Treatment of Alzheimer's Disease. *International Journal of Molecular Sciences* **2019**, *20*, 22, doi:10.3390/ijms20030498.

   IF: 4,556 (2019) MNiSW: 140

2. Czarnecka, K.; Lisiecki, P.; Szewczyk, E.; Chufarova, N.; Wojtowicz, P.; **Krecisz, P.**; Szymanski, P. New acridine derivatives as promising agents against methicillin-resistant staphylococci - From tests to in silico analysis. *Computational Biology and Chemistry* **2020**, *88*, 6, doi:10.1016/j.compbiolchem.2020.107321.

IF: 2,877 (2020) MNiSW: 70

3. Czarnecka, K.; Girek, M.; Wójtowicz, P.; **Kręcisz, P**.; Skibiński, R.; Jończyk, J.; Łątka, K.; Bajda, M.; Walczak, A.; Galita, G.; et al. New Tetrahydroacridine Hybrids with Dichlorobenzoic Acid Moiety Demonstrating Multifunctional Potential for the Treatment of Alzheimer's Disease. *International Journal of Molecular Sciences* **2020**, *21*, doi:10.3390/ijms21113765.

IF: 5,923 (2020) MNiSW: 140

4. Zawada, K.; Czarnecka, K.; Girek, M.; **Kręcisz, P.**; Trejtnar, F.; Mandíková, J.; Jończyk, J.; Bajda, M.; Staśkiewicz, M.; Wójtowicz, P.; et al. New hybrids of tacrine and indomethacin as multifunctional acetylcholinesterase inhibitors. *Chemical Papers* **2020**, doi:10.1007/s11696-020-01295-y.

IF: 2,097 (2020) MNiSW: 40

5. Dominiak, Z.; Huras, H.; **Kręcisz, P.**; Krzeszowski, W.; Szymański, P.; Czarnecka, K. Promising results in development of male contraception. *Bioorganic & Medicinal Chemistry Letters* **2021**, 128005, doi:https://doi.org/10.1016/j.bmcl.2021.128005.

IF: 2,823 (2020) MNiSW: 70

6. Skrzypek, A.; Matysiak, J.; Karpińska, M.; Czarnecka, K.; **Kręcisz, P.**; Stary, D.; Kukułowicz, J.; Paw, B.; Bajda, M.; Szymański, P.; et al. Biological evaluation and molecular docking of novel 1,3,4-thiadiazole-resorcinol conjugates as multifunctional cholinesterases inhibitors. *Bioorganic Chemistry* **2021**, *107*, 104617, doi:https://doi.org/10.1016/j.bioorg.2020.104617.

IF: 5,275 (2020) MNiSW: 100

7. Czylkowska, A.; Szczesio, M.; Raducka, A.; Rogalewicz, B.; **Kręcisz, P.**; Czarnecka, K.; Szymański, P.; Pitucha, M.; Pawlak, T. Cytotoxic Activity against A549 Human Lung Cancer Cells and ADMET Analysis of New Pyrazole Derivatives. *International Journal of Molecular Sciences* **2021**, *22*(13), 6692, doi: https://doi.org/10.3390/ijms22136692

IF: 5,923 (2020) MNiSW: 140

**Łącznie:**

*Suma IF:* ***29,474***

*Suma MNiSW:* **700**

Publikacje w czasopismach polskich nieindeksowanych

1. **Kręcisz, P.**; Czarnecka, K.; Szymański, P. Od starych po innowacyjne – najbardziej obiecujące cząsteczki w farmacji. Aptekarz Polski 2018, 148 (126e), 5-11.

Doniesienia zjazdowe

1. Lisiecki, P.; **Kręcisz, P.**; Dudkiewicz, B. Kasety SCCmec u metycylinoopornych szczepów S. pseudintermedius izolowanych z infekcji od zwierząt towarzyszących człowiekowi. XX Sympozjum naukowe Postępy w Medycynie Zakażeń, 2-3 grudnia 2016, Warszawa.

2. Kałużyńska, Z.; **Kręcisz, P.**; Lisiecki, P. Oporność szczepów Staphylococcus pseudintermedius izolowanych z infekcji od zwierząt na antybiotyki klasy MLSB. I Sesja Młodych Mikrobiologów Środowiska Łódzkiego, 23 czewca 2017, Łódź.

# Streszczenie

Medycyna nuklearna jest obecnie jednym z najprężniej rozwijających się kierunków medycznych. Efektem tego stanu rzeczy jest silny rozwój badań nad nowymi radiofarmaceutykami, co było inspiracją do badań prezentowanych w pracy doktorskiej.

Celem przedstawionej pracy doktorskiej było zebranie informacji na temat obecnego stanu wiedzy o najnowszych radiofarmaceutykach, opracowanie metod pozwalających na uzyskanie danych o parametrach fizykochemicznych i stabilności substancji biologicznie czynnych pochodnych 1,2,3,4-tetrahydroakrydyny będących nośnikami „zimnych" izotopów atomów wykorzystywanych w medycynie nuklearnej, a także usprawnienie procesu projektowania oraz otrzymywania nowych substancji leczniczych wykorzystujących techniki chromatograficzne, które w przyszłości z powodzeniem można będzie zastosować w badaniach nad nowymi radiofarmaceutykami.

Wyniki badań dostarczyły informacji o właściwościach fizykochemicznych jodopochodnych 1,2,3,4-tetrahydroakrydyny będących „zimnymi" radiofarmaceutykami. Opracowane pochodne zawierały w swojej strukturze atom jodu, który domyślnie zostanie zastąpiony izotopem promieniotwórczym. Uzyskane dane dotyczyły między innymi wartości logarytmu P oraz pKa dla 2-jodo-N-[4-(1,2,3,4-tetrahydroakrydyno-9-amino)butylo]benzamidu, 3-jodo-N-[4-(1,2,3,4-tetrahydroakrydyno-9-amino)butylo]benzamidu i 4-jodo-N-[4-(1,2,3,4-tetrahydroakrydyno-9-amino)butylo]benzamidu. Pozwoliły one na ocenę wpływu położenia podstawnika (atomu jodu) w pierścieniu aromatycznym na kluczowe pod względem farmakokinetyki właściwości fizykochemiczne związku. 3-jodo-N-[4-(1,2,3,4-tetrahydroakrydyno-9-amino)butylo]benzamid został poddany również badaniu stabilności chemicznej. Próbki zostały analizowane z użyciem techniki HPLC. Przy użyciu tej metody dokonano pełnej walidacji zgodnie z raportem Q2 wydanym przez Międzynarodową Radę ds. Harmonizacji. Wyniki badań dostarczyły cennych informacji o fotolabilności układu, co pozwoliło na opracowanie prawidłowego sposobu przechowywania i transportu badanych analogów tego związku. Kluczowym elementem opracowywania nowych substancji leczniczych jest ich prawidłowe oczyszczenie po procesie syntezy. Dlatego proces ten został poddany optymalizacji, której wynikiem było opracowanie strategii optymalizacji rozdziału chromatografii typu FLASH z wykorzystaniem techniki TLC. Koncepcja ta pozwala na precyzyjne ustalenie warunków rozdziału gradientowego mającego na celu eliminację niekorzystnych efektów zastosowania techniki mokrej podaży próbki oraz uzyskiwania czystych frakcji badanego związku w określonym czasie retencji bez względu na skalę procedury. Opracowana strategia w znaczący sposób usprawnia i przyspiesza proces oczyszczania substancji biologicznie czynnych co ma znaczenie w procesie oczyszczania radiofarmaceutyków, które z uwagi na specyficzny czas połowicznego rozpadu izotopów promieniotwórczych wymagają szybkich, powtarzalnych i wydajnych procedur.

# Abstract

Nuclear medicine and imaging are currently one of the most dynamically developing directions in medical sciences. The outcome is the strong development of research on new radiopharmaceuticals, which was the inspiration for the research presented in this dissertation.

The aim of this dissertation was to collect information on the current state of knowledge about the latest radiopharmaceuticals, to develop methods to obtain data on the physicochemical parameters and stability of biologically active 1,2,3,4-tetrahydroacridine derivatives that are carriers of non-radioactive isotopes of elements used in nuclear imaging, as well as streamlining the process of designing and obtaining new medicinal substances using chromatographic techniques, which in the future can be successfully applied in research on new radiopharmaceuticals.

The study results provided information on the physicochemical properties of 1,2,3,4-tetrahydroacridine iodine derivatives, which are "cold" radiopharmaceuticals. The developed derivatives contained in their structure the iodine element, which will be finally replaced by a radioactive isotope. The obtained data concerned log P and pKa values for 2-iodo-N-[4-(1,2,3,4-tetrahydroacridine-9-amino)butyl]benzamide, 3-iodo-N-[4-(1,2,3,4-tetrahydroacridine-9-amino)butyl] benzamide and 4-iodo-N-[4-(1,2,3,4-tetrahydroacridine-9-amino)butyl]benzamide, which allowed to assess the effect of iodine substituent placement in the aromatic ring on the crucial physicochemical properties of the compound in terms of pharmacokinetics. 3-iodo-N-[4-(1,2,3,4-tetrahydroacridine-9-amino)butyl]benzamide was also subjected to a chemical stability test. The samples were analyzed by HPLC using a fully validated method according to report Q2 issued by the International Council for Harmonization. The results of the research provided valuable information on the photolabile of the structure, and allowed for the development of the proper method of storage and transport of the tested analogues of this compound. One of the most important element in the development of new medicinal substances is their correct purification after the synthesis process. This process was optimized, the result of which was the development of a TLC optimization strategy for the separation of FLASH chromatography. This strategy allows for precise determination of the gradient separation conditions, which is aimed at eliminating the unfavorable effects of wet load technique and obtaining pure fractions of the tested compound within a specified retention time, regardless of the scale of the procedure. The developed strategy significantly improves and accelerates the purification process of biologically active substances, which is important in the purification process of radiopharmaceuticals, which, due to the specific half-life of radioactive isotopes, require fast, repeatable and efficient procedures.